Aus der Medizinischen Klinik
mit Schwerpunkt Infektiologie und Pneumologie
der Medizinischen Fakultät Charité-Universitätsmedizin Berlin

DISSERTATION

Role of mitochondria for survival of alveolar epithelial cells after pneumolysin challenge

zur Erlangung des akademischen Grades
Doctor medicinae (Dr. med.)

vorgelegt der Medizinischen Fakultät
Charité – Universitätsmedizin Berlin

von Iris Vera von Wunsch-Rolshoven Teruel
aus Berlin

Datum der Promotion: 04.06.2021

Preface

Parts of this thesis were published in

Nerlich A, von Wunsch Teruel I, Mieth M, Hönzke K, Rückert JC, Mitchell TJ, Suttorp N, Hippenstiel S, Hocke AC: **Reversion of pneumolysin induced executioner caspase activation redirects cells to survival**. *The Journal of Infectious Diseases*; 12 October 2020; jiaa639, https://doi.org/10.1093/infdis/jiaa639.

Table of contents

List of figures

List of tables

List of abbreviations

$\Delta\Psi_m$	Mitochondrial membrane potential
AIF	Apoptosis-inducing factor
Apaf-1	Apoptotic protease activating factor 1
ARDS	Acute respiratory distress syndrome
ATeam	Adenosine 5′-triphosphate indicator based on epsilon subunit for analytical measurements
ATP	Adenosine triphosphate
BAK	Bcl-2 antagonist/killer
BAX	Bcl-2-associated X protein
Bcl-2	B-cell lymphoma-2
Ca^{2+}	Calcium ion
$[Ca^{2+}]_c$	Cytosolic calcium
$[Ca^{2+}]_m$	Mitochondrial calcium
CAP	Community acquired pneumonia
CDC	Cholesterol-dependent cytolysin
CFP	Cyan fluorescent protein
CO_2	Carbon dioxide
cps	Capsule
DAMPs	Damage-associated molecular patterns
DAPI	6-diamidin-2-phenylindol
DIC	Differential interference contrast
DMSO	Dimethyl sulfoxide
DNA	Deoxyribonucleic acid
Drp1	Dynamin-related protein 1
FIS1	Mitochondrial fission protein 1
FRET	Förster resonance energy transfer
h	Hours
H^+	Hydrogen ion / proton
IL	Interleukin
MCU	Mitochondrial Ca^{2+} uniporter
min	Minute(s)

List of abbreviations

MPT	Mitochondrial permeability transition
mPTP	Mitochondrial permeability transition pore
mtDNA	Mitochondrial DNA
Na^+	Sodium ion
NADH	Nicotinamide adenine dinucleotide hydrogen
NF-κB	Nuclear factor κB
NLRP3	Nod-like receptor family pyrin domain-containing 3
OD	Optical density
PBS	Phosphate-buffered saline
PLY	Pneumolysin
PUMA	p53 upregulated modulator of apoptosis
PRR	Pattern recognition receptor
RNA	Ribonucleic acid
ROI	Region of interest
Rpm	Revolutions per minute
SD	Standard deviation of the mean
sec	Second(s)
SIM	Structured illumination microscopy
S.pn.	*Streptococcus pneumoniae*
TNF	Tumor necrosis factor
TMRE	Tetramethylrhodamine ethyl ester
YFP	Yellow fluorescent protein

Zusammenfassung

Laut Weltgesundheitsorganisation ist die Pneumonie weltweit die vierthäufigste Todesursache. Der häufigste Erreger der ambulant erworbenen Pneumonie ist das Bakterium *Streptococcus pneumoniae* (*S.pn.)*. Schwere Pneumokokkenpneumonien können ein akutes Lungenversagen verursachen, das durch diffuse Alveolarschäden mit nachfolgendem Lungenödem charakterisiert ist. Es wird angenommen, dass das porenbildende *S.pn.* Toxin Pneumolysin (PLY) entscheidend zur Lungenödembildung beiträgt. Die Porenbildung durch PLY verursacht in Alveolarepithelzellen einen schnellen Calciumeinstrom in die Mitochondrien. Dies führt zu einem Verlust des mitochondrialen Membranpotentials, zu mitochondrialer Fragmentierung, zur Aktivierung der Effektorcaspasen-3/7 und schließlich zum Zelltod. Ein Überleben von Alveolarepithelzellen nach PLY-Exposition könnte jedoch die Pneumokokkenpneumonie-assoziierte Mortalität und Morbidität reduzieren. Allerdings ist bisher unbekannt, welche zellulären Parameter zum Überleben von Alveolarepithelzellen nach PLY-Exposition beitragen.

Ziel dieser Arbeit war es, das Überleben von Alveolarepithelzellen nach PLY-Exposition *in vitro* zu untersuchen und zelluläre Parameter zu bestimmen, die mit dem Überleben von Alveolarepithelzellen nach PLY-Exposition assoziiert sind. Dazu wurden A549-Zellen und primäre Alveolarepithelzellen Typ II nach PLY-Exposition *in vitro* über einen Zeitraum von 18 h mittels Lebendzellmikroskopie untersucht. Die durch maschinelles Lernen optimierte Bildanalyse ermöglichte die kontinuierliche longitudinale Beurteilung des Zellüberlebens und der Caspase-3/7-Aktivierung individueller Zellen sowie die Korrelation mit den oben genannten mitochondrialen Parametern und der Autophagie-induktion in einzelnen Zellen.

Überraschenderweise konnten Zellen identifiziert werden, die eine PLY-Exposition trotz deutlicher Caspase-3/7-Aktivierung überlebten. Die A549-Zellen erholten sich von mitochondrialer Fragmentierung, Verlust des mitochondrialen Membranpotentials sowie der Abnahme mitochondrialer ATP-Produktion. Die Analyse der Mitochondrien auf Einzelzell-ebene identifizierte eine niedrigere Amplitude des initialen Calciumeinstroms in die Mitochondrien sowie einen folgenden schnelleren Calciumausstrom aus den Mitochondrien als entscheidende Parameter für das Überleben nach PLY-Exposition. Entsprechend führte die Hemmung des mitochondrialen Calciumausstroms zu vermehrtem Zelltod. Zudem gibt diese Studie erste Hinweise darauf, dass der zelluläre

Prozess der Autophagieinduktion für das Überleben von Alveolarepithelzellen nach PLY-Exposition relevant ist.

Schlussfolgernd stellt sich die mitochondriale Calciumregulation als ein entscheidender Parameter für die Kontrolle des Überlebens gegenüber Zelltod von Alveolarepithelzellen nach PLY-Exposition *in vitro* dar. Diese neuen Erkenntnisse könnten einen therapeutischen Ansatz bieten, um Alveolarschäden zu begrenzen und dadurch den Ausgang schwerverlaufender Pneumokokkenpneumonien zu verbessern.

Abstract

According to the World Health Organization, pneumonia is the 4th most common cause of death worldwide. The main cause of community-acquired pneumonia (CAP) is the bacterium *Streptococcus pneumoniae* (*S.pn.)*. Acute respiratory failure is a major complication of severe pneumococcal pneumonia, characterized by severe damage of the alveoli resulting in pulmonary edema. Pneumolysin (PLY), a pore-forming toxin which is produced by *S.pn.*, is thought to contribute to edema formation. In alveolar epithelial cells, PLY pore formation leads to rapid mitochondrial calcium ($[Ca^{2+}]_m$) influx resulting in loss of mitochondrial membrane potential, mitochondrial fragmentation, activation of executioner caspases-3/7 and finally cell death. Survival of alveolar epithelial cells after PLY challenge might contribute to limited mortality and morbidity following *S.pn.*-mediated CAP. However, it is currently unknown which cellular parameters determine whether alveolar epithelial cells are able to survive after PLY challenge.

The aim of the present study was thus to investigate the survival of alveolar epithelial cells after PLY challenge and characterize cellular parameters associated with cell survival *in vitro*. The alveolar epithelial cell line A549 and primary alveolar epithelial type II cells were investigated after PLY challenge for 18 hours using live-cell imaging. By establishing a machine learning-based single cell analysis method, it was possible to longitudinally track individual cells and relate cellular parameters, including cell survival and caspase-3/7 activation, with the above mentioned mitochondrial parameters as well as further cellular parameters such as autophagy induction.

Surprisingly, a significant number of alveolar epithelial cells survived the PLY challenge despite having shown clear caspase-3/7 activation. Cells were able to recover from mitochondrial fragmentation, loss of mitochondrial membrane potential and drop down of mitochondrial ATP production. The in-depth analysis of mitochondria on a single cell level identified the $[Ca^{2+}]_m$ influx amplitude and $[Ca^{2+}]_m$ efflux rate as decisive parameters for survival after PLY challenge. Accordingly, inhibition of $[Ca^{2+}]_m$ efflux resulted in a decrease of surviving A549 cells. Further findings indicated that induction of autophagy might be important for the survival of alveolar epithelial cells after PLY challenge.

In summary, regulation of $[Ca^{2+}]_m$ was identified as a critical parameter for controlling cell survival after PLY challenge in alveolar epithelial cells *in vitro*. This might serve as useful insight for future therapies to prevent and treat severe pneumococcal pneumonia by limiting alveolar damage.

1 Introduction

1.1 Community-acquired pneumonia

Community-acquired pneumonia (CAP) is an acute infection of the lower respiratory tract [1]. Pneumonia is the most common cause of death in low-income countries according to the World Health Organization. Worldwide it ranks 4th on the list of most common causes of death [2]. It kills more children worldwide than any other single cause of death, accounting for 18 % of all deaths in children under five years [3].

CAP is defined as a pneumonia that develops in immune-competent patients who have not been hospitalized recently [4]. As a major cause of morbidity and mortality, CAP is responsible for an enormous clinical and economic burden for healthcare systems worldwide [5]. In Germany alone, about 660,000 people suffer from CAP each year [4]. With a hospitalization rate of around 46.5 %, CAP poses a high economic burden in Germany [6]. The risk factors for CAP are male sex, age ≥ 65 years, and chronic comorbidities such as chronic cerebrovascular or neurologic disease, chronic cardiovascular disease, chronic lung disease and diabetes mellitus [6]. Furthermore, mortality is increased in these risk groups [5, 6].

Pneumonia can be caused by a variety of microorganisms. The most common pathogen causing CAP is *Streptococcus pneumoniae* (*S.pn.*) [1, 5]. Other causes include bacteria such as *Haemophilus influenzae, Legionella spp., Mycoplasma pneumoniae, Chlamydophila pneumoniae, Staphylococcus aureus,* and gram-negative bacteria, as well as rhino-, adeno- and coronaviruses and fungi [1].

1.1.1 Clinical features

The symptoms of CAP typically include fever or hypothermia, flu-like symptoms, fatigue and respiratory symptoms such as productive cough and dyspnea. Additionally, patients can suffer from circulatory symptoms and impaired consciousness. During the physical examination, signs such as tachypnea, tachycardia and arterial hypotension can be objectified. A focal auscultatory abnormality pointing to a specific location of an infiltrate should be confirmed by a chest x-ray [4].

To determine the severity of CAP, and therefore decide whether patients should be treated in an inpatient or outpatient care setting, the CRB-65 score was developed, based

on the parameters of confusion, respiratory rate, blood pressure and age [7]. If at least one of the criteria (Table 1) is met, hospital admission should be considered [4].

Parameter	**CRB-65 criteria**
Impaired consciousness	Newly arisen
Respiratory rate	≥ 30/min
Blood pressure (systolic / diastolic)	< 90 mmHg / ≤ 60 mmHg
Age	≥ 65 years

Table 1: CRB-65 criteria

Possible complications in patients with CAP are pleurisy, pleural effusions, pleural empyema and lung abscesses [4, 8]. Severe CAP can result in acute respiratory failure, as well as sepsis and comorbidity- or sepsis-associated extrapulmonary organ dysfunction [4].

A common cause for acute respiratory failure in severe CAP is acute respiratory distress syndrome (ARDS). ARDS is an acute life-threatening lung injury which is clinically defined as the acute onset of hypoxemia, bilateral lung opacities on chest radiograph and a non-cardiogenic pulmonary edema [9]. Pneumonia is the most common cause of ARDS and sepsis can also enhance the likelihood of development of ARDS. ARDS occurs as a consequence of alveolar injury, which together with an excessive inflammatory response and further tissue damage leads to increased permeability of the alveolar-capillary barrier. This results in the accumulation of edema fluid in the alveoli and a consequent pulmonary gas exchange failure, and therefore almost always requires mechanical ventilation support [10].

1.1.2 Prevention and therapy

Pneumococcal vaccines can help protect against serious and potentially fatal pneumococcal infections [1]. There are two different classes of pneumococcal vaccines available. Pneumococcal polysaccharide contains purified polysaccharides and covers 23 serotypes [11]. Pneumococcal conjugate vaccines contain polysaccharides of either 10 or 13 serotypes which are coupled to a carrier protein [12].

The German national vaccination schedule recommends that infants and children under the age of 2 years should be vaccinated with one of the conjugate vaccines. People

between the ages of 2 to 60 years should only be vaccinated if they belong to a risk group. Risk groups include, amongst others, patients with a chronic disease or under immunosuppression. Adults ≥ 60 years of age should be vaccinated with the 23-valent polysaccharide vaccine [13].

When patients do fall ill of CAP, the recommended antibacterial treatments are penicillin and its derivatives, macrolides and cephalosporins [4]. Unfortunately, there is an increasing worldwide problem regarding antibiotic resistance. Around 20-30 % of *S.pn.* are estimated to be multidrug-resistant, meaning resistant against more than three different antibiotic groups [14]. Furthermore, it has to be noted that since the development of antibiotics in the 1930s, it has not been possible to reduce the mortality rate of pneumonia. In spite of effective intensive care unit treatment and antibiotic therapy, around 12.2 % of hospital-treated pneumonia patients still die in Germany, according to the German Network for Community Acquired Pneumonia registry [15]. Treatment and pulmonary recovery are further complicated by the release of several virulence factors such as pneumolysin (PLY) when the *S.pn.* bacteria die [16]. PLY contributes to increased permeability of the alveolar-capillary barrier as will be detailed below. It is assumed that during severe pneumonia the alveolar-capillary barrier dysfunction promotes edema formation leading to acute respiratory failure [10, 17]. The known mechanisms underlying these phenomena will be covered in detail in the following chapters.

1.2 Pneumococcal pneumonia

1.2.1 Streptococcus pneumoniae

S.pn. is a lancet-shaped, gram-positive, facultative aerobic bacteria that comes in pairs [18]. It is an opportunistic pathogen that colonises the mucosal surfaces of the human upper respiratory tract, especially the nasopharynx [18, 19]. The colonisation of the nasopharyngeal mucosa occurs during early childhood [20]. The spreading and transmission of *S.pn.* through contaminated respiratory secretions is fostered through close contacts [18]. Nasopharyngeal colonisation is usually asymptomatic [18]. It can either be cleared, or *S.pn.* can spread directly via the airway to the usually sterile regions of the lower respiratory tract, causing pneumonia [19]. It can also progress to cause other invasive diseases such as otitis media, sinusitis, meningitis and sepsis [21].

To date, 100 different *S.pn.* serotypes have been identified [22]. They all express different capsule polysaccharides. Interestingly, just around 20 serotypes are responsible for more

than 80 % of invasive pneumococcal infections [23]. Apparently, these serotypes have an increased capacity to cause invasive disease. They must have gathered a collection of genes that allow them to shift the pathogen-host balance, thus facilitating the transition from colonisation to invasion [18, 19]. The proteins encoded by these genes which enable *S.pn.* to colonise and invade the host are called virulence factors.

1.2.2 Pneumococcal virulence factors

S.pn. possesses many virulence factors with different functions that are crucial for colonisation and invasion of the host. The composition of the expressed virulence factors differs, depending on the different *S.pn.* serotypes and depending on the target tissue and pneumococcal phenotype (colonising or invasive) [18]. The most important and best studied include the toxin PLY, the polysaccharide capsule and the surface-associated proteins (Figure 1). The multiple effects of PLY will be detailed in chapter 1.3.

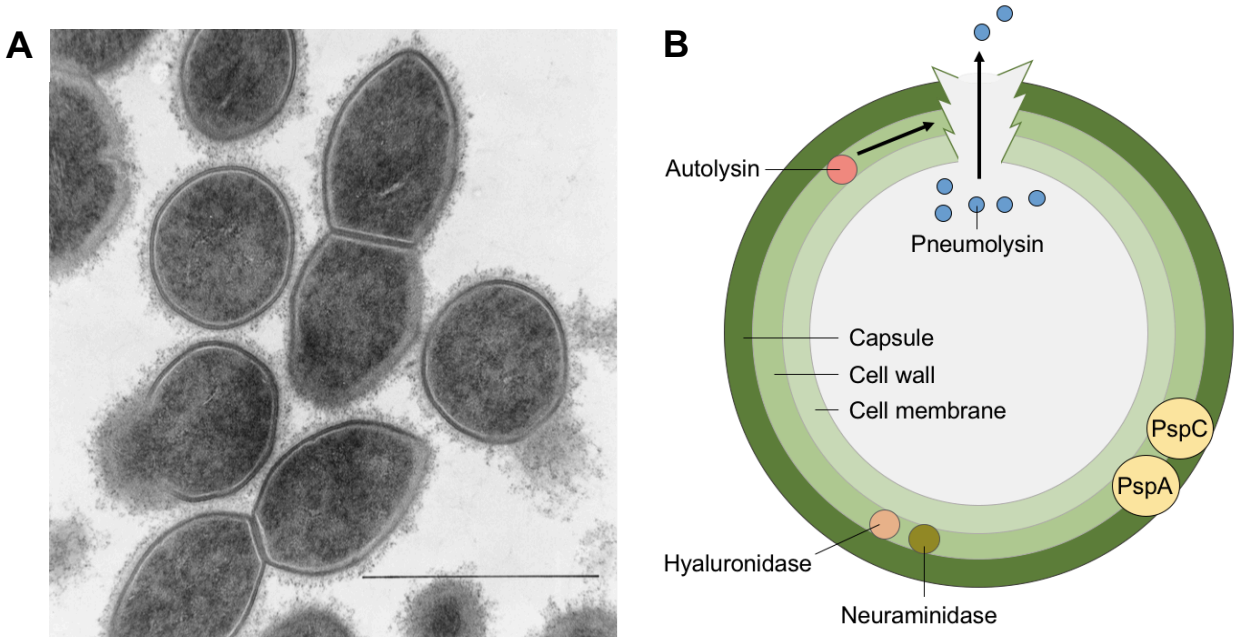

Figure 1. *Streptococcus pneumoniae* and its virulence factors. (**A**) Electron micrograph of non-encapsulated pneumococci. Bar represents 1 µm. (**B**) Virulence factors of *Streptococcus pneumoniae*. Important virulence factors are the capsule, the cell wall, pneumolysin, LPXTG-anchored proteins such as hyaluronidase and neuraminidase, and choline-binding proteins such as autolysin pneumococcal surface proteins A and C (PspA and PspC). Figures were adapted and modified from [19, 24].

The polysaccharide capsule is crucial during colonisation as it prevents mucociliary clearance by interfering with mucus binding [25]. Furthermore, it inhibits complement activity and protects *S.pn.* from opsonophagocytosis during invasive infection [26, 27].
Additionally, *S.pn.* owns a variety of proteins that are bound to its surface and act as virulence factors. They are either anchored via LPXTG (a gram-positive attachment motif), or via interaction with choline present in the pneumococcal cell wall [19].
LPXTG-anchored proteins include neuraminidase and hyaluronidase. Neuraminidase is important during colonisation as it demasks receptors for adherence by cleaving the glycopeptides and glycolipids of host cells [28-30]. Hyaluronidase helps *S.pn.* spread in the tissue by breaking down hyaluronic acid in the extracellular matrix [31].
Choline-binding proteins include autolysin, pneumococcal surface protein A and pneumococcal surface protein C. Autolysin is a cell wall degrading enzyme. Degradation of the cell wall not only leads to the release of highly inflammatory cell wall fragments but also to the release of PLY [32-34]. Pneumococcal surface protein A interferes with the complement system which impedes complement-driven opsonisation [35]. By binding lactoferrin it additionally protects against the bactericidal effects of free lactoferrin [36]. Pneumococcal surface protein C (also called choline-binding protein A) facilitates adhesion and uptake of bacteria into nasopharyngeal cells by binding human secretory immunoglobulin A [37, 38].

1.2.3 Pathogenesis of pneumococcal pneumonia

Through breathing, not only oxygen but also microbes are frequently inhaled into the respiratory tract. Even though humans are constantly exposed to pathogens, they are normally able to resist pathogen attacks thanks to the innate and adaptive immune system [39]. The innate immune system is a non-specific defence which can respond rapidly to a broad range of microorganisms [40]. Unlike adaptive immunity, innate immunity has little or no memory of prior exposure to pathogens [41].
Combined with the cough reflex, mucociliary clearance serves as a first line of defence of the innate immune system to prevent pathogens from reaching the lower respiratory tract [42, 43]. Molecules that can directly target pathogens such as lactoferrin and lysozyme are carried within the mucus [43, 44]. Some pathogens like *S.pn.* are able to overcome the mucociliary apparatus with the help of virulence factors such as the polysaccharide capsule [25].

In both the upper and lower respiratory tract, epithelial cells serve as an anatomical barrier to protect from tissue invasion [43, 45]. Dendritic cells within the respiratory mucosa of the nose and conducting airways can detect invading microorganisms, catch them and bring them to the draining lymph nodes where the adaptive immunity will be mobilised [46].

Once invading microbes have reached the alveoli, macrophages are the first cells of the innate immune system they will encounter. Cells of the innate immune system can detect pathogens non-specifically with cell surface receptors [40]. These receptors are called pattern recognition receptors (PRRs). PRRs detect pathogen-associated molecular patterns (PAMPs), which are conserved molecular patterns of pathogens that cannot be found in the human host. PRRs are additionally able to detect cellular stress through so-called damage-associated molecular patterns (DAMPs). DAMPs are usually intracellular components such as mitochondrial deoxyribonucleic acid (mtDNA) that are secreted during pathological processes in order to minimize tissue damage [47].

The recognition of PAMPs through immune cells such as macrophages leads to phagocytosis of the pathogen [41]. The pneumococcal antiphagocytic components are its polysaccharide capsule and PLY [48]. Once alveolar macrophages have recognized PAMPs or DAMPs, they start producing a large number of different chemokines and cytokines, which will eventually activate the adaptive immune system and recruit more immune cells such as monocytes, neutrophils and lymphocytes [39, 41].

While immune cell recruitment is necessary for microbial clearance, an overwhelming immune cell recruitment can lead to an uncontrolled hyperinflammatory response and subsequent lung tissue damage [10]. Injury of alveolar epithelial and endothelial cells causes loss of alveolar-capillary barrier integrity [10, 17]. The ensuing pulmonary edema, containing cell debris, bacteria and immune cells, accumulates in the alveolar space, causing impaired oxygen exchange which, if severe, leads to ARDS and acute respiratory failure [10]. Furthermore, systemic spreading of the invading pathogen facilitated by the epithelial and endothelial barrier dysfunction can result in sepsis and septic shock [49, 50]. During pneumococcal pneumonia, PLY further aggravates epithelial and endothelial barrier dysfunction through its cytotoxic and pro-inflammatory properties, as detailed below.

Resolution of ARDS requires reabsorption of the pulmonary edema and repair of the epithelial and endothelial barriers. For reabsorption of the pulmonary edema, sodium and

chloride are absorbed across the apical surface of alveolar epithelial cells and sodium is extruded on the basolateral membrane by the sodium-potassium pump. This creates an osmotic gradient which facilitates absorption of water from the alveoli [51]. Thus, effective reabsorption requires metabolically active cells and the restoration of the alveolar epithelial cell barrier. Reepithelialization of the epithelial surface occurs mainly by proliferation of alveolar epithelial type II cells which can differentiate into type I cells [51, 52]. Alveolar epithelial type I cells are flattened non-dividing cells that cover around 95 % of the alveolar surface, being responsible for gas exchange [53]. Alveolar epithelial type II cells line the remainder of the alveolus. They are an essential part of the human alveolar epithelium as next to their proliferating properties they also produce surfactants [54]. Surfactants lower the surface tension in alveoli and lack of surfactant can lead to alveolar collapse and respiratory failure [52, 54].

1.3 Pneumolysin

1.3.1 General

PLY is a toxin that belongs to the group of cholesterol dependent cytolysins (CDC) [48]. CDCs commonly oligomerize upon binding to cell membranes with subsequent pore formation [55]. PLY is a 53 kDa protein composed of 471 amino acids. Like all other CDCs, it consists of 4 domains, of which the c-terminal domain (domain 4) composes the cholesterol-binding unit [55, 56]. The protein is released by autolysin (another pneumococcal virulence factor) during bacterial lysis, via an autolysin-independent mechanism or under the influence of bacteriolytic antibiotics [56, 57]. PLY is released as a monomer and binds to cholesterol. This is followed by oligomerization of multiple monomers, which leads to the formation of inactive pre-pores. After a conformational change, the actual membrane-perforating pore is formed [58-60].

PLY has multiple actions on eukaryotic cells ranging from direct cytotoxic effects to activation of pro-inflammatory responses. All clinically relevant *S.pn.* strains produce PLY, while PLY-deficient *S.pn.* mutants are less virulent [61-64].

1.3.2 Cytotoxic properties of pneumolysin

Through its cytotoxic properties PLY induces cell death in different cell types. The kind of cell death induced by PLY depends both on toxin dose and cell type [65].

At high doses, formation of a large number of pores totally disrupts the compartmentalization of the cell membrane, which leads to cell lysis [66]. At lower doses PLY pore formation leads to leakage of cytoplasmic proteins and ions [56]. Among other things, a rapid cytosolic influx of the second messenger calcium (Ca^{2+}) then occurs which activates apoptotic pathways as detailed in chapter 1.6 [67-69].

PLY facilitates the invasion of *S.pn.* into the lower respiratory tract through inhibition of mucociliary clearance by damaging the ciliated epithelium and impairing ciliary function [66, 70, 71]. In the alveoli, PLY also damages endothelial cells and contributes to pulmonary haemorrhage and edema [72-74]. Combined with cell death of respiratory epithelial cells, this not only leads to clinically deleterious lung injury, but also enables *S.pn.* to invade lung tissue and enter the blood stream [63, 73, 75]. PLY-positive *S.pn.* also cause the separation of epithelial tight junctions [70]. Loss of epithelial and endothelial barrier function is a major complication of pneumococcal pneumonia as it can lead to acute respiratory failure and sepsis.

1.3.3 Pro-inflammatory properties of pneumolysin

PLY is also responsible for strong pro-inflammatory activities that play a role during the pathogenesis of pneumonia. Dysregulated immune responses to PLY lead to excessive lung inflammation and potentially lung injury – both of which can also facilitate the spreading of *S.pn.* and development of acute respiratory failure.

In sublytic concentrations, PLY activates the p38 mitogen-activated protein kinase signalling pathway through a sublethal number of pores and the subsequent osmotic stress [76]. Its activation has been shown to be important for the production of cytokines such as interleukin-8 (IL-8), which is known to promote cell recruitment, especially neutrophils, to sites of infection [77].

PLY activates a large number of genes in eukaryotic cells [78]. Microarray analysis of a monocyte cell line that had been infected either with either wild type *S.pn.* or a PLY-deficient mutant showed that more than 140 genes were induced by PLY. Among those genes were proinflammatory proteins such as IL-8, mannose-binding lectin 1, macrophage inflammatory protein-1 β and monocyte chemotactic protein 3 [78].

It has been reported that PLY interacts with the innate immune system through the recognition of PLY by TLR4 and TLR2 [79, 80]. TLR4-deficient mice show a higher vulnerability for invasive pneumococcal infections and more lethal outcomes compared with wild type mice [80]. The detection of PLY by TLR4 activates NF-κB signalling and

inflammatory cytokine production, particularly tumor necrosis factor α (TNF-α), IL-6 and IL-1β [79]. This induces recruitment of further immune cells like neutrophils, inflammatory monocytes and dendritic cells [39]. Furthermore, it leads to changes in epithelial barrier permeability and an increase of total protein levels in the lung [81]. It has also been shown that PLY activates TLR4-independent innate immune responses through NOD-like receptor family pyrin domain-containing 3 (NLRP3) inflammasome activation, leading to the release of IL-1β and IL-18 [81, 82].

PLY further enables the persistence and invasion of *S.pn.* in pulmonary tissue and into the blood stream by the activation of complement [83, 84]. Complement activation is crucial for pneumococcal clearance, and both the classical and alternative pathways are required [84]. It has been assumed that the continuous activation of complement factors leads to a diminished availability of complement factors for opsonisation [83].

1.4 Mitochondria

Mitochondria are cell organelles in the cytoplasm. Because of their compartmentalised structure they provide an ideal space for different biochemical processes such as the production of adenosine triphosphate (ATP), beta-oxidation, steroidogenesis and ketogenesis [85]. Mitochondria are essential for cellular energy production and play a central role in the regulation of Ca^{2+} homeostasis and cell death, as well as activation of the innate immune system, as will be detailed below.

Mitochondria have an inner and an outer membrane. The space between the inner and outer membrane is called the intermembrane space. It contains important proteins for mitochondrial biogenesis, energy metabolism and apoptosis. A prominent example is cytochrome c, which is a component of the electron transport chain and plays an important role in apoptosis [86].

The internal compartment of mitochondria, surrounded by the inner membrane, is the mitochondrial matrix [86]. In the matrix biosynthetic reactions such as the citric acid cycle occur. The citric acid cycle leads to the accumulation of reduced nicotinamide adenine dinucleotide hydrogen (NADH) in the mitochondrial matrix where it is then used for oxidative phosphorylation [85]. The mitochondrial matrix is also the site where mtDNA is stored and replicated, and where transcription and protein biosynthesis take place [87].

While the outer mitochondrial membrane has many pores that allow the passage of ions and molecules as large as small proteins, the inner membrane is impermeable except

through specific transporters [85]. The inner membrane forms invaginations, called cristae, that extend deeply into the mitochondrial matrix [86]. This increases the surface area of the inner membrane. The inner membrane contains the protein complexes for oxidative phosphorylation. Oxidative phosphorylation is the oxygen-dependent production of ATP driven by an electrochemical gradient across the inner mitochondrial membrane [85]. Due to the electron transfer from NADH and oxygen, protons are pumped from the matrix through the inner mitochondrial membrane into the inner membrane space, resulting in the mitochondrial membrane potential ($\Delta\Psi_m$). The ATP synthase uses this electrochemical proton gradient to generate ATP from adenosine diphosphate and phosphate ions [85]. Mitochondria are the main source of ATP, which is an energy-rich molecule that propels fundamental cell functions.

The number and location of mitochondria differs according to cell type and function**.** Mitochondrial distribution to locations of high energy demand is facilitated by motor proteins along microtubules and the actin filament [88, 89].

Mitochondria are highly dynamic and the shape of mitochondria is very variable from small granular to highly filamentous structures [90]. In the cell, they form a tubular network that constantly changes by fission and fusion processes [88]. Fission and fusion processes are very important. They control the efficient distribution of mitochondria within the cell and allow the exchange of lipid membranes and intramitochondrial content such as mtDNA between mitochondria [90, 91].

Mitochondrial fission and fusion are regulated by a family of dynamin-related GTPases [90, 92]. Mitofusins 1 and 2 regulate the fusion of the outer mitochondrial membrane, whereas optic atrophy protein 1 promotes the fusion of the inner membrane [88, 89]. Mitochondrial fission requires the GTPase dynamin-related protein 1 (Drp1) and mitochondrial fission protein 1 (FIS1) [92].

Dysregulation of fission and fusion processes and consequent changes in mitochondrial morphology lead to a substantial reduction of mitochondrial functions [88]. Mitochondria undergo dramatic morphological changes during apoptosis resulting in fragmented mitochondria [93, 94]. Remarkably, inhibition of Drp1 or FIS1 delays or even blocks cell death, implicating mitochondrial fission as an important step in apoptosis [93, 95].

1.4.1 Mitochondrial activation of the innate immune system

Mitochondria play an important role regarding the regulation of different signalling pathways of the innate immune system [47, 96]. Mitochondria are an important source of DAMPs and different studies show their importance in the process of inflammation.

Among other things, it has been described that mitochondrial dysfunction leads to the release of DAMPs such as mtDNA, cytochrome c and mitochondrial transcription factor A [47]. In alveolar epithelial cells specifically, our group has shown that stimulation with PLY leads to release of mtDNA [97]. A study by Zhang *et al.* demonstrated that the intravenous injection of clinically relevant amounts of mtDNA caused a strong inflammatory response in the lung [98].

1.4.2 Mitochondrial calcium regulation

Mitochondria also play an important role regarding intracellular Ca^{2+} storage, buffering and signalling. Well-balanced intracellular Ca^{2+} concentrations are of utmost importance for cellular functioning [99-101].

The outer mitochondrial membrane is freely permeable to small molecules such as ions, while the inner membrane is ion-impermeable [102]. Three transporters present in the inner mitochondrial membrane seem to play a role in Ca^{2+} homeostasis. The mitochondrial Ca^{2+} uniporter (MCU) helps in the uptake of Ca^{2+} into mitochondria [103, 104]. The H^+/Ca^{2+} exchanger mHCX and the Na^+/Ca^{2+} exchanger NCLX pump Ca^{2+} from the mitochondria to the cytosol [101]. The molecular identity of mHCX is controversial and so far it has only been described in isolated mitochondria [99, 101]. The Ca^{2+} efflux properties of NCLX, on the other hand, are generally accepted today [101, 105]. NCLX can be inhibited by the selective blocker CGP-37157 [101]. The mitochondrial calcium ($[Ca^{2+}]_m$) efflux by NCLX is much slower than the influx via the MCU [106]. Hence, NCLX is the rate limiting determinant for controlling Ca^{2+} fluxes in mitochondria [105].

When the $[Ca^{2+}]_m$ influx exceeds the efflux rate, mitochondria efflux Ca^{2+} through the opening of the mitochondrial permeability transition pore (mPTP) leading to cell death, as will be detailed below [101, 107].

1.5 Apoptosis

Apoptosis is a form of regulated cell death that serves as a mechanism to eliminate infected and malignant cells without triggering an inflammatory process [108]. Two main

apoptosis activation pathways have been described: the extrinsic and the intrinsic pathway.

Many of the characteristic morphological and biochemical changes that occur during classical apoptosis result from activation of a family of cysteine proteases called caspases, which can be divided into the initiator and the effector caspases. Activated initiator caspases-8, -9 and -10 cleave and thereby activate effector caspases-3, -6 and -7 [109]. The activation of the executioner caspases results in cell shrinkage, chromatin condensation and DNA fragmentation. Other characteristic morphological features include membrane blebbing and formation of apoptotic bodies [109]. Apoptotic bodies are membrane vesicles that contain cell content. *In vivo*, they are engulfed by phagocytic cells and degraded in lysosomes. Since the plasma membrane remains intact during apoptosis, apoptotic death is generally considered as an non-inflammatory process [110]. Necrosis, on the other hand, is characterized by cell swelling and rupture. Subsequent leakage of cell contents is followed by inflammation of the surrounding tissue. *In vitro*, or if apoptotic cells are not cleared, their plasma membranes rupture and release pro-inflammatory intracellular contents through secondary necrosis [111].

1.5.1 Extrinsic apoptosis pathway

The extrinsic pathway is triggered by disturbances of the extracellular microenvironment which activate so-called cell death receptors that are located in the plasma membrane. Such death receptors include the TNF receptor 1 and the CD95/Fas receptor, as well as the TNF-related apoptosis-inducing ligand receptors-1 and -2. After binding extrinsic ligands (e.g. TNF-α), they interact with different intracellular receptors and form multiprotein complexes. These induce the activation of caspases-8 and -10 which consequently activate caspases-3, -6 and -7 [85, 109].

1.5.2 Intrinsic apoptosis pathway

The intrinsic pathway is initiated from inside the cell and displays a reaction to stress because of intracellular homeostatic perturbations such as cytosolic Ca^{2+} overload, oxidative stress or DNA damage [109, 112]. This pathway is also called the mitochondrial pathway, indicating the essential role of mitochondria.

Mitochondrial outer membrane permeabilization (MOMP) plays a crucial role in the intrinsic pathway. MOMP leads to release of pro-apoptotic proteins to the cytosol, and

can also elicit cell death through the loss of vital mitochondrial functions such as loss of $\Delta\Psi_m$ and cessation of mitochondrial ATP synthesis [112, 113].

Intrinsic apoptosis is mainly controlled by pro- and anti-apoptotic members of the B-cell lymphoma 2 (Bcl-2) protein family [85]. After apoptotic signals, pro-apoptotic Bcl-2 proteins such as p53 upregulated modulator of apoptosis (PUMA) are increasingly expressed to activate Bcl-2-associated X protein (BAX), Bcl-2 antagonist/killer 1 (BAK) or truncated BH3 interacting-domain death agonist (tBID). In physiological conditions, BAX resides in the cytosol. However, upon apoptosis induction, BAX inserts into the outer membrane where it forms pores – alone or in association with BAK or tBID – resulting in MOMP [114, 115]. Anti-apoptotic Bcl-2 proteins such as Bcl-2 and Bcl-2-like 1 can inhibit the apoptotic activities of BAX and BAK – either through inhibition of oligomerization or indirectly by promoting the cytosolic translocation of BAX [109].

MOMP leads to loss of $\Delta\Psi_m$ and facilitates the release of pro-apoptotic proteins such as cytochrome c or apoptosis-inducing factor (AIF) to the cytosol. Once released, cytochrome c binds to apoptotic protease activating factor 1 (Apaf-1), which in the presence of ATP/dATP triggers its oligomerization. After this, pro-caspase-9 is recruited and undergoes autoactivation. The protein complex comprising cytochrome c, Apaf-1 and caspase-9 is called the “apoptosome”. Activated caspase-9 cleaves downstream caspases like caspase-3, -6 and -7, which culminates in cell death [109].

In the past few years, there has also been accumulating evidence that programmed cell death can also occur caspase-independently. The causes can be an irreversible loss of mitochondrial functions as well as the release of caspase-independent death factors such as AIF. AIF can lead to chromatin condensation and DNA fragmentation without caspase activation [116]. It appears that AIF plays a critical role in the death of certain cell types such as neurons [117, 118].

1.5.3 Mitochondrial permeability transition

Another mechanism that can lead to cell death through permeabilization of the outer mitochondrial membrane is the opening of the mPTP. Its opening is called mitochondrial permeability transition (MPT) and can be triggered by multiple stimuli such as mitochondrial Ca^{2+} overload or oxidative stress [119, 120]. The mPTP is a mega pore between the inner and outer mitochondrial membrane, and its exact composition is still debated [120].

The opening of the mPTP allows water and small molecules (up to 1.5 kDa) to pass through, which results in the loss of $\Delta\Psi_m$ as ions equilibrate across the membranes. This can lead to depletion of ATP and ultimately necrotic cell death [99, 120].

Although mPTP opening has mostly been associated with necrotic cell death, it has also been reported to trigger apoptosis by activation of caspase-dependent and caspase-independent mechanisms through cytochrome c and AIF release [116, 121]. The exact mechanism underlying the release of these pro-apoptotic proteins is still unclear. One model is that water entering the mitochondria through the open mPTP results in mitochondrial swelling and rupture of the outer mitochondrial membrane. Rupture of the outer mitochondrial membrane might then release pro-apoptotic components of the intermembrane space [99, 107].

1.6 Pneumolysin-induced apoptosis

PLY has been reported to induce apoptosis in a number of cell types including neuronal cells, macrophages and respiratory epithelial cells [68, 97, 122, 123]. The induction of apoptosis can be harmful or potentially beneficial during *S.pn.* infection. Understanding the molecular mechanisms and consequences of apoptosis in each setting is essential for potential therapeutic interventions. Most studies on PLY-induced apoptosis have been conducted on neuronal cells.

1.6.1 Pneumolysin-induced apoptosis in brain tissue

PLY is a major trigger of apoptosis in the brain and implicated in the apoptosis of neurons, microglia and brain microvascular endothelial cells [67, 68, 122, 124]. In this context, PLY exerts a harmful effect, as it contributes to disease progression and neuronal cell death causing neurological impairment.

A study by Stringaris *et al.* showed that buffering of intracellular calcium ($[Ca^{2+}]_c$) with BAPTA-AM and inhibition of the mPTP using bongkrekic acid, improved survival of human neuronal cells following stimulation with PLY [68]. Human neuronal cells that had been co-incubated with the pan-caspase inhibitor ZVAD were partly protected against PLY-induced toxicity which suggests that caspases are involved in PLY-induced cell death [68]. Using human brain microvascular endothelial cells, it was also shown that PLY-induced apoptosis was dependent on the activation of caspases [124].

On the other hand, studies by Bermpohl *et al.* and Braun *et al.* in murine brain models showed that apoptosis of endothelial cells and neuronal cells was caspase independent

and independent of TLR2 or TLR4 activation [67, 69, 122]. Intracellular $[Ca^{2+}]_c$ increase induced MOMP and release of AIF [122]. The use of murine primary cells instead of human cell lines might possibly explain these differences.

Interestingly, all of these studies on brain tissue cells indicated that apoptosis after PLY stimulation was induced through $[Ca^{2+}]_c$ influx and the ensuing effects on mitochondria. Apoptosis of cochlear hair cells showed similar mechanisms since $[Ca^{2+}]_c$ influx and mitochondrial toxicity also triggered apoptosis [125].

1.6.2 Pneumolysin-induced apoptosis in the respiratory tract

PLY has been implicated in the apoptosis of alveolar macrophages, epithelial cells and endothelial cells [72, 97, 123, 126].

In a study by Dockrell *et al.* PLY-deficient mutant *S.pn.* induced less apoptosis in infected macrophages than PLY-producing strains [123]. Bongkrekic acid, an inhibitor of the mPTP, decreased PLY-induced apoptosis of macrophages in a study by Marriott *et al.* [126]. Apoptosis of inflammatory macrophages seems to be caspase dependent and involves TLR4 [127].

Epithelial and endothelial cell apoptosis, on the other hand, contributes to tissue injury. It was shown that pore formation by PLY in human alveolar epithelial cells leads to a strong $[Ca^{2+}]_m$ influx, which induces rapid opening of the mPTP, mitochondrial fragmentation, loss of $\Delta\Psi_m$ and decrease of ATP production. This is followed by release of mtDNA and activation of executioner caspases-3 and -7. The PLY induced dose-dependent $[Ca^{2+}]_m$ influx correlated with caspase-3/7 activation. Interestingly, cytochrome c or AIF release could not be detected [97].

1.7 Anastasis

MOMP and subsequent activation of executioner caspases-3 and -7 was widely considered a point of no return regarding the initiation of apoptosis, yet recent findings show that this is not always the case. When MOMP only affects a limited number of mitochondria, sublethal caspase activation occurs and cells are able to survive. This process has been termed minority or incomplete MOMP [121, 128].

Additionally, a variety of primary cells, cell lines and cancer cells exposed to transient apoptotic stimuli can survive partial activation of executioner caspases and initiation of apoptosis [129, 130]. This still poorly characterized process has been termed anastasis, a Greek word meaning “rising to life” [129, 130].

Anastasis is defined as an active process during which the expression of a number of genes is upregulated. Two stages of anastasis were revealed through transcriptome profiling. During the early phase, genes that are associated with transcription, stress response and regulation of cell death are upregulated. During the late phase, anastatic cells undergo cytoskeletal rearrangement and morphological changes and become more migratory. One of the messenger RNAs that was highly induced in the early anastasis phase was the transcription factor Snail. Silencing Snail, which is known to downregulate E-cadherin, prevented cell recovery [130].

Anastasis only occurs when cells are transiently treated with potentially lethal chemicals such as staurosporine [129, 130]. In this context, it is interesting to note that cells are able to repair PLY pores to some extent, via shedding patches of damaged plasmalemma into the extracellular milieu [131, 132]. Therefore, treatment with sublytic toxin concentrations can be considered a transient stimulus.

It is tempting to speculate that alveolar epithelial cells might also be able to recover from apoptosis initiation after stimulation with sublytic PLY concentrations. Survival of alveolar epithelial cells could be of great advantage during *S.pn.* pneumonia, as it would maintain the alveolar-capillary integrity, and thus decrease the risk of pulmonary edema formation resulting in acute respiratory failure. Furthermore, the survival especially of alveolar epithelial type II cells could be essential, as their proliferation restores alveolar epithelial surfaces after lung injury.

1.8 Aims of the study

CAP is a common infectious disease that places a high burden on society due to its high prevalence, mortality and morbidity. Complications of CAP include acute respiratory failure, which is characterized by severe damage of the alveoli resulting in pulmonary edema. The most common pathogen causing CAP is *S.pn.* which produces the pore-forming toxin PLY, thereby contributing to the development of pulmonary edema by driving alveolar injury. As the extent of alveolar injury correlates with clinical severity, improved survival of alveolar epithelial cells after PLY challenge during *S.pn.* pneumonia may benefit clinical outcomes.

It is well established that in alveolar epithelial cells, PLY pore formation leads to mitochondrial calcium influx $[Ca^{2+}]_m$, resulting in loss of mitochondrial membrane potential, mitochondrial fragmentation, executioner caspases-3/7 activation and finally cell death. Furthermore, recent studies demonstrated that various different types of eukaryotic cells are able to survive activation of executioner caspases and initiation of apoptosis. However, it is still unclear whether alveolar epithelial cells survive PLY-mediated activation of executioner caspases-3/7, and the mechanisms underlying survival of PLY-mediated induction of cell death are also unclear.

Therefore, it was the aim of this project to investigate the following questions:

1. Can alveolar epithelial cells survive PLY-induced activation of executioner caspases-3/7?

2. Which cellular parameters are associated with increased survival of alveolar-epithelial cells after PLY challenge?

2 Materials and methods

2.1 Materials

2.1.1 Human lung alveolar epithelial cell line A549

The cell line used in this work was the A549 cell line from ATCC (CCL-185). It is a human epithelial lung cell line which was extracted from a lung carcinoma of a 58-year old Caucasian man in 1972. These cells have the properties of type II pulmonary epithelial cells [133].

2.1.2 Primary human alveolar epithelial type II cells

Fresh human lung explants for isolation of primary human alveolar epithelial type II cells (phAEC II) were obtained from adult patients undergoing lung resection at the thoracic surgery centres of Helios Klinikum Emil von Behring Zehlendorf, DRK Klinikum Mitte, Vivantes Klinikum Berlin Neukölln and Charité Campus Mitte. The tumour-free lung tissue probes were from patients of whom the majority had a lung cancer. Written informed consent was obtained. The study was approved by the local institutional review board (Ethics committee of the Charité Universitätsmedizin Berlin, Germany, EA2/079/13) and performed in accordance with the approved guidelines.

2.1.3 *Streptococcus pneumoniae* D39Δ*cps* and D39Δ*cps*Δ*ply*

The *S.pn.* strains used for this work were the D39 derived capsule locus (*cps*) deletion mutant D39Δ*cps* and additionally the PLY-deficient double mutant D39Δ*cps*Δ*ply*. These pneumococcal strains were kindly provided by Prof. Dr. Sven Hammerschmidt from the University of Greifswald, Germany.

2.1.4 Stimulants

Description	Manufacturer
Pneumolysin	Prof. Dr. Timothy Mitchell, University of Birmingham, United Kingdom
Oligomycin	Sigma-Aldrich

Table 2: Stimulants

2.1.5 Inhibitors

Description	Manufacturer
Pan-caspase inhibitor Z-VAD-FMK (ZVAD)	Merck Millipore
NCLX inhibitor CGP-37157	Sigma-Aldrich

Table 3: Inhibitors

2.1.6 Enzymes

Description	Manufacturer
DNase (Bovine Pancreas)	Calbiochem
Trypsin/EDTA (1X)	Sigma-Aldrich
Trypsin type I	Sigma-Aldrich

Table 4: Enzymes

2.1.7 Plasmids

Description	Origin
mitoATeam ($AT1.03^{YEMK}$ with N-terminal mitochondrial signal sequence)	Prof. Hiromi H. Imamura, University of Kyoto, Japan

Table 5: Plasmids

2.1.8 Cell culture media and additives

Human lung alveolar epithelial cell line A549

Description	Composition
Culture medium	Ham's F12, 500 ml FCS, 10 % L-glutamine, 1 %

Stimulation medium	Phenol red-free Ham's F12, 500 ml FCS, dialyzed, 2 % L-glutamine, 1 %
Galactose medium	DMEM + L-glutamine, – D-glucose, 500 ml FCS, dialyzed, 2 % D-(+)-galactose, 1 %
Freezing medium	Ham's F12, 500 ml FCS, 10 % DMSO, 10 %

Table 6: Media and additives for A549 cells

Primary human alveolar epithelial type II cells

Description	Composition
Culture medium	RPMI 1640, 500 ml FCS, 10 % L-glutamine, 1 %
Stimulation medium	RPMI 1640, 500 ml FCS, 2 % L-glutamine, 1 %

Table 7: Media and additives for primary human alveolar epithelial type II cells

2.1.9 Bacterial culture of *Streptococcus pneumoniae*

Description	Composition
Growth medium for *Streptococcus pneumoniae*	Todd Hewitt broth, 30 g, autoclaved Yeast extract, 0,5 % Aqua dest., ad 1000 ml

Freezing medium for *Streptococcus pneumoniae*	Todd Hewitt medium, 80 %, autoclaved Glycerine, 20 %, sterile

Table 8: Bacterial culture of *Streptococcus pneumoniae*

2.1.10 Chemicals and reagents

Item	**Manufacturer**
CellEvent Caspase-3/7 Green Detection Reagent	Life Technologies
CYTO-ID autophagy detection kit	Enzo Life Sciences
D-(+)-galactose	Sigma-Aldrich
Dimethyl sulfoxide (DMSO)	Sigma-Aldrich
DMEM + L-glutamine, – D-glucose	Life Technologies
Ethanol	Roth
Fetal calf serum	GE Healthcare
FCS, dialyzed	Life Technologies
Glutamine	Life Technologies
Glycerine	Roth
Ham's F12	Biochrome
Hank's Balanced Salt Solution (HBSS)	Thermo Fischer Scientific
Isopropanol	Roth
MitoTracker Orange CMTMRos	Life Technologies
Opti-MEM	Thermo Fischer Scientific
Pancoll separating medium	PAN-Biotech
Phosphate buffered saline (PBS)	Life Technologies
Rhod2-AM	Life Technologies
RPMI 1640	Gibco

SiR-actin	Spirochrome
SiR-DNA	Spirochrome
Tetramethylrhodamine ethyl ester perchlorate (TMRE)	Life Technologies
Todd Hewitt broth	BD
Trypan blue	Sigma-Aldrich
ViaFect™ Transfection Reagent	Promega
Yeast extract	BD

Table 9: Chemicals and reagents

2.1.11 Consumables

Item	**Manufacturer**
Cell culture flask (75 cm^2)	Sarstedt
Centrifuge tubes (25 and 50 ml)	Falcon
Columbia blood agar plates	BD
Combitips (1, 2.5, 5 and 10 ml)	Eppendorf
Cryogenic vials (1.5 and 2 ml)	Roth
Falcons (15 ml, 50 ml)	Corning
Inoculating loop	Sarstedt
SuperFrost® microscope slides	Thermo Fischer Scientific
Pasteur pipette	Sarstedt
Pipettes (10, 200 and 1000 µl)	Corning
Petri dishes (10 cm)	Falcon
Pipette tips with filter (10, 200, 1000 µl)	Biozym
Reaction tubes (0,5, 1 and 2 ml)	Sarstedt
Serological pipettes (2, 5, 10 and 25 ml)	Falcon
Sterile gauze strainer (40, 70 and 100 µm)	Falcon

Tissue culture flask (75 cm^2)	Sarstedt
µ-Slide, 8-well (ibiTreat)	Ibidi
Cell culture flask (75 cm^2)	Sarstedt
Centrifuge tubes (25 and 50 ml)	Falcon
Columbia blood agar plates	BD

Table 10: Consumables

2.1.12 Equipment

Item	**Manufacturer**
Counting chamber, Neubauer Improved	Laboroptik
Autoclave Varioklav, type 75S u 135S	H+P Labortechnik AG
Centrifuge, Biofuge primo	Heraeus Instruments
Confocal microscope, LSM 780	Zeiss
Super-resolution microscope with structured illumination, ELYRA PS.1	Zeiss
Fridge, (4°C/-20°C) LCv 4010 MediLine	Liebherr
Freezer, (-80°C) HERAfreeze™	Thermo Fisher Scientific
Incubator, Heraeus	Thermo Fisher Scientific
Phase-contrast microscope, Wilovert S	Hund
Photometer, Uvikon X2	BioTek
Sterile work bench HERAsafe™, KS	Thermo Fisher Scientific
Vacuum pump, Vacusafe	INTEGRA Biosciences AG
Vortex mixer, Labdancer	IKA
Water bath, WBT 6	Roth

Table 11: Equipment

2.1.13 Software

Program	Supplier
Adobe Photoshop Elements 18.0	Adobe Systems
CellProfiler software version 3.1.5	Open source
ImageJ	Open source
Prism 8.3.0	GraphPad
Python 3.6	Open source
ZEN 2.1	Zeiss

Table 12: Software

2.2 Methods

2.2.1 Cell culture

The handling of cell cultures was done routinely in a laboratory under a sterile workbench. The laboratory had a S2 biosafety level. Only sterile materials were used. The cultivation, stimulation and infection of all cells was routinely done at 37 °C, 5 % CO_2 and 95 % humidity in an incubator. All substances used were warmed up to 37 °C before use.

2.2.1.1 Thawing of A549 cells

The frozen cells stored in cryovials were quickly thawed at 37 °C in a water bath. Afterwards, they were resuspended in 10 ml of culture medium and centrifuged for 5 min at 900 rpm. The supernatant was aspirated, and the cells were seeded in a cell culture flask with fresh culture medium.

2.2.1.2 Preparing cryo stocks

For cryostorage, detached A549 cells were transferred into 15 ml tubes and centrifuged for 5 min at 900 rpm. The supernatant was aspirated, and the cell pellets were resuspended in freezing medium and transferred into cryovials. To prevent cell damage during this freezing process, the cryovials were first placed in an isopropanol-filled box for at least 24 h at -80 °C. Afterwards, the cryovials were kept in liquid nitrogen for long-term storage.

2.2.1.3 Cultivation of A549 cells

The cells were generally kept in tissue culture flasks filled with culture medium at 37 °C in an atmosphere of 5 % CO_2. The cultivation media used was Ham's F12 with FBS at a concentration of 10 % and L-glutamine at a concentration of 1 %. No antibiotics were added. Cells were split two to three times a week when reaching a confluence of 70-80 %. For splitting, the medium was removed completely, and cells were washed twice with 10 ml of PBS. To remove the adherent cells from the bottom of the flasks, they were incubated with 2 ml trypsin/EDTA. The enzymatic reaction of trypsin was stopped by adding the previously removed medium. Next, the cell suspension was centrifuged at 900 rpm. The supernatant was then aspirated, and the cell pellet resuspended in fresh culture medium and distributed in a ratio of 1:5 or 1:10 into the tissue culture flasks containing fresh medium.

The cell count had to be determined for the experiments. For this purpose, 10 µl of the cell suspension were mixed with 10 µl of trypan blue. In all 4 quadrants of a counting chamber, viable cells were counted under a microscope. The number of cells per ml was then calculated using the following formula: number of cells/ml = number of cells in all 4 quadrants / 2 × 10^4 (constant of the counting chamber). The culture medium was diluted depending on the number of cells needed per well.

For live-cell imaging, the cells were cultivated on 8-well Ibidi µ-slides (ibiTreat) with a cell count of 30,000 per well. Stimulation or infection was conducted 3 days after seeding when the cells formed a confluent monolayer. On the evening prior to the day of the experiment, the culture medium was replaced with medium containing 2% of FCS. This is a common procedure to put the cells in a state of “starvation” before infection or stimulation experiments.

2.2.1.4 Transient transfection of A549 cells

For FRET based determination of mitochondrial ATP, the A549 cells were transiently transfected with a plasmid encoding the mitochondrial ATP sensor called mitoATeam. ATeam stands for “adenosine 5′-triphosphate indicator based on epsilon subunit for analytical measurements”. This ATP sensor was developed by Imamura *et al.* The mitochondrial location of mitoATeam was accomplished through adding a mitochondrial signal sequence to the N-terminal end of the sensor [134].

The cells were seeded with a cell count of 30,000 per well with a volume of 250 µl in a 8-well µ-slide. The following day 30 µl of OptiMEM and 0.4 µg of plasmids encoding mitoATeam were each mixed in 1.5 ml reaction tubes. Afterwards, 1 µl ViaFectTM transfection reagent was added to each tube, and the mixture was incubated at room temperature for 15 min. Meanwhile, 170 µl of fresh medium was added to the seeded cells after removal of the old medium. Following the 15 min of incubation, 30 µl of the transfection mixture was also added to those cells. After 6 h, the whole transfection medium mixture was aspirated and replaced with fresh medium. The following day, the efficiency of the transfection was checked using a fluorescence microscope and the culture medium was once more replaced with fresh medium. For experiments, the medium was replaced with 200 µl of medium two days post-transfection, either with or without 0.1 µg/ml of PLY for stimulation.

The activity of the mitochondrial ATP sensor mitoATeam was tested using oligomycin, which is an inhibitor of the mitochondrial ATP synthase. Cells were stimulated with

10 µg/ml of oligomycin for 30 min, following previous incubation with galactose-containing medium for 24 h. Galactose enhances the oxidative metabolism and consequently makes them susceptible to mitochondrial inhibitors such as oligomycin. Before each measurement, the Ibidi µ-slides were calibrated inside of the confocal microscope which had been pre-set to 37 °C and 5 % CO_2.

2.2.1.5 Isolation of primary human type II alveolar epithelial cells

phAEC II were isolated from human lung tissue as described previously [135]. In short, human lung tissue was finely minced and transferred into HBSS. The tissue was digested with trypsin and DNase for 40 min at 37 °C. After inactivation of enzymes and recovery of the cells using 30 % FCS, the digested tissue was filtered serially through sterile gauze strainers. Macrophages and fibroblasts were removed based on differential adhesion to tissue culture plates or by density gradient using a separating medium. All isolation steps were performed at 37 °C or room temperature. After the final centrifugation step, the phAEC II cells were cultured in RPMI 1640 medium with 10 % FCS and stored for a maximum of four days. For stimulation experiments phAEC II were harvested by trypsinisation and seeded in Ibidi µ-slides containing phenol red-free Ham's F12 medium with 2 % FCS and 1 % L-glutamine. The experiment with phAEC II stimulated with 0.2 µg/ml PLY was conducted with the help of Dr. Andreas Nerlich.

2.2.2 Bacterial culture

All work with bacterial strains was done in a sterile work environment under the S2 biosafety level. The bacterial cultivation always took place at 37 °C, 5 % CO_2 and 95 % humidity. All materials and equipment were disinfected and autoclaved after usage.

2.2.2.1 Storing of *Streptococcus pneumoniae*

S.pn. strains were spread on warm Columbia blood agar plates with 5 % sheep blood medium using inoculation loops, creating a three-phase streaking pattern. After 8-10 h of incubation, isolated colonies were transferred to a new agar plate and reincubated for 8-10 h. Then, using a sterile cotton swap, the colonies that had grown on this last agar plate were transferred to freezing medium to be stored at -80 °C in cryogenic vials.

2.2.2.2 Cultivation of *Streptococcus pneumoniae*

For cultivation of the *S.pn.* strains, the content of the cryogenic vials was spread on the aforementioned agar plates using an inoculation loop (on the morning of the day before the experiments).

After being incubated for 8-10 h, isolated colonies were transferred with cotton swabs to the Todd Hewitt broth with 0.5 % yeast extract. The number of transferred bacteria was determined by measuring the optical density (OD) at 600 nm in a photometer. The OD was supposed to be from 0.03 to 0.05. Until usage, the bacterial suspension was either stored on ice or directly incubated in a water bath at 37 °C until reaching an OD of 0.3 to 0.4 in the early midlog phase.

2.2.2.3 Cell infection with *Streptococcus pneumoniae*

After reaching the optimal concentration, the bacterial suspension was centrifuged at 4000 rpm for 10 min, the supernatant discarded, and the bacterial pellet resuspended in the same amount of preheated Ham's F12 medium supplemented with 2 % FCS. Starting with this bacterial suspension, a concentration of 10^8 cfu/ml was generated using the following formula: OD of 0.1 = 10^8 cfu/ml. The suspension was diluted until reaching a concentration of 2.5 × 10^5 cfu/ml and 200 µl of this suspension were added to 50,000 cells per well, which resulted in a multiplicity of infection of 1. The A549 cells were incubated for 18 h.

To check whether the initial number of bacteria actually contained the correct concentration of *S.pn.* strains, bacterial suspensions were serially diluted in PBS, put on agar plates and incubated at 37 °C overnight. The following day, the initial actual multiplicity of infection could be calculated based on the counted colonies on the plates. Infection of A549 cells with *S.pn.* strains was executed with the help of Dr. Maren Mieth.

2.2.3 Cell stimulation

2.2.3.1 Pneumolysin

PLY (stock concentration of 1065 µg/ml) was diluted in cell culture medium until reaching a concentration of 0.1 µg/ml or 0.2 µg/ml and then added to cells.

2.2.3.2 ZVAD and CGP-37157

The pan-caspase inhibitor ZVAD and the NCLX inhibitor CGP-37157 were diluted with cell culture medium until reaching a concentration of 10.7 µM and 10 µM, respectively.

CGP-37157 was added to the cells 15 min prior to PLY stimulation. ZVAD was added to the cells 30 min prior to PLY stimulation and when PLY was added.

2.2.3.3 Negative control

When cells in other wells were stimulated or infected, the same amount of cell culture medium was substituted in a control well. These cells were incubated as long as stimulated cells. The analysis of these cells was used as negative control.

2.2.4 Live-cell microscopy

Live-cell microscopy was used for the analysis of caspase-3/7 activation, actin, mitochondrial membrane potential, $[Ca^{2+}]_m$ flux, mitochondrial morphology, and autophagy, as well as the detection of intracellular ATP. Live-cell microscopy makes it possible to analyse non-fixated living cells in their ideal environment. In this way, cells can be stimulated, and the consequences of the stimulation can be observed throughout the whole experiment. Due to the incubator built inside the microscopes the cells stay in a stable environment of 37 °C and 5 % CO_2. All cell culture media used were preheated before being added to the cells.

Live-cell imaging was performed on a LSM 780 confocal laser-scanning microscope using a 40× water immersion objective (C-Apochromat Corr. M27, numerical aperture 1.2) and on a ELYRA PS.1 super-resolution microscope with structured illumination using a 63× oil immersion objective (Plan-Apochromat objective Corr. M27, numerical aperture 1.4). Images were acquired with the ZEN 2.1 program.

2.2.4.1 Confocal microscopy

To be able to measure different cellular parameters, fluorescent dyes were used. They have the property that after absorbing light of certain wavelength they emit light of a longer wavelength. When absorbing light, the electrons of the fluorescent dye jump to a higher energy level. Once the electron jumps back to its ground level, it emits a longer wavelength photon. This specific emission wavelength can then be measured using filters and detectors inside the microscope.

In thicker probes, the standard fluorescent microscopes also measure light signals that are above or below the focal plane. This leads to a loss of image quality. To circumvent this problem, confocal microscopes have a built-in pin hole just before the detector. This pin hole only lets light signals through that come from a specific spot within the focal plane, leading to a better image quality. Furthermore, instead of flooding the entire probe

evenly in light, a single spot of focused light is rapidly transitioned across the probe resulting in many single spot images. These single spot images can then be put together digitally to create one fluorescent image of the whole scanned probe.

Through the shifting of the focal plane, it is possible to cut a thick probe into many optical slices which can then be put back together digitally to form a three-dimensional stack. If these optical slices are simply put on top of each other, a two-dimensional image representing either the highest (maximum intensity projection) or sum of all intensities (sum intensity projection) of the three-dimensional stack can be generated.

When emission spectra of fluorescent dyes (such as CellEvent Caspase-3/7 Green Detection Reagent and CYTO-ID dye) are very similar, spectral imaging can be used to properly differentiate them. Spectral imaging collects information across a wide range of emission wavelengths at the same time for each pixel. The resulting spectral image stack is commonly referred to as a lambda stack. Since each fluorescent dye has a unique spectral signature, this can then be used to assign the specific contribution of that dye to individual pixels of the lambda stack based on reference spectra. This makes it possible to reassign colour to regions that would otherwise appear mixed. This post-imaging process is called linear unmixing.

2.2.4.2 Structured illumination microscopy

Structured illumination microscopy (SIM) is a technique that allows the acquisition of super-resolution images. This technique was used in this work for a refined visualization of the morphology of mitochondria that had been labelled with the MitoTracker Orange CMTMRos dye.

Briefly, SIM works by using a patterned illumination, usually a grid, to excite the probe. The grid's position and orientation are changed a number of times, and the emitted fluorescence signal is recorded for each one of those positions. Following processing with a specialized algorithm, this information can be extracted from the raw data of these multiple images, to produce a reconstructed final image that has a resolution approximately twice that of diffraction-limited instruments (such as confocal microscopes). SIM images were acquired with five phase shifts and three rotations of the structured illumination grid and a z-step size of 120 nm.

2.2.4.3 Labelling of nuclei

SiR-DNA is based on the fluorophore silicon rhodamine (SiR) and the DNA minor groove binder bisbenzimide (Hoechst). Labelling of nuclei with SiR-DNA (1 µM) was done for 2 h at 37 °C and 5 % CO2 before the stimulation experiments started. SiR-DNA was excited at a wavelength of 633 nm and emission was collected between 634 nm and 758 nm.

2.2.4.4 Analysis of caspase-3/7 activation

For measurements of caspase-3/7 activation CellEvent Caspase-3/7 Green Detection Reagent was added in a concentration of 1:500 to the cell culture medium with or without PLY. The substrate is a nucleic acid-binding dye which is conjugated to a four-amino acid peptide (DEVD). This peptide sequence impedes the dye binding to DNA, so that no fluorescent signal can be measured initially. Only when activated caspase-3/7 is present is the dye cleaved from the DEVD peptide and can bind to the DNA, which produces a fluorescence signal in the cell nucleus.

Caspase-3/7 activation was measured before and after PLY stimulation every 10 min over a time span of 18 h**.** The caspase-3/7 sensor was excited at a wavelength of 488 nm and emission was collected between 488 – 561 (confocal) and 495 - 550 nm (SIM), respectively.

2.2.4.5 Visualization of actin polymerization

Labelling of the actin cytoskeleton with SiR-actin (1 µM) was done for 1 h at 37 °C and 5 % CO_2 before the stimulation experiments started. SiR-actin is based on the fluorophore silicon rhodamine (SiR) and the actin binding natural product jasplakinolide, which is a filamentous actin stabilizing cell toxin. It enables the labelling of filamentous actin inside living cells.

Actin polymerization was measured before and after PLY stimulation over a time span of 18 h, first every 30 min and later every hour**.** SiR-actin was excited at a wavelength of 633 nm and emission was collected between 634 nm and 758 nm.

2.2.4.6 Analysis of mitochondrial membrane potential

Cells were incubated for 30 min with 10 nM tetramethyl-rhodamine methyl ester (TMRE) at 37 °C and 5 % CO_2. Depending on the membrane potential of mitochondria, TMRE accumulates inside the mitochondria. When the mitochondrial membrane depolarizes the dye diffuses out of the mitochondria, which leads to a reduction of the fluorescent signal.

After incubation, the excess fluorescent dye was washed off three times with HBSS and cell culture medium with or without PLY was added.

The mitochondrial membrane potential was measured before and after PLY stimulation every 10 min over a time span of 18 h. TMRE was excited at a wavelength of 561 nm and emission was collected between 561 nm and 633 nm. For the evaluation of the mitochondrial membrane potential, the TMRE signal of the dying and surviving cells was normalized to control.

2.2.4.7 Analysis of mitochondrial calcium influx

Cells were incubated for 30 min with 4.45 µM Rhod2-AM at 37 °C and 5 % CO_2 using FBS-free medium, followed by three washing steps with HBSS. The mitochondrial calcium indicator is a molecule that exhibits an increase in fluorescence upon binding Ca^{2+}.

The mitochondrial calcium load was measured before and after PLY stimulation over a period of 18 h. Since Ca^{2+} changes occur rapidly, images were taken continuously before and 30 min after stimulation, and thereafter every 10 min. Rhod2-AM was excited at a wavelength of 561 nm and emission was collected between 561 nm and 633 nm.

2.2.4.8 Visualization of mitochondrial morphology

To label mitochondria, cells were incubated for 30 min at 37 °C and 5 % CO_2 with 100 nM of the MitoTracker Orange CMTMRos dye dissolved in DMSO. After incubation, the excess fluorescent dye was washed off three times with PBS and cell culture medium with or without PLY was added.

The mitochondrial morphology was visualized immediately before stimulation, and 1 h and 6 h after addition of PLY. For SIM, MitoTracker Orange was excited at a wavelength of 561 nm and emission was collected between 570 and 620 nm. Randomly chosen dying and surviving cells were used to compare the morphology of mitochondria after PLY stimulation. This experiment was conducted with the help of Dr. Andreas Nerlich.

2.2.4.9 Measurement of mitochondrial ATP concentration

For the determination of mitochondrial ATP concentrations, the transfection of the ATP sensor mitoATeam was done as described in chapter 2.2.1.4.

The measurement was based on Förster resonance energy transfer (FRET). FRET is a phenomenon which describes the energy transfer from a donor, which is an excited light-sensitive molecule, to another molecule which acts as an acceptor. For an efficient energy

transfer, a maximum distance of 10 nm is required and the emission spectrum of the donor should overlap with the absorption spectrum of the acceptor [136].

The FRET-based mitochondrial ATP sensor mitoATeam consists of two fluorescent proteins that are coupled together. The cyan fluorescent protein (CFP) acts as the donor and the yellow fluorescent protein (YFP) as the acceptor (Figure 2). CFP and YFP are genetically linked through the ε subunit of the F_oF_1-ATP synthase from *Bacillus subtilis*. The physiological role of the ε subunit is the regulation of the F_oF_1-ATP synthase activity depending on the ATP concentration. Upon binding ATP, the subunit undergoes a conformational change from a relaxed into a folded form. Consequently, the distance between CFP and YFP is reduced, which intensifies the FRET effect and leads to more fluorescence emission at 527 nm. In the relaxed form (in the absence of ATP) the distance between CFP and YFP increases, thus the FRET effect is reduced, and fluorescent signals are emitted at 475 nm.

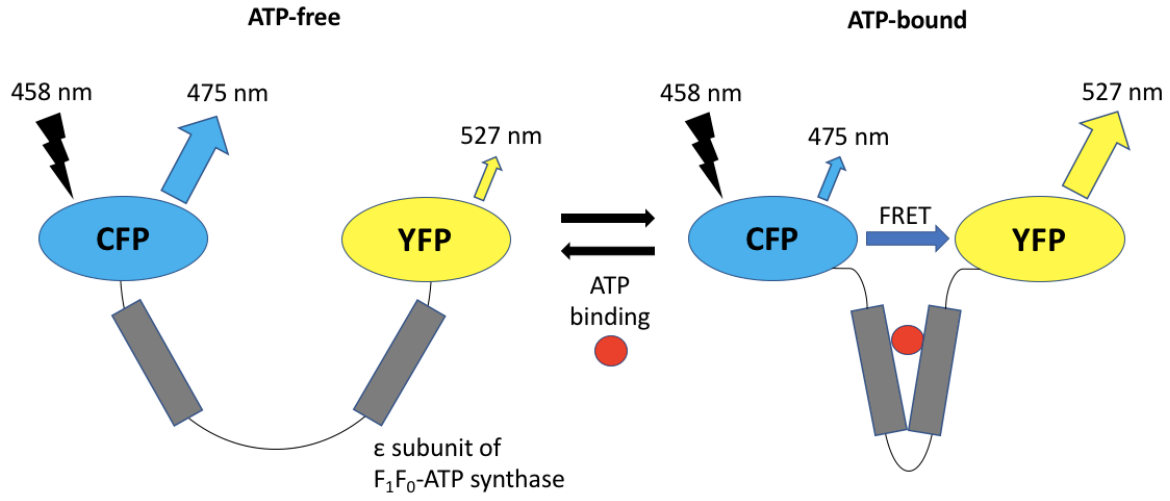

Figure 2. Schematic drawing of the Förster resonance energy transfer (FRET) effect. The donor CFP and the acceptor YFP are connected by the ε subunit of the *Bacillus subtilis* F_oF_1-ATP synthase. In the ATP-free form (left), the extended conformation of the ε subunit separates the two fluorescent proteins, resulting in a low FRET effect. In the ATP-bound form, the conformational change of the ε subunit draws the two fluorescent proteins close to each other, which increases the FRET effect.

FRET signals were measured by spectral confocal microscopy. Therefore, lambda stacks were acquired using 458 nm excitation, and emission was detected between 415 nm and 691 nm. The ATP content is expressed as the normalized ratio of the YFP/CFP peak intensity at 530 nm (YFP) and 478 nm (CFP).

The mitochondrial ATP concentration was determined just before stimulation, directly after, every 30 min for 2 hours and thereafter every hour for a total time period of 18 h. Stimulation with 10 µg/ml oligomycin served as positive control.

2.2.4.10 Analysis of autophagy

To analyse autophagy, cells were incubated with CYTO-ID dye (CYTO-ID Autophagy Detection Kit) for 30 min and then cell culture medium with or without PLY was added. The cationic amphiphilic tracer dye CYTO-ID selectively labels autophagic vacuoles.
Autophagic vesicles were visualized before and directly after PLY stimulation, and thereafter every hour over a time period of 18 h**.** The fluorescent signal of CYTO-ID was measured in lambda mode using 488 nm excitation and emission was detected between 415 nm and 691 nm.

2.2.5 Single cell analysis

In experiments in which labelling of nuclei was possible, a machine learning-based approach was established (see below) to analyse different cellular parameters in individual cells at different time points. For all other experiments, different approaches had to be employed.
For quantification of ATP levels and actin polymerization, a region of interest (ROI) was drawn manually around individual cells at different time points within the ZEN 2.1 software. Thereby, the intensity of fluorescent signals of each individual cell could be measured over time. Cells were separated into a surviving or dying fraction based on morphology, cell detachment and caspase-3/7 activation. For individual cell analysis of ATP levels and actin polymerization, at least 5 or 10 cells were analysed in each surviving and dying cell population, respectively.
For quantification of autophagy, a semi-automatic approach was established. First, the pencil tool in the Fiji software was used to add spots to individual nuclei at each measured time point based on the differential interference contrast (DIC) channel. Within the software CellProfiler, these spots (PrimaryObjects) could then be used to track individual cells over time. Furthermore, these spots served as seed points to define the region around them as cytoplasm (SecondaryObjects). Within the cytoplasm, Cyto-ID vesicles could then be identified and counted using CellProfiler. Cells were divided into surviving and dying cells using a manually defined threshold for the caspase-3/7 intensity for each experiment.

All semi-automatic and machine learning-based single cell analysis approaches were conducted with the help of Dr. Andreas Nerlich.

2.2.5.1 Machine learning and image processing

For detection of cell nuclei, the convolutional neural network StarDist was used as it was developed specifically for segmentation of nuclei [137].

Training of the convolutional neural network

Training data sets were generated by randomly selecting 10 images of experiments of unstimulated and PLY-stimulated A549 cells at different time points. Next, around 200 nuclei of A549 cells per image were marked by manually drawing around the edges of each nucleus using the Fiji software [138].

Images used for training were first resized from 2048 × 2048 pixels to 1024 ×1024 pixels. This enabled faster training without influencing predictive quality. Next, training data were augmented before training by horizontal and vertical flips, 90° rotations, elastic deformations and Gaussian filtering. Additionally, these 1024 × 1024 pixel images were split into four 512 × 512 pixel images.

All of these steps resulted in a total number of 700 images. Of these images, 80 % were used for training and 20 % for testing. The training was performed on a Nvidia Titan X GPU. Details on the training parameters of the convolutional neural network are summarized in table 13. These training parameters were adapted from StarDist.

Parameter	Value
n_rays	32
n_channel_in	1
unet_n_depth	3
unet_kernel_size	[3, 3]
unet_n_filter_base	32
net_conv_after_unet	128
net_input_shape	[null, null, 1]
train_shape_completion	true
train_completion_crop	32
train_patch_size	[512, 512]
train_dist_loss	mae
train_epochs	100
train_steps_per_epoch	200
train_learning_rate	0.0003
train_batch_size	8
train_tensorboard	true
train_checkpoint	weights_best.h5
train_reduce_lr	"factor": 0.5, "patience": 10, "verbose": true

Table 13: Parameters of the convolutional neural network StarDist

Nuclei prediction

The time-lapse image data of each 18 h experiment with PLY-stimulated and unstimulated A549 cells consisted of around 100-150 frames/images, depending on the experiment. Each image had to be further processed with the Fiji software. Amongst other things, the size had to be adapted to 1024 × 1024 pixels for nuclei prediction. Furthermore, slight positional shifts of the ibidi slide after PLY stimulation impaired later tracking in some experiments. Therefore, we corrected this shift using the MultiStackRegistration Plugin version 1.45 which realigned the images (https://github.com/miura/MultiStackRegistration).

Finally, the image data was split into the different channels and the SiR-DNA channel was extracted to be subjected to nuclei prediction by StarDist. Next, the predicted nuclear masks for each frame/image were added to the image stack as an additional channel.
For Figure 17 B, the acquired z-stacks were split into individual channels, maximum intensity projections of the SiR-DNA channel and sum intensity projections of the caspase-3/7 channel were generated, and individual nuclei were predicted with StarDist. For quantification, the nuclear mask images were added to an image stack containing the projections as additional channel.

Tracking and analysis with CellProfiler

Afterwards, images were analysed using CellProfiler software version 3.1.5 [139]. For quantification of signals in the nuclei, the masks predicted by StarDist were used. For the cytoplasm a 15-pixel wide, ring-shaped region around the nucleus was used as a proxy. Cells were tracked, and intensity measurements were obtained using built-in measurement modules in CellProfiler. For Figure 17 B cells were classified as alive or dead based on a MADIntensity value as a threshold in CellProfiler.

Tracking of primary human alveolar epithelial type II cells

Tracking of phAEC II (Figure 9) was done manually in randomly chosen cells using TrackMate [140]. Caspase-3/7 sensor intensity was quantified using a spot size of 40 pixels, and tracked cells were assigned manually to the surviving/dying fraction based on interpretation of caspase-3/7 signal, morphology and cell detachment.

2.2.5.2 Final data analysis

Final data analysis was performed in Python 3.6 and Prism 8.3.0. The fluorescent caspase-3/7, SiR-actin, TMRE and Ca^{2+} signals are expressed as F/F_0 ratio, where F is the signal intensity at each time point and F_0 is the average baseline signal intensity obtained before stimulation.
The influx amplitude of Ca^{2+} was calculated by subtracting the mean baseline value from the maximal peak fluorescence value. Efflux rates in Figure 15 were obtained by fitting a biexponential decay model over a period of ~80 min after reaching the maximum amplitude. For Figure 16, the efflux rates were derived from a linear fit of the change in the fluorescence over a period of ~28 min after reaching the maximum amplitude.

2.2.6 Statistical analysis

Values are expressed as mean ± standard deviation (SD) from at least three independent experiments. Welch's t-test was used for comparison of two groups, and Welch ANOVA followed by Benjamini, Krieger and Yekutieli two stage false discovery rate correction was used for comparison of three or more groups. Both tests assume that the groups of data are sampled from Gaussian populations, but without assuming that the groups have the same SD. Exact *P* values are indicated in the figures. GraphPad Prism 8.3.0 was used for the statistical analysis.

3 Results

3.1 Caspase-3/7 activation during *Streptococcus pneumoniae* infection is pneumolysin-dependent

It was recently shown that A549 cells treated with purified PLY showed strong mitochondrial alterations and caspase-3/7 activation - especially when a high toxin concentration of 1 µg/ml was applied [97]. To date, it had not been tested whether caspase-3/7 activation is also induced at physiological levels of PLY, as produced by *S.pn.*

Therefore, A549 cells were infected either with either PLY-producing *S.pn.* D39Δ*cps* or PLY-deficient mutant *S.pn.* D39Δ*cps*Δ*ply*. While infection of A549 cells with PLY-deficient mutant *S.pn.* did not result in caspase-3/7 activation after 18 h, PLY-producing *S.pn.* induced caspase-3/7 activation, as reflected by increased fluorescence intensities (Figure 3).

This shows that caspase-3/7 is not only activated by purified PLY, but also by PLY produced by living *S.pn.* bacteria in the cells investigated. Furthermore, it underlines that caspase-3/7 activation during *S.pn.* infection is PLY-dependent.

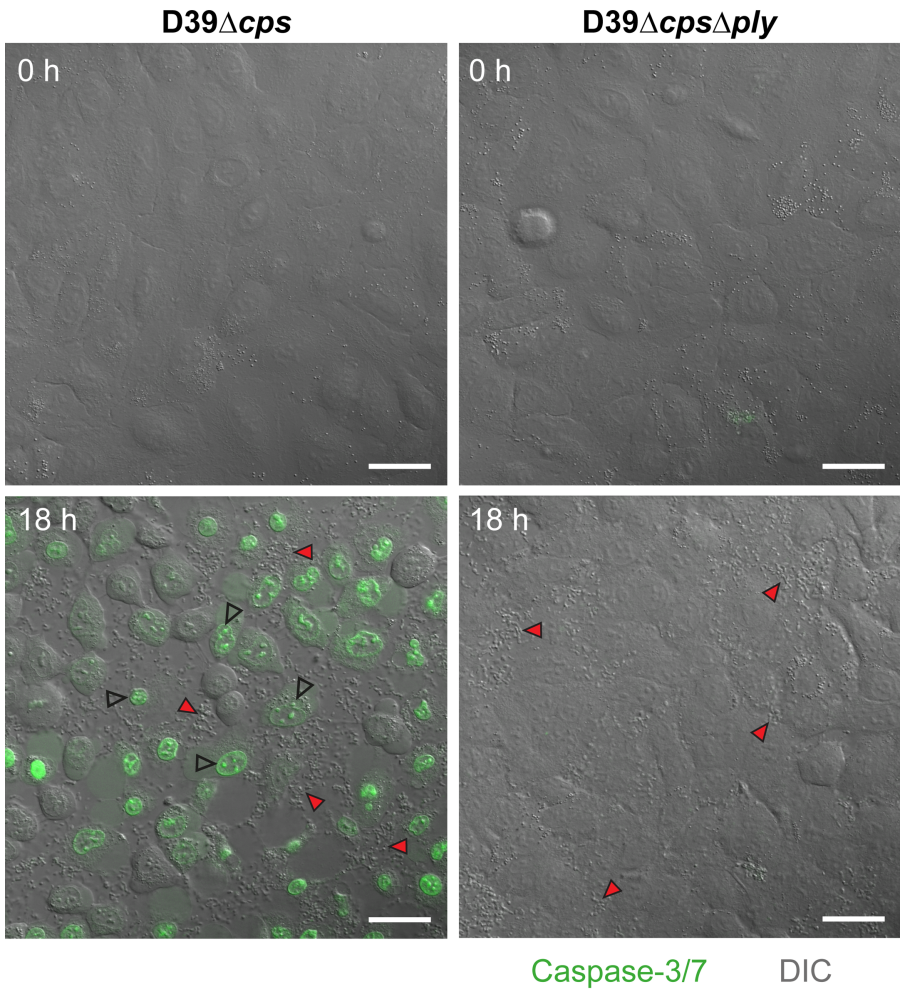

Figure 3. PLY-dependent caspase-3/7 activation after pneumococcal infection. A549 cells were analysed by confocal live-cell microscopy for 18 h to compare caspase-3/7 activation during infection with either PLY-producing *Streptococcus pneumoniae* (*S.pn.*) D39Δ*cps* or PLY-deficient *S.pn.* D39Δ*cps*Δ*ply*. Cells were visualized using differential interference contrast (DIC) for cellular morphology and for proof of bacterial infection (grey, red arrowheads on *S.pn.* bacteria) as well as caspase-3/7 activation (green). Black open arrowheads indicate exemplary dying cells with strong caspase-3/7 activation. At the beginning (0 h, upper panels), cells showed normal morphology. Infection with PLY-producing *S.pn.* D39Δ*cps* led to strong caspase-3/7 activation compared with PLY-deficient mutants D39Δ*cps*Δ*ply* (18 h, right, lower panel). Depicted is one representative experiment out of six. Scale bars represent 30 µm. Figure reproduced in entirety from supplementary figure 1 from original publication [141].

3.2 A549 cells can survive caspase-3/7 activation

Next, it was tested whether lower concentrations of purified PLY would also lead to caspase-3/7 activation in A549 cells.

Challenging A549 cells with concentrations of 0.1 µg/ml PLY led to caspase-3/7 activation in most of the cells (Figure 4 A). Interestingly, among the A549 cells with detectable caspase-3/7 activation, live-cell microscopy revealed two different cellular phenotypes (Figure 4).

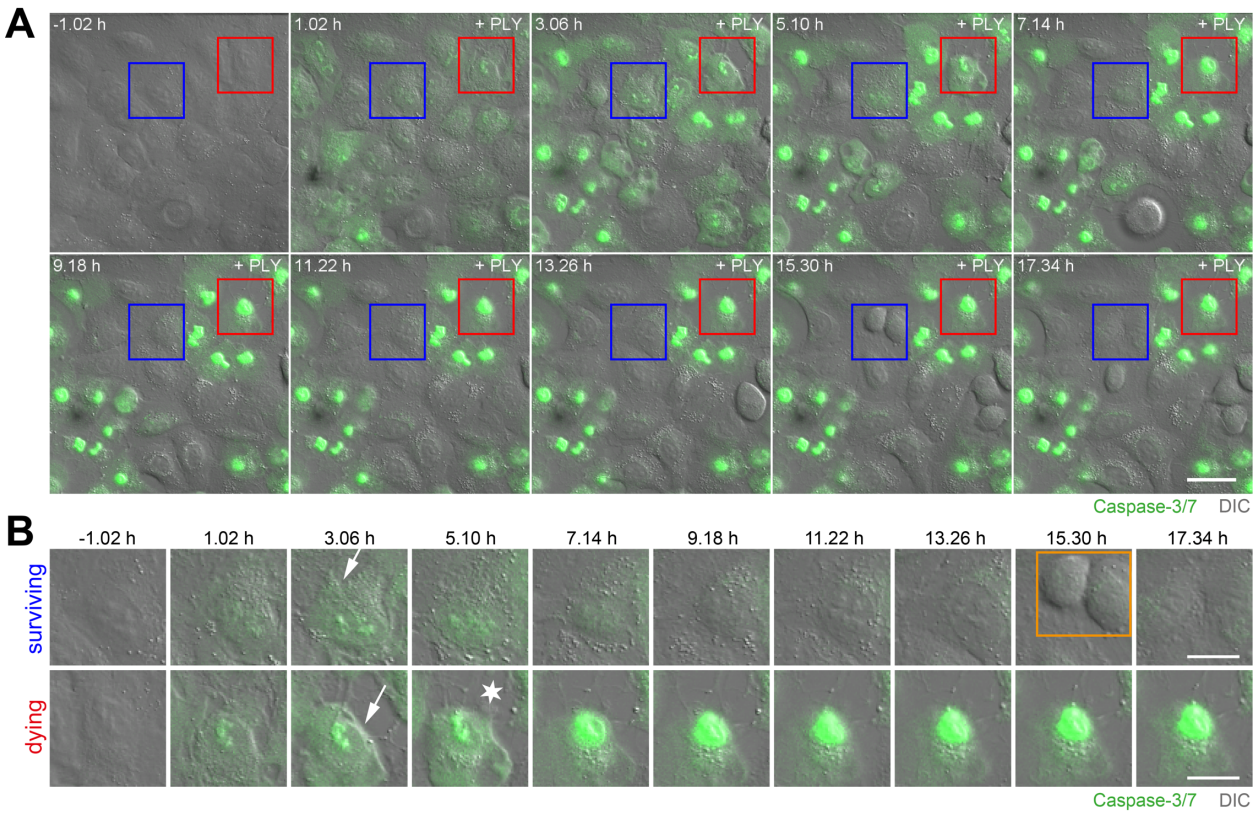

Figure 4. Survival of PLY-treated A549 cells after caspase-3/7 activation. A549 cells were stimulated with 0.1 µg/ml PLY and caspase-3/7 activation was imaged by confocal live-cell microscopy for up to 18 h after stimulation. (**A**) Representative time-lapse images of A549 cells visualizing cellular morphology by differential interference contrast (DIC, grey) and caspase-3/7 activation (green). All cells showed activation of caspase-3/7 and the red box indicates a representative dying cell, while the blue box indicates a cell that recovered and subsequently divided. Scale bar represents 30 µm. (**B**) Enlarged images of the representative surviving and dying cells shown in (A). In addition, apoptotic characteristics such as cell shrinkage (arrow) leading to gap formation (star) were observed. The orange rectangle indicates cell division of a surviving cell. Scale bars represent 15 µm. Figure adapted from figure 1 from original publication [141].

One subpopulation of cells showed a strong caspase-3/7 activation and died over the course of the experiment (Figure 4 A [red rectangle] and B). The dying cells showed increasing activated caspase-3/7 signals, and no cell motility (data not shown) when cell death was final. Some dead cells detached completely from the cell layer and moved out of focus (data not shown). Surprisingly, another subpopulation of cells was detected in which caspase-3/7 activation was induced which peaked at around 3 h (Figure 4 A [blue rectangle] and B). In this subpopulation of cells, the overall caspase-3/7 activation decreased over the course of the experiment until barely any activation of caspases was detectable after 17.30 h.

Both populations showed typical apoptotic features such as cell shrinkage (Figure 4 B - arrow) - that accompanied caspase-3/7 activation. In dying cells, the cell retraction was so pronounced that it led to gap formation (Figure 4 B - star). In the surviving population, with the disappearance of caspase-3/7 signal, cell shrinkage reversed.

Moreover, cells that survived the toxin stimulation after caspase-3/7 activation were able to divide again after several hours of recovery (Figure 4 B, [orange rectangle, 15.30 h]).

For quantification of these processes at a single cell level and to separate both subpopulations, a machine learning-based segmentation method was implemented and combined with an automatic cell tracking and analysis pipeline (Figure 5).

For this purpose, the nuclei of A549 cells were stained with a marker called SiR-DNA. The cells were then stimulated with 0.1 µg/ml PLY and their fate was followed over a course of 18 h by live-cell imaging using a laser scanning confocal microscope.

Nuclei were identified based on positive nuclear marker staining, and were segmented using a machine learning-based algorithm (Figure 5 A). The recognition of nuclei enabled the automatic tracking of individual cells with the help of the CellProfiler software and the measurement of different cellular parameters in the nuclei and cytoplasm of each cell. Therefore, it was possible to measure the caspase-3/7 signal in individual cells at different time points.

To separate the surviving and dying cell populations, tracked cells of four representative test data sets were manually assigned to their respective population based on cell morphology, cell movement, cell detachment, SiR-DNA signal and caspase-3/7 activation at each measured time point until 18 h.

Next, the maximum caspase-3/7 activation level of surviving cells was determined for each experiment, and subsequently, the mean maximum caspase-3/7 activation in surviving cells was calculated from these four representative experiments (43.30 ± 2.73; Figure 5 B). From then on, this caspase-3/7 activation threshold value of 43.3 was used to automatically assign cells to either the surviving or dying population. Figure 5 C exemplifies the separation of both cell populations in a representative experiment using this thresholding strategy.

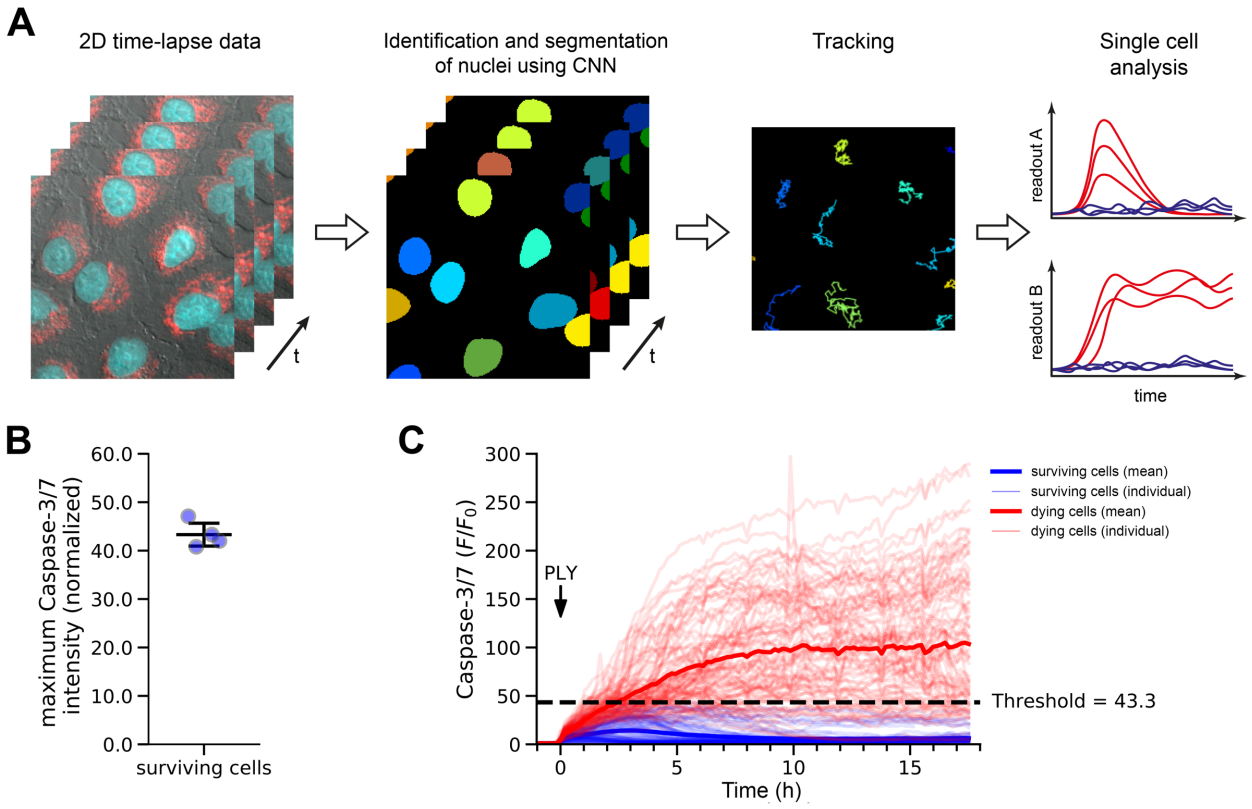

Figure 5. Machine learning-based analysis pipeline and caspase-3/7 threshold determination. (**A**) Data sets were acquired by confocal live-cell microscopy. Individual cells were identified and segmented using the convolutional neural network (CNN) StarDist. Illustration of how cells were segmented and tracked, and how signals in the nucleus and cytoplasm of individual cells were quantified. (**B**) A549 cells were stimulated with 0.1 µg/ml PLY for up to 18 h, and all surviving cells were manually identified based on caspase-3/7 activation signal, SiR-DNA signal and cell movement. Subsequently, the maximal signal of the caspase-3/7 activation in surviving cells was determined for each experiment (mean ± SD from n = 4 independent experiments). (**C**) Illustration of the separation of both cell populations in a representative experiment using the caspase-3/7 activation threshold determined in (B). Traces from individual cells are shown as thin lines and the threshold value is indicated by the bold dashed line (blue: surviving cells, red: dying cells). Figure reproduced in entirety from supplementary figure 2 from original publication [141].

After separation into a surviving and dying population, the nuclear caspase-3/7 activation in each individual A549 cell was determined before and after stimulation with 0.1 µg/ml PLY over a period of 18 h. As already illustrated in Figure 4 A and B, an increase of caspase-3/7 signal (1 h - 5 h) after stimulation could be observed in both surviving and dying cells (Figure 6). However, while the nuclear caspase-3/7 activity increased constantly in the dying cells, it stayed below the threshold in the surviving population and declined over the course of the experiment. No increase of caspase-3/7 activation was detectable in unstimulated control cells.

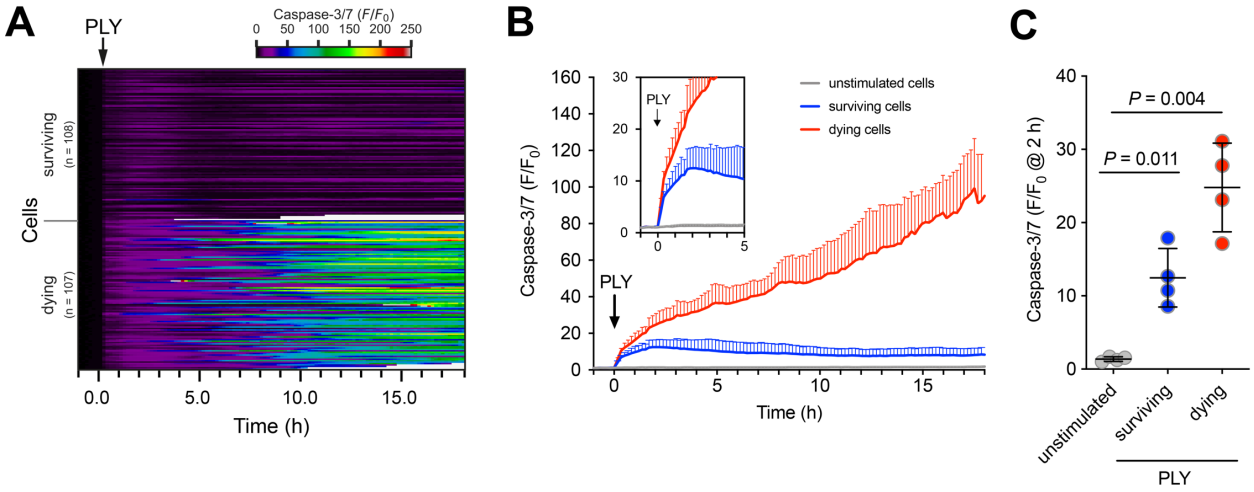

Figure 6. Survival of PLY-treated A549 cells after caspase-3/7 activation. A549 cells were stimulated with 0.1 µg/ml PLY and caspase-3/7 activation was imaged by confocal live-cell microscopy for up to 18 h after stimulation. (**A**) Normalized intensity of caspase-3/7 activation of individually tracked cells (n = 215) stimulated with PLY from one representative experiment are displayed as heatmap. Cells were separated based on caspase-3/7 activation threshold (Figure 5) into surviving and dying populations. White traces indicate cells that moved out of the field of view (surviving cells), or cells that underwent cell death, detached from the cell layer and moved out of focus (dying cells). (**B**) Quantification of normalized intensity of caspase-3/7 activation in the surviving and dying cell population and unstimulated control cells (mean ± SD from n = 4 independent experiments). The inset shows a zoom-in on the first five hours after stimulation. (**C**) Normalized caspase-3/7 activation in unstimulated control cells and surviving/dying cells two hours after medium exchange/stimulation with PLY (mean ± SD from n = 4 independent experiments, Welch ANOVA). Figure adapted from figure 1 from original publication [141].

3.3 Pan-caspase inhibition increases A549 cell survival after pneumolysin stimulation

Since the activation of caspase-3/7 seems to be involved in the PLY-induced cell death of A549 cells, it was hypothesized that inhibition of PLY-mediated caspase activation leads to increased cell survival. To test this hypothesis, A549 cells were stimulated with 0.1 µg/ml PLY in the presence or absence of the pan-caspase inhibitor ZVAD.

In the presence of 10.7 µM ZVAD, the sum signal of caspase-3/7 activation in A549 cells following PLY stimulation was reduced compared with control cells which had solely been treated with DMSO (Figure 7 A). Nevertheless, the reduction of caspase-3/7 activation was not complete in ZVAD-treated cells following PLY stimulation. Unstimulated A549 cells showed no caspase-3/7 activation.

The measurements on a single cell level confirmed the reduction of caspase-3/7-activation in ZVAD-treated cells following PLY stimulation (Figure 7 B). The separation of cells into a surviving and dying population, using the above-mentioned caspase-3/7 activation threshold of 43.3, revealed that after stimulation with 0.1 µg/ml PLY, more A549 cells survived that had been treated with ZVAD compared with cells that had only been treated with DMSO.

Treatment with ZVAD led to a 1.5-fold increase of surviving cells after PLY stimulation compared with DMSO-treated cells (Figure 7 C). After PLY stimulation and under ZVAD-treatment, 87.41 ± 8.73% of tracked A549 cells survived, while under DMSO-treatment only 52.65 ± 10.42% cells survived. Unstimulated cells showed no decrease of surviving cells.

These results show that pan-inhibition of caspases leads to an increased number of surviving A549 cells after stimulation with 0.1 µg/ml PLY. Furthermore, these results underline the implication of caspase-3/7 activation in cell death processes following PLY stimulation.

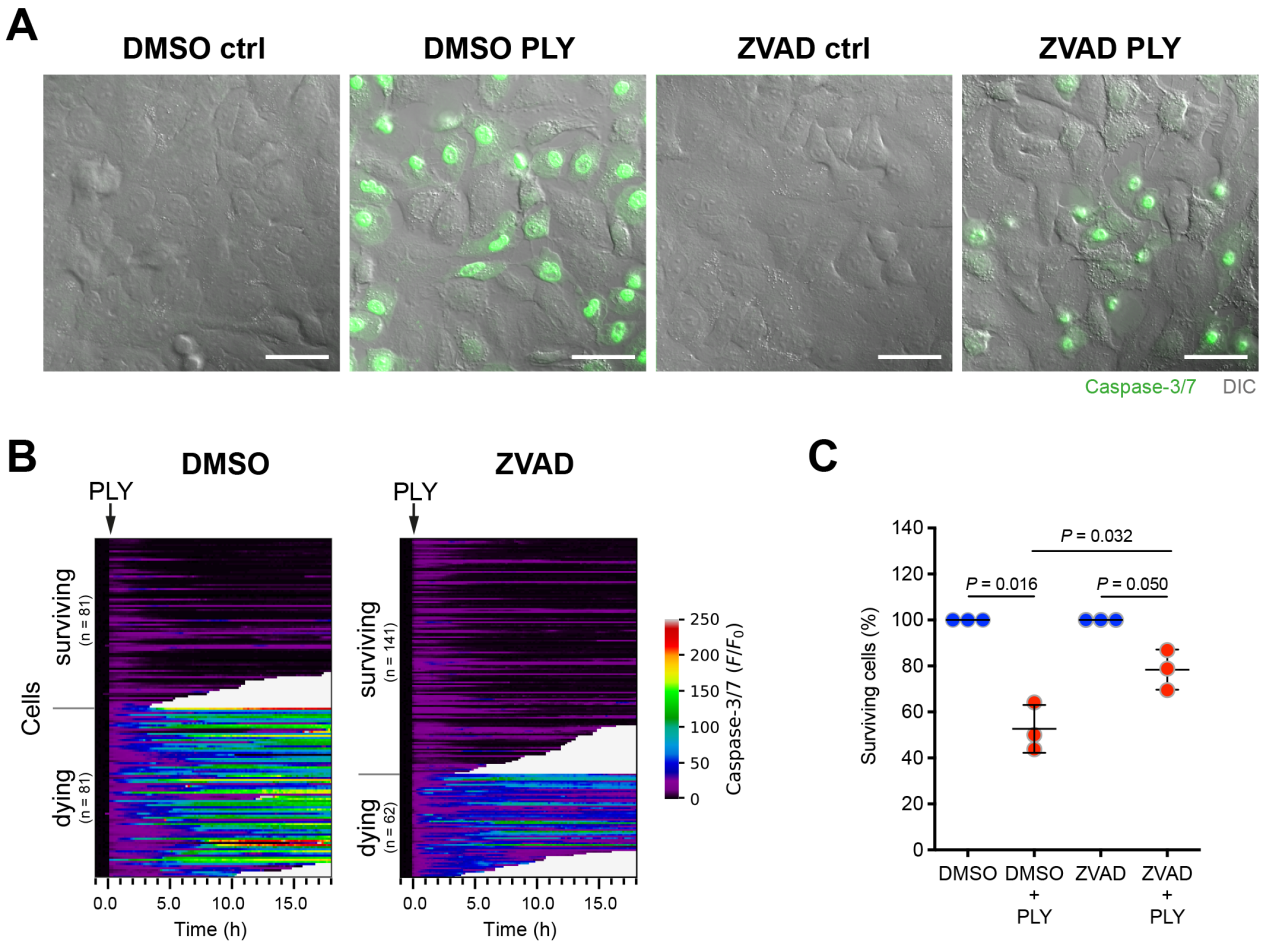

Figure 7. Pan-caspase inhibition increases number of surviving cells after PLY stimulation. A549 cells were preincubated with DMSO or 10.7 µM pan-caspase inhibitor ZVAD. Subsequently, cells were stimulated with 0.1 µg/ml PLY in presence of DMSO or ZVAD and caspase-3/7 activation was imaged by confocal live-cell microscopy. (**A**) Representative end point images of A549 cells visualizing cellular morphology by differential interference contrast (DIC, grey) and caspase-3/7 activation (green) 18 h after stimulation. Scale bars represent 40 µm. (**B**) Normalized intensities of caspase-3/7 activation of individually tracked cells (DMSO: n = 162, ZVAD: n = 203) stimulated with PLY from one representative experiment are displayed as heatmap. Cells were separated based on caspase-3/7 activation threshold (Figure 5) into surviving and dying populations. White traces indicate cells that moved out of the field of view (surviving cells), or cells that underwent cell death, detached from the cell layer and moved out of focus (dying cells). (**C**) Quantification of surviving/dying cells detected during the 18 h time course, expressed as surviving fraction (mean ± SD from n = 3 independent experiments, Welch ANOVA). Figure adapted from figure 2 from original publication [141].

3.4 Reversal of actin polymerization in surviving cells after pneumolysin stimulation

Actin cytoskeletal changes in alveolar epithelial cells can result in disruption of cell layers which can lead to epithelial barrier dysfunction [55, 65].

The first experiments showed that cell bodies of dying A549 cells retracted, leading to gap formation, while surviving cells recovered, regaining their pre-exposure cell morphology. To better visualize these morphological alterations, cytoskeletal changes were analysed in surviving and dying cells by the visualization of actin polymerization using SiR-actin dye. SiR-actin dye emits fluorescence upon binding to filamentous actin. Since the emission wavelengths of SiR-actin and SiR-DNA overlap, it was not possible to stain the nuclei in these experiments and automatically track cells over time. A manual approach was chosen to separate A549 cells into a surviving and dying fraction. Cells were separated manually - based on cell morphology, cell movement and cell detachment.

Figure 8 A and B show caspase-3/7 activation and changes of the actin cytoskeleton of A549 cells exposed to 0.1 µg/ml PLY. In line with the previous experiments, around 1 h after PLY stimulation surviving and dying cells showed an increase of caspase-3/7 activation, which disappeared in the surviving fraction while increasing in the dying fraction (Figure 8 A-C). The actin polymerization signal dropped slightly in all cells after stimulation with 0.1 µg/ml PLY (Figure 8 A and D). This was also observed in control experiments when medium was exchanged (data not shown).

Starting around 1 h after PLY stimulation, surviving and dying cells showed a slight increase of actin polymerization (Figure 8 B and D). The actin polymerization signal kept increasing in dying cells until the end of the experiment (Figure 8 A-C). Dying cells retracted, leading to gap formation (Figure 7 B - star). The drop down of actin polymerization signal and caspase-3/7 signal in dying cells at later time points is due to cell detachment of dying cells which floated out of focus (data not shown).

Figure 8 B shows a representative surviving cell. Just like the dying cells, it showed increased actin polymerization after PLY stimulation. Surviving cells showed a significant increase of actin polymerization, though it was not as pronounced as in dying cells (Figure 8 D and E). At around 5.40 h the representative surviving cell displayed morphological alterations such as cell retraction (Figure 8 B – arrow), but it recovered from this over

time. At 18.06 h cell shrinkage and actin polymerization was completely reversed in surviving cells (Figure 8 B and D).

These results show how even low concentrations of PLY (0.1 µg/ml) can lead to cell shrinkage and consequently gap formation in cell layers of alveolar epithelial A549 cells. Furthermore, it was visualized how surviving cells recover from actin polymerization and cell shrinkage, indicating that surviving cells might be able to restore cell-cell contacts and rebuild alveolar epithelial cell layers.

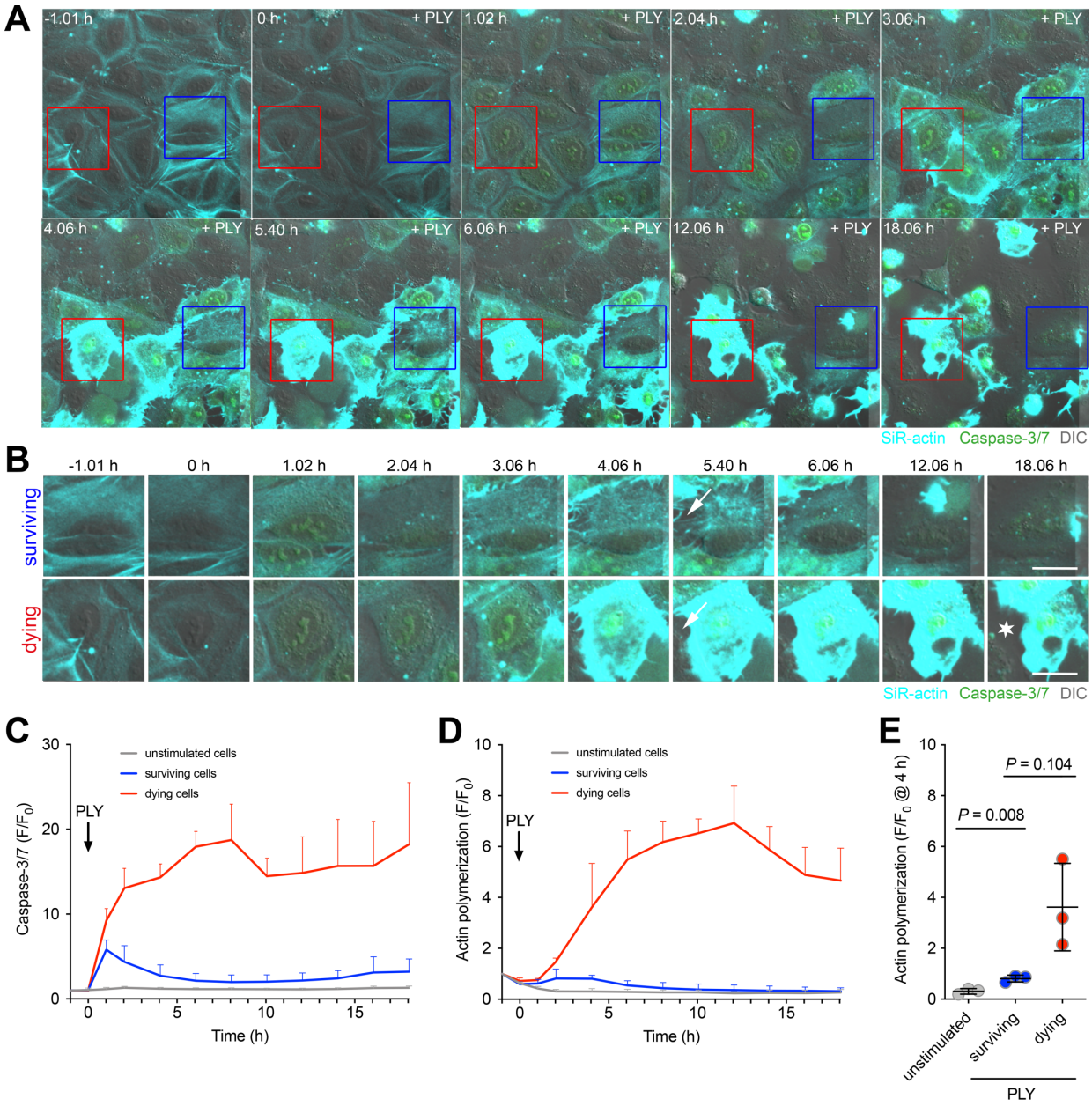

Figure 8. Reversal of actin polymerization in surviving cells after PYL stimulation. A549 cells were stimulated with 0.1 µg/ml PLY and caspase-3/7 activation and changes of actin cytoskeleton were imaged by confocal live-cell microscopy for up to 18 h after stimulation. (**A**) Representative time-lapse images of A549 cells visualizing cellular morphology (DIC, grey), caspase-3/7 activation (green) and actin polymerization (cyan). The blue box indicates a cell that recovered, while the red box indicates a representative dying cell. Scale bar represents 30 µm. (**B**) Enlarged images of the representative surviving and dying cells shown in (A). Cell shrinkage (arrow) leading to gap formation (star) can be observed. Scale bars represent 15 µm. (**C**) Quantification of normalized intensity of caspase-3/7 activation in the surviving and dying cell population and unstimulated control cells (mean ± SD from n = 3 independent experiments). (**D**) Quantification of normalized intensity of actin polymerization in the surviving and dying cell population and unstimulated control cells (mean ± SD from n = 3 independent experiments). (**E**) Normalized actin polymerization signal in unstimulated control cells and surviving/dying cells four hours after medium exchange/stimulation with PLY (mean ± SD from n = 3 independent experiments, Welch ANOVA).

3.5 Survival of primary human alveolar epithelial type II cells after pneumolysin stimulation

A549 cells are an immortalized tumour cell line from the alveolar environment. To further validate the findings presented so far, primary human alveolar epithelial type II cells (phAEC II) were isolated from fresh and living human lung tissue.

Stimulation with 0.1 µg/ml PLY did not lead to caspase-3/7 activation in these primary cells (data not shown), therefore a higher concentration was applied. Hence, phAEC II were stimulated with 0.2 µg/ml PLY and their fate was tracked over time, together with caspase-3/7 activation (Figure 9). For these experiments, nuclei were not labelled. A manual approach was therefore chosen. Cells were separated manually, based on cell morphology, cell movement, cell detachment and caspase-3/7 activation.

Similarly to A549 cells, a subpopulation of cells was able to recover after activation of executioner caspases-3/7. Dying cells showed a higher caspase-3/7 activation. Furthermore, they detached from the monolayer and moved out of focus which impeded further tracking of dead cells.

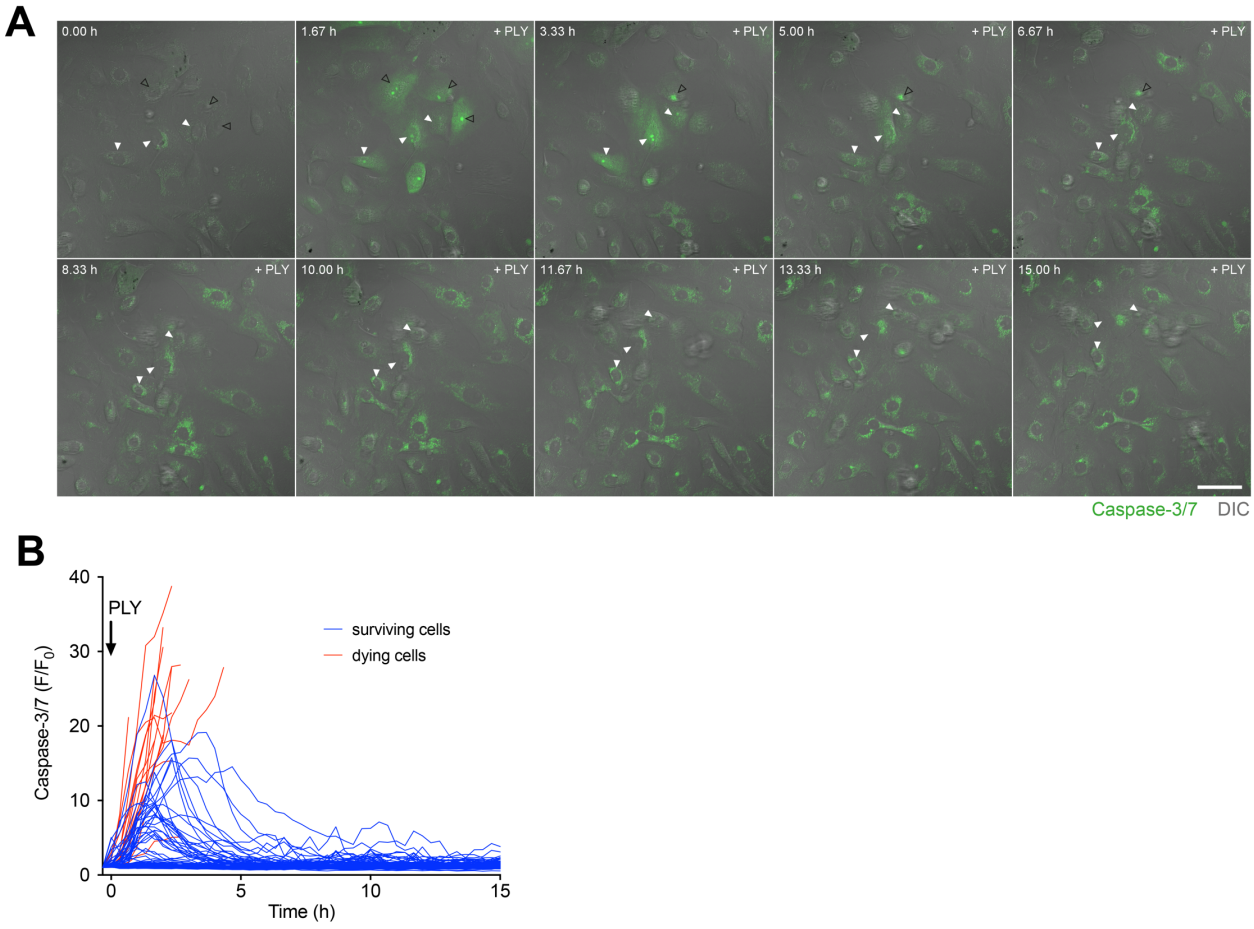

Figure 9. Survival of PLY-treated primary human alveolar epithelial type II cells (phAEC II) after caspase-3/7 activation. phAEC II were stimulated with 0.2 µg/ml PLY and caspase-3/7 activation was imaged by confocal live-cell microscopy for 15 h after stimulation. (**A**) Representative time-lapse images of phAEC II. Cells are visualized by differential interference contrast (DIC, grey) and cell fate was investigated by caspase-3/7 activation (green). Black open arrowheads indicate dying cells with strong caspase-3/7 activation, white arrowheads indicate recovering cells. Scale bar represents 50 µm. (**B**) Normalized intensities of caspase-3/7 activation of manually tracked individual cells (n = 102) stimulated with PLY from one exemplary experiment are displayed (blue: surviving cells, red: dying cells). For the dying cells, maxima of caspase-3/7 activation values are shown before they underwent cell death, detached from the cell layer and moved out of focus. Figure adapted from supplementary figure 3 from original publication [141].

3.6 Reversal of mitochondrial fragmentation in surviving cells after pneumolysin stimulation

It had been demonstrated in another study by Nerlich *et al.* that PLY stimulation in A549 cells leads to significant mitochondrial dysfunctions [97]. Among others, strong mitochondrial fragmentation was detected after stimulation with 1.0 µg/ml of PLY (Figure 10**,** for illustration, published in [97]).

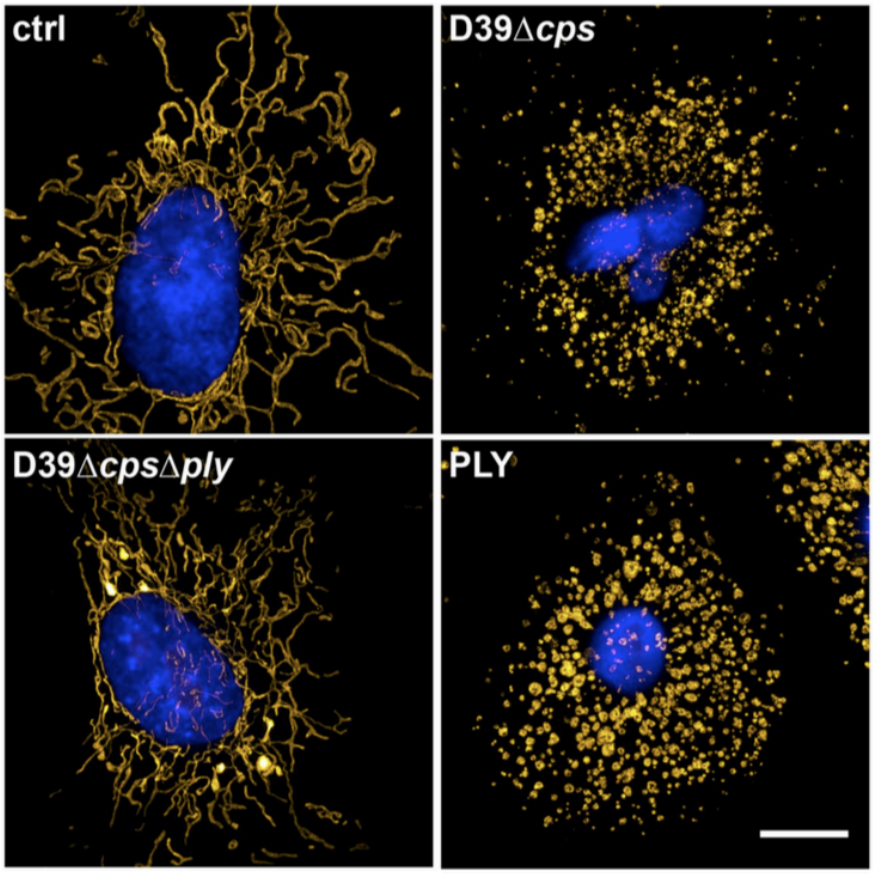

Figure 10. **PLY induces mitochondrial fragmentation in A549 cells.** A549 cells were labelled with MitoTracker Orange and subsequently infected with either PLY-producing *Streptococcus pneumoniae* (*S.pn.*) D39Δ*cps* or PLY-deficient *S.pn.* D39Δ*cps*Δ*ply* for 5 h, stimulated with 1.0 µg/ml PLY for 15 min or left untreated (ctrl). Cells were fixed, stained with 6-diamidin-2-phenylindol (DAPI) and mitochondrial morphology was analysed by structured illumination microscopy. Mitochondria were pseudocoloured using YellowHot LUT and a reconstructed widefield image of the nucleus is shown in blue. Scale bar represents 5 µm. **This figure is from [97].**

The previous results showed that a significant number of A549 cells were able to recover from caspase-3/7 activation and survive after stimulation with 0.1 µg/ml PLY. Since the study by Nerlich *et al.* showed how strongly mitochondria are affected when exposed to PLY, mitochondrial affection was hypothesized as crucial for cellular survival after PLY challenge.
To further analyse the role of mitochondria in this setting, mitochondria of A549 cells were labelled with MitoTracker Orange and stimulated with 0.1 µg/ml PLY. Before and after PLY stimulation, caspase-3/7 activation and A549 survival was monitored and mitochondrial morphology of surviving and dying cells was compared.

Before stimulation, A549 cells exhibited interconnected and elongated mitochondria. Stimulation with 0.1 µg/ml PLY caused caspase-3/7 activation and fragmentation of the mitochondrial network after 1 h in A549 cells (Figure 11).
Around 6 h after stimulation, cells that were able to clear the caspase-3/7 activation (Figure 11 A) also showed a reversed mitochondrial network from fragmentation to elongation (Figure 11 B). On the other hand, in dying cells mitochondria further fragmented and displayed small, round and more numerous organelles (Figure 11 C).
These results indicate that mitochondria, at least as provable by this imaging method, were able to recover from PLY-induced mitochondrial fragmentation.

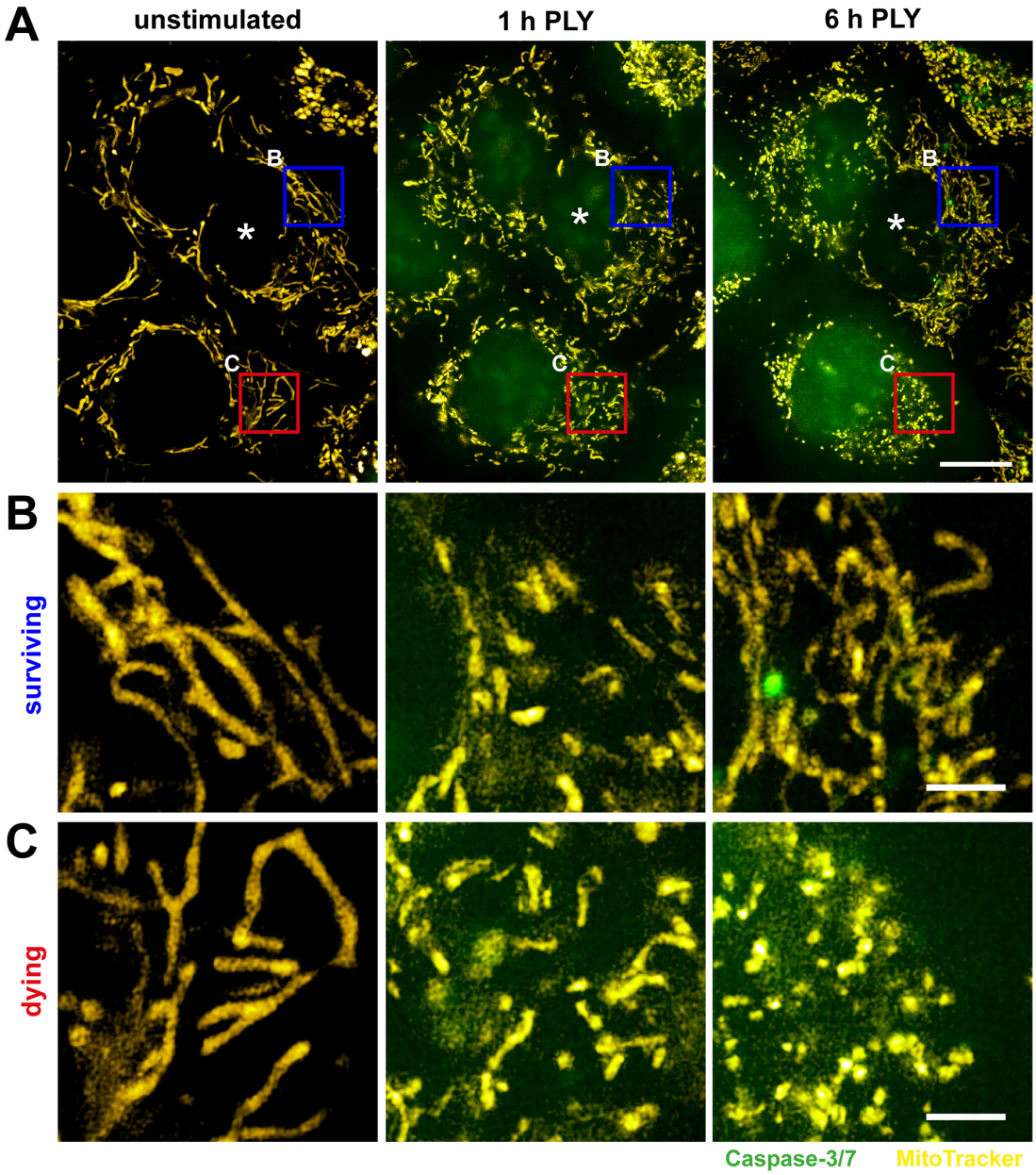

Figure 11. Reversal of mitochondrial fragmentation in surviving cells after PLY stimulation. (**A**) A549 cells labelled with MitoTracker Orange and subsequently stimulated with 0.1 µg/ml PLY in the presence of the caspase-3/7 sensor. Changes of mitochondrial morphology in living cells were analysed by live-cell structured illumination microscopy. Mitochondria are pseudocoloured using YellowHot look-up table and a widefield image of caspase-3/7 activation is shown in green. Asterisks indicate a surviving cell. Representative images taken from three independent experiments are shown. Scale bar represents 10 µm. (**B**) Enlargement of the region indicated by the blue rectangle in (A), illustrating reversal from mitochondrial fragmentation in a surviving cell. (**C**) Enlargement of the region indicated by the red rectangle in (A), illustrating complete mitochondrial fragmentation in a dying cell. Scale bars in (**B**) and (**C**) represent 2 µm. Figure adapted from figure 3 from original publication [141].

3.7 Recovery of mitochondrial membrane potential in surviving cells after pneumolysin stimulation

It can be hypothesized that such severe mitochondrial morphological alterations as described above must be accompanied by significant changes in mitochondrial functionality. Therefore, it was tested whether, and how, surviving and dying cells differed regarding loss of $\Delta\Psi_m$ and depletion of mitochondrial ATP levels. A decrease of $\Delta\Psi_m$ has been observed in response to many apoptotic stimuli, as well as to PLY [69, 97, 142].

To test if differences in $\Delta\Psi_m$ were detectable in the two cell populations, mitochondria were loaded with TMRE. TMRE is a cationic dye that accumulates in mitochondria and diffuses out of them when $\Delta\Psi_m$ decreases. Similarly to the caspase-3/7 activity measurements, changes of $\Delta\Psi_m$ were monitored automatically in individual A549 cells for 18 h after PLY stimulation and furthermore normalized to control.

Immediately after stimulation with 0.1 µg/ml PLY, there was an initial drop of $\Delta\Psi_m$ in A549 cells (Figure 12). Whilst $\Delta\Psi_m$ decreased further in the dying cell population, it recovered partially in the surviving cells (Figure 12 A-C). This finding indicates that mitochondria of surviving A549 cells were able to partially recover their functionality.

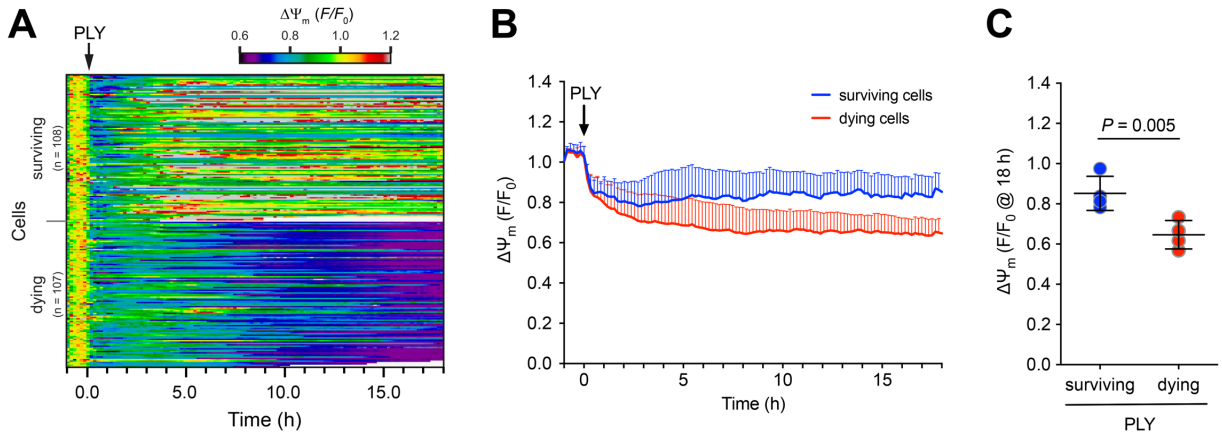

Figure 12. Reversal of loss of mitochondrial membrane potential in surviving cells after PLY stimulation. A549 cells were stimulated with 0.1 µg/ml PLY in the presence of TMRE to analyse mitochondrial membrane potential ($\Delta\Psi_m$) and imaged by confocal live-cell microscopy for up to 18 h after stimulation. (**A**) Normalized $\Delta\Psi_m$ of individual cells (n = 215) stimulated with PLY from one representative experiment are displayed as heatmap. Cells were separated based on caspase-3/7 activation threshold (Figure 5) into surviving and dying cells. White traces indicate cells that moved out of the field of view (surviving cells), or cells that underwent cell death, detached from the cell layer and moved out of focus (dying cells). (**B**) Quantification of normalized $\Delta\Psi_m$ in the surviving and dying cell population (mean ± SD from n = 4 independent experiments). (**C**) Normalized $\Delta\Psi_m$ in the surviving and dying cell population at 18 h after stimulation with PLY (mean ± SD from n = 4 independent experiments, Welch's t-test). Figure adapted from figure 4 from original publication [141].

3.8 Partial recovery of mitochondrial ATP production in surviving cells after pneumolysin stimulation

Since $\Delta\Psi_m$ is the driving force for ATP synthesis in [85], the mitochondrial ATP concentration was also monitored. Cells were transfected with the mitochondrial FRET-based ATP sensor mitoATeam and spectral-FRET analysis was used to assess the effect of 0.1 µg/ml PLY on mitochondrial ATP production.

A region of interest was drawn around the mitochondria of individual cells and the intensities of the YFP and CFP signal were measured. The ATP content is expressed as the normalized ratio of the YFP/CFP peak intensity at 530 nm (YFP) and 478 nm (CFP), respectively. The higher the ATP concentrations are, the lower the CFP signal is, since CFP and YFP are closer to each other and there is more FRET effect. Therefore, the higher the YFP/CFP ratio is, the higher the ATP levels are.

For all mitoATeam-based experiments, the inhibitor of F_0F_1-ATP synthase oligomycin was added to A549 cells as positive control since it induces a decrease of ATP content. Figure 13 B shows how ATP levels drop right after addition of oligomycin.

Cells were separated manually, based on cell morphology, cell movement and cell detachment. Figure 13 A shows the mitochondrial ATP levels of individual surviving and dying A549 cells over a time period of 18 h, from three different experiments. Both cell populations revealed an initial drop of mitochondrial ATP levels after stimulation with 0.1 µg/ml PLY. The recovery of mitochondrial ATP levels after PLY challenge was heterogenous in both cell populations.

Some dying cells showed an increase of mitochondrial ATP levels after the initial drop down. However, starting at around 1.5 h, mitochondrial ATP levels could no longer be measured in cells from this population, as the cells were dead (Figure 13 A and B).

Conversely, mitochondrial ATP levels could be measured in surviving cells until the end of the experiment. Most of the surviving cells recovered to their pre-toxin exposure ATP levels, but not all of them (Figure 13 A and B). These findings correlate with the partial recovery of $\Delta\Psi_m$ after stimulation with 0.1 µg/ml PLY, since $\Delta\Psi_m$ is the driving force for mitochondrial ATP production.

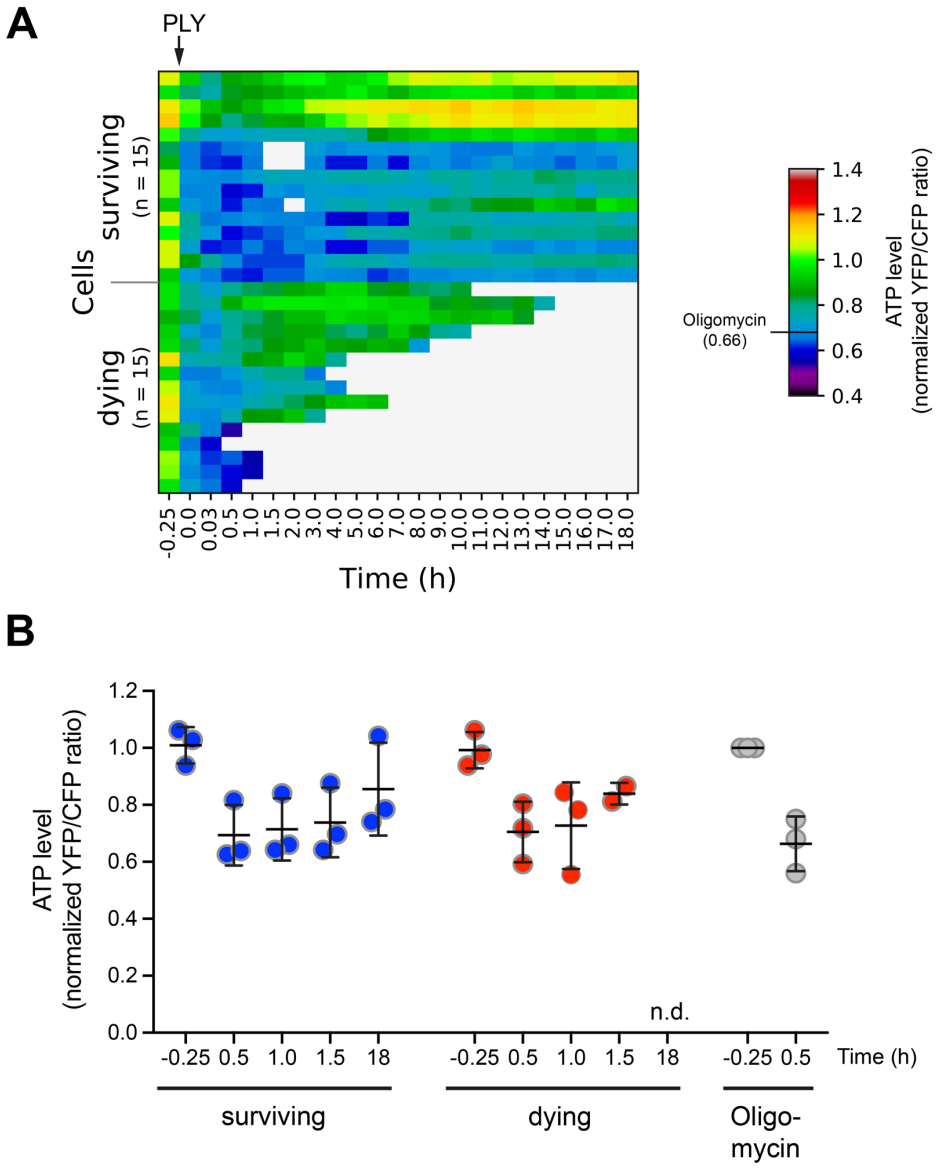

Figure 13. Partial recovery of mitochondrial ATP production in surviving cells after PLY stimulation. A549 cells were transfected with a plasmid encoding a FRET-ATP sensor targeted to mitochondria. 48 hours post transfection, cells were left unstimulated or stimulated with 0.1 µg/ml PLY in medium. Cells stimulated with 10 µg/ml oligomycin for 30 min served as positive control. The ATP content is expressed as normalized ratio of the YFP/CFP peak intensity at 530 nm (YFP) and 478 nm (CFP), respectively. (**A**) Normalized ATP levels of five individual cells stimulated with PLY from three independent experiments are displayed as heatmap. Cells were separated manually into dying and surviving cells. White traces indicate cells that were temporarily out of focus (surviving cells), or cells that underwent cell death, detached from the cell layer and moved out of focus (dying cells). The mean value obtained in cells treated with oligomycin is indicated in the colour bar. (**B**) Quantification of normalized ATP levels in the surviving and dying cell population and oligomycin treated cells at the indicated time points (mean ± SD from n = 3 independent experiments, n.d. = not detectable). Figure reproduced in entirety from supplementary figure 4 from original publication [141].

3.9 Mitochondrial calcium levels correlate with surviving and dying cell populations after pneumolysin stimulation

PLY related pore formation is known to increase cytosolic Ca^{2+}, which leads to a strong Ca^{2+} influx into mitochondria [97, 131]. It is well established that mitochondrial Ca^{2+} ($[Ca^{2+}]_m$) overload plays a crucial role in the initiation of different forms of cell death [107, 112]. To understand if and how $[Ca^{2+}]_m$ changes might be decisive for the survival of alveolar cells, $[Ca^{2+}]_m$ changes were analysed in A549 cells after stimulation with 0.1 µg/ml PLY. Unstimulated cells served as baseline control.

After PLY stimulation, an immediate increase of $[Ca^{2+}]_m$ was observed in almost all cells. In some cells $[Ca^{2+}]_m$ levels declined slowly (Figure 14, black arrowheads), while this occurred significantly faster in other cells (Figure 14, white arrowheads). Interestingly, this latter fraction belonged to the surviving population of cells, which was determined by evaluation of morphology and caspase-3/7 activation.

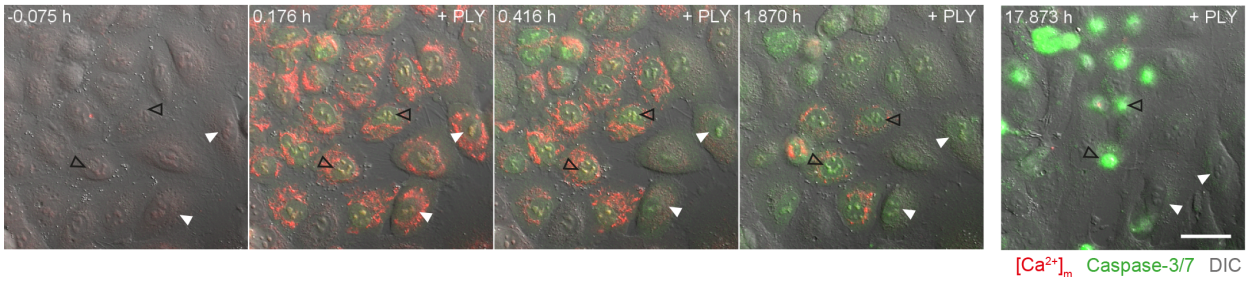

Figure 14. Mitochondrial calcium increase and decrease in surviving and dying cells after PLY stimulation. A549 cells were loaded with mitochondrial Ca^{2+} ($[Ca^{2+}]_m$) indicator Rhod-2-AM and stimulated with 0.1 µg/ml PLY in the presence of caspase-3/7 activation sensor. Representative time-lapse images of A549 cells visualizing cellular morphology by differential interference contrast (DIC, grey), $[Ca^{2+}]_m$ (red) and caspase-3/7 activation (green) at the beginning (-0.075 h – 1.870 h) and shortly before the ending (17.873 h) of the experiment. White arrowheads indicate representative surviving cells, black open arrowheads indicate representative cells that die. Scale bar represents 30 µm. Figure adapted from figure 5 from original publication [141].

Next, individual cells were tracked based on nuclear labelling, and separated into a surviving and dying fraction based on the established caspase-3/7 activation threshold. This enabled the quantification of the observed $[Ca^{2+}]_m$ differences in both populations (Figure 15 A - E).

The analysis of the integrated $[Ca^{2+}]_m$ signal (area under curve (AUC) analysis) indicated a slightly decreased integrated $[Ca^{2+}]_m$ signal response in the surviving population (Figure 15 B). The quantification of $[Ca^{2+}]_m$ showed that surviving cells displayed a lower $[Ca^{2+}]_m$ influx peak at the beginning (Figure 15 C) and had a slightly lower $[Ca^{2+}]_m$ influx amplitude (Figure 15 D). Notably, surviving cells had a ~1.58-fold increased $[Ca^{2+}]_m$ efflux rate (Figure 15 E). Thus, surviving A549 cells cleared Ca^{2+} faster out of their mitochondria.

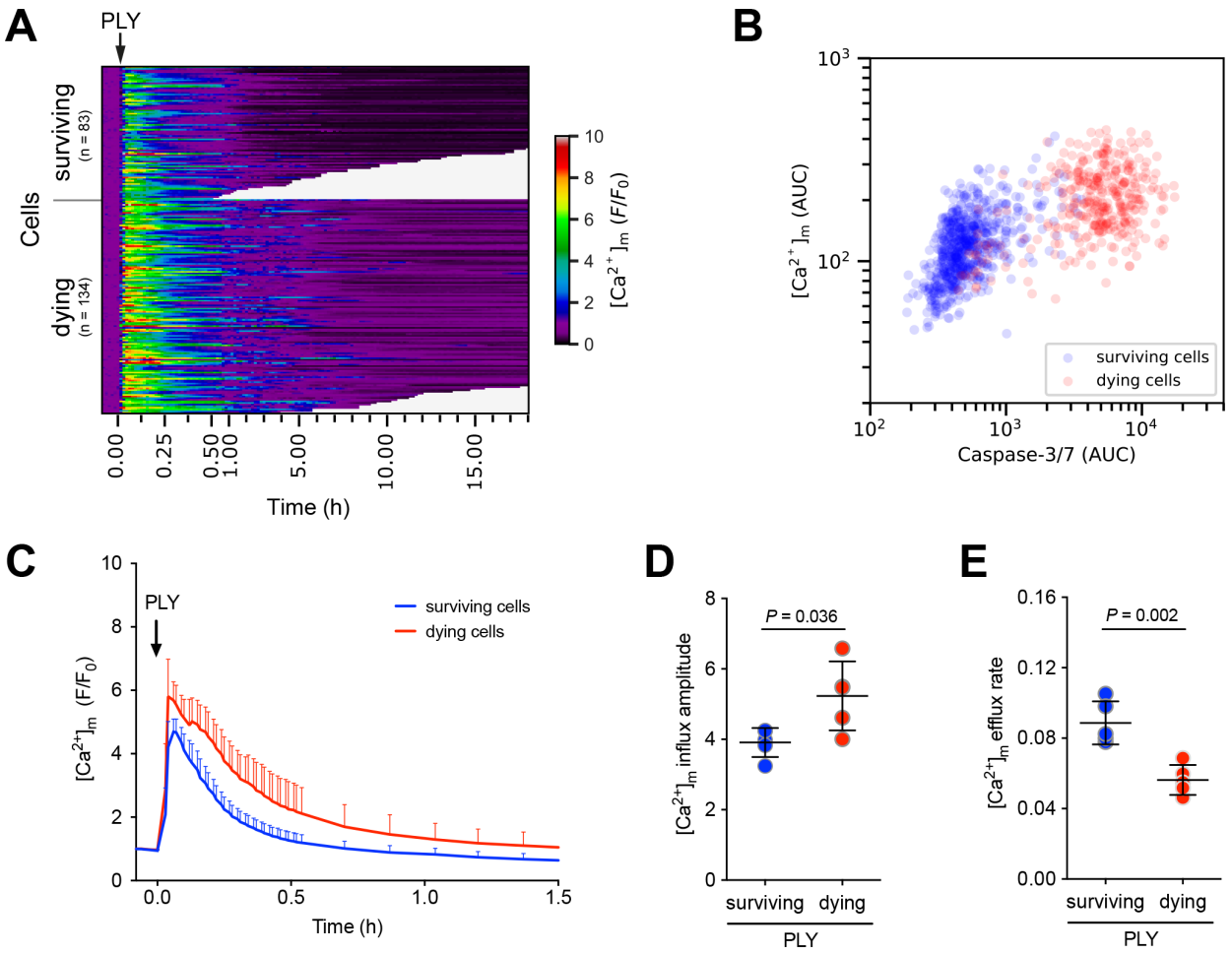

Figure 15. Mitochondrial calcium level correlates with surviving and dying cell populations after PLY stimulation. A549 cells were loaded with mitochondrial Ca^{2+} ($[Ca^{2+}]_m$) indicator Rhod-2-AM and stimulated with 0.1 µg/ml PLY in the presence of caspase-3/7 activation sensor. (**A**) Normalized intensity of $[Ca^{2+}]_m$ of individual cells (n = 217) stimulated with PLY from one representative experiment are displayed as heatmap. Cells were separated based on caspase-3/7 activation threshold (Figure 5) into surviving and dying populations. White traces indicate cells that moved out of the field of view (surviving cells), or cells that underwent cell death, detached from the cell layer and moved out of focus (dying cells). (**B**) 2D scatter plot showing area under curve (AUC) values for $[Ca^{2+}]_m$ and caspase-3/7 activation for the surviving and dying population. Data are pooled from 5 independent experiments. (**C**) Quantification of normalized intensity for $[Ca^{2+}]_m$ in the surviving and dying cell population within 1.5 h after stimulation (mean ± SD from n = 5 independent experiments). (**D** and **E**) Determination of $[Ca^{2+}]_m$ influx amplitude (D) and $[Ca^{2+}]_m$ efflux rates (E) of the data shown in (C). Data represent mean ± SD from n = 5 independent experiments; Welch's t-test. Figure adapted from figure 5 from original publication [141].

3.10 Inhibition of mitochondrial calcium efflux reduces the number of surviving cells after pneumolysin stimulation

The previous results indicated that the $[Ca^{2+}]_m$ efflux capacity might be decisive for survival of A549 cells stimulated with 0.1 µg/ml PLY. If $[Ca^{2+}]_m$ efflux is important for survival, its inhibition should result in a decrease of surviving cells. Therefore, by pharmacological treatment of the mitochondrial Na^+/Ca^{2+} exchanger NCLX, it was tested, whether or not $[Ca^{2+}]_m$ efflux inhibition would result in a decrease of surviving cells.

Consequently, A549 cells were treated with either DMSO or 10 µM CGP-37157 and stimulated with 0.1 µg/ml PLY. CGP-37157 is an established inhibitor of the Na^+/Ca^{2+} exchanger NCLX [143]. Therefore, NCLX should inhibit the efflux of $[Ca^{2+}]_m$. In order to quantify this, $[Ca^{2+}]_m$ influx peak as well as $[Ca^{2+}]_m$ efflux rate were determined under treatment with CGP-37157 or DMSO, before and after stimulation with 0.1 µg/ml PLY (Figure 16 A and B).

After PLY stimulation, the $[Ca^{2+}]_m$ influx amplitude was not significantly altered under CGP-37157 treatment compared with DMSO-treated cells (Figure 16 B and C). This indicated that CGP-37157 treatment did not influence PLY-induced $[Ca^{2+}]_m$ influx.

Conversely, after stimulation with 0.1 µg/ml PLY, cells treated with CGP-37157 showed a reduction of $[Ca^{2+}]_m$ efflux rate by ~2.30 fold compared with DMSO-treated cells (Figure 16 B and D). This confirmed that CGP-37157 partially inhibits $[Ca^{2+}]_m$ efflux after PLY stimulation.

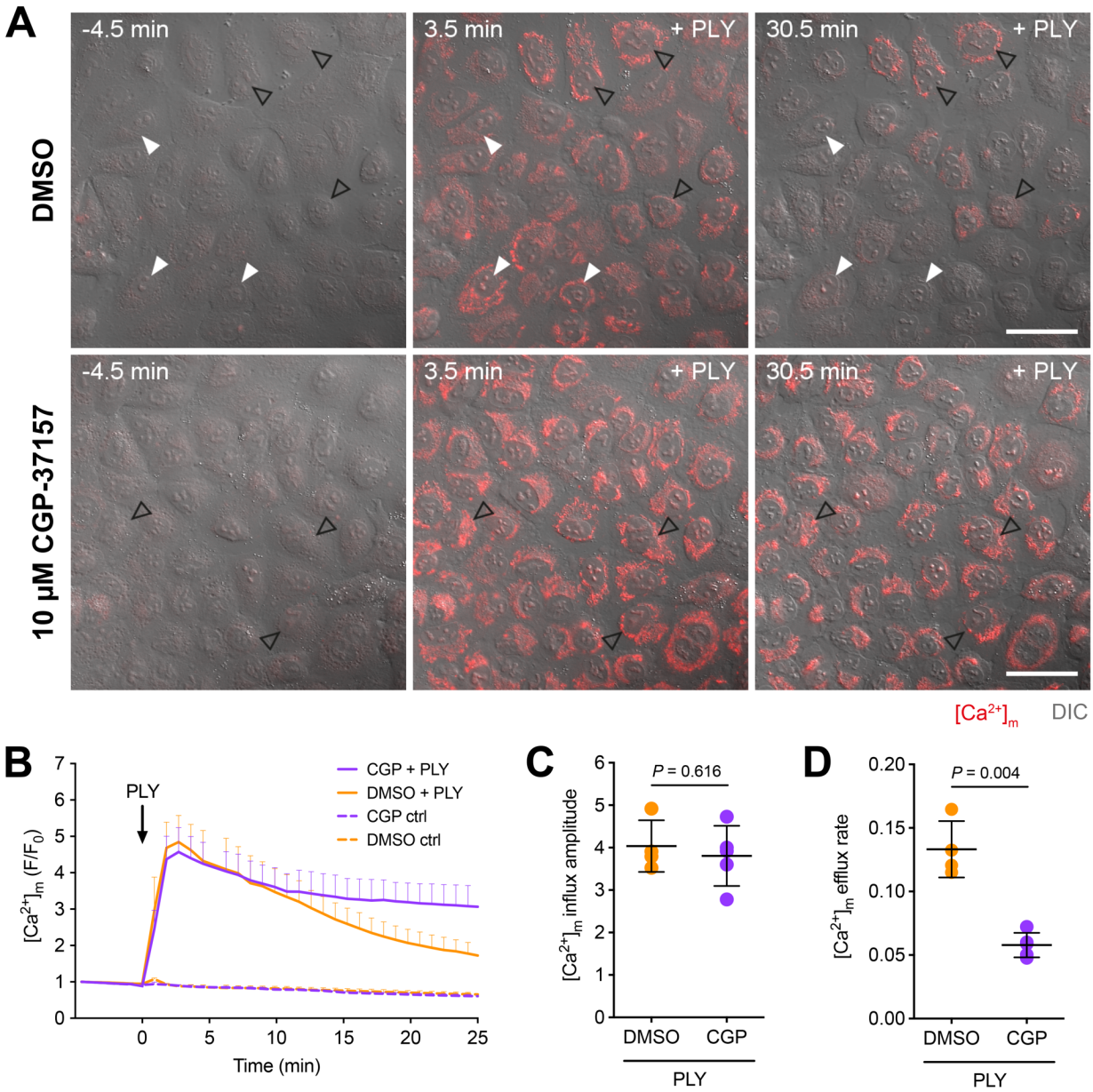

Figure 16. Treatment with CGP-37157 reduces mitochondrial efflux rates after PLY stimulation. A549 cells preincubated with DMSO or 10 µM CGP-37157 and subsequently loaded with Rhod-2-AM were stimulated with 0.1 µg/ml PLY for up to 30 min. (**A**) Representative time-lapse images of $[Ca^{2+}]_m$ responses in DMSO and CGP-37157-treated cells, respectively. Cells are visualized by differential interference contrast (DIC, grey) and $[Ca^{2+}]_m$ is shown in red. White arrowheads indicate exemplary cells with fast decaying $[Ca^{2+}]_m$ and black open arrowheads indicate exemplary cells with slowly decaying $[Ca^{2+}]_m$. Scale bars represent 40 µm. (**B**) Mean $[Ca^{2+}]_m$ changes, normalized to baseline, plotted as function of time (n ≥ 3). (**C** and **D**) Determination of $[Ca^{2+}]_m$ influx amplitude (C) and $[Ca^{2+}]_m$ efflux rates of (D) of the data shown in (B). Data represent mean ± SD from n ≥ 4 independent experiments; Welch's t-test. Figure adapted from figure 6 from original publication [141].

After having established that the $[Ca^{2+}]_m$ efflux rate was decreased under CGP-37157 treatment, the quantification of surviving and dying A549 cells followed.

Treatment with CGP-37157 led to a ~1.75-fold decrease of surviving cells 20 h after stimulation with 0.1 µg/ml PLY compared with DMSO-treated cells (Figure 17 A and B). Under DMSO treatment 61.21 ± 16.13 % of tracked A549 cells survived, while under CGP-37157 treatment only 31.97 ± 18.37 % of cells survived. Unstimulated cells showed no decrease of surviving cells (Figure 17 B).

These results indicate that $[Ca^{2+}]_m$ efflux is decisive for the survival of A549 cells after stimulation with 0.1 µg/ml PLY.

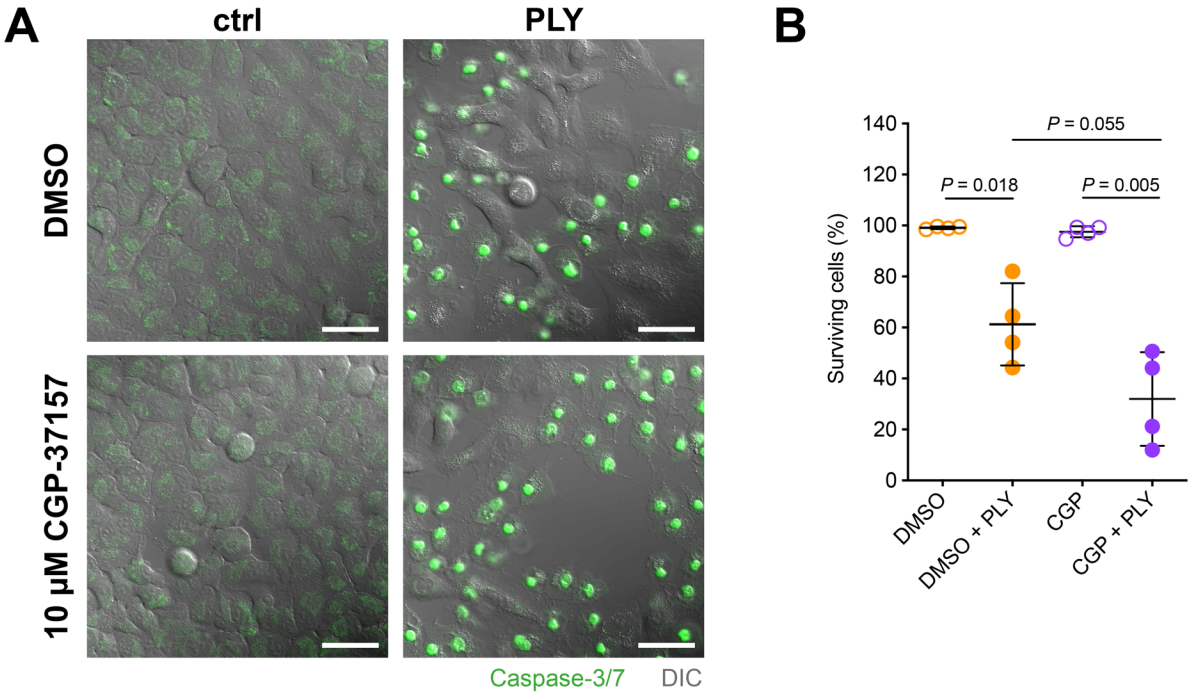

Figure 17. Inhibition of mitochondrial calcium efflux reduces the number of surviving cells after PLY stimulation. A549 cells preincubated with DMSO or 10 µM CGP-37157 and subsequently loaded with Rhod-2-AM were stimulated with 0.1 µg/ml PLY for up to 30 min. (**A**) Representative image data of DMSO- and CGP-37157-treated cells left unstimulated or stimulated with 0.1 µg/ml PLY in the presence of the caspase-3/7 activation sensor for 20 h. Cells are visualized by differential interference contrast (DIC, grey) and caspase-3/7 activation is shown in green. Scale bars represent 40 µm. (**B**) Quantification of surviving/dying cells after 20 h expressed as surviving fraction (mean ± SD from n = 4 independent experiments, Welch ANOVA). Figure adapted from figure 6 from original publication [141].

3.11 Increase of autophagic vesicles in surviving cells

Surviving cells displayed strong mitochondrial alterations such as $\Delta\Psi_m$ and fragmentation which could be reversed. Healthy mitochondrial function is essential for cell survival and removal of damaged mitochondria, e.g. by autophagy, can prevent cell death [144]. Therefore, enhanced autophagy after PLY stimulation might enable the removal of damaged mitochondria and thereby contribute to survival.

The aim was to test for enhanced autophagy after stimulation with 0.1 µg/ml PLY, and whether it correlates with the cellular fate of both subpopulations. Quantification of autophagic vesicles was determined by labelling them with Cyto-ID. Based on a manually defined threshold of caspase-3/7 intensity for each of these experiments, A549 cells were separated into a surviving and dying fraction. Next, Cyto-ID spots were counted automatically in the cytoplasm of each cell.

Unstimulated A549 cells showed no increase of autophagic vesicles after exchange of medium (Figure 18 A and B). Interestingly, after stimulation with 0.1 µg/ml PLY an increase of autophagic vesicles was detectable in both subpopulations (Figure 18 A and B). The increase of autophagic vesicles was significantly higher in surviving cells after PLY stimulation (Figure 18 C). Around 5 h after PLY-stimulation, 13.69 ± 1.55 autophagic vesicles were detectable per surviving cell compared with 7.58 ± 1.75 per dying cell.

In conclusion, these results indicate that both surviving and dying cells augment autophagy after stimulation with 0.1 µg/ml PLY, and that autophagy is more pronounced in surviving cells.

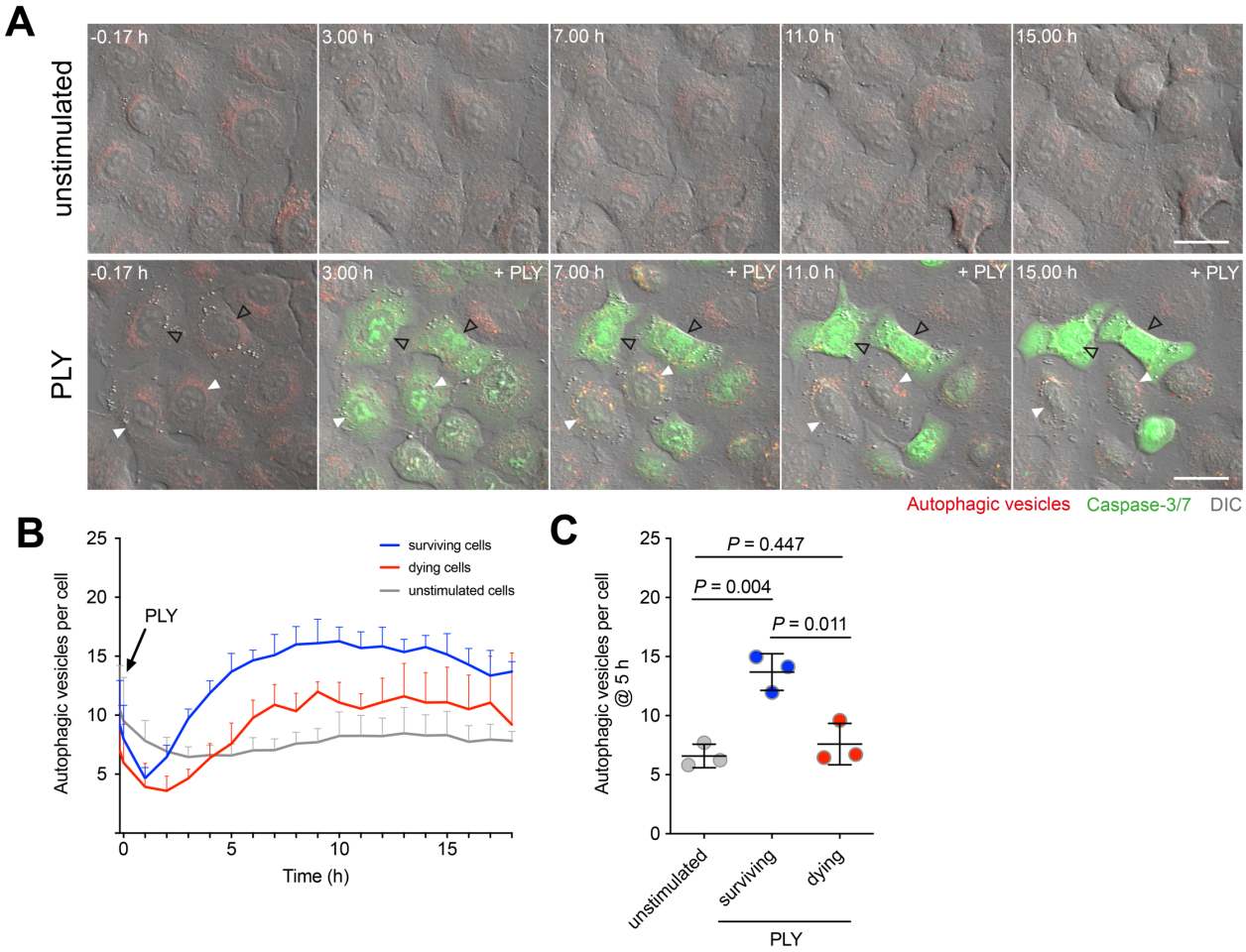

Figure 18. Amount of induced autophagic vesicles correlates with cellular survival and death after PLY treatment. A549 cells were left unstimulated or stimulated with 0.1 µg/ml PLY and caspase-3/7 activation, and accumulation of Cyto-ID-positive autophagic vesicles was imaged by spectral confocal live-cell microscopy for 18 h after stimulation. (**A**) Representative time-lapse images of A549 cells visualizing cellular morphology by differential interference contrast (DIC, grey), activation of caspase-3/7 (green) and autophagic vesicles (red). The upper panel shows unstimulated cells and the lower panel shows PLY-stimulated cells. White arrowheads indicate recovering cells with increased amounts of autophagic vesicles, black open arrowheads indicate dying cells with strong caspase-3/7 activation. Scale bar represents 25 µm. (**B**) Quantification of the number of autophagic vesicles per cell in the surviving and dying cell population and unstimulated control cells (mean ± SD from n = 3 independent experiments). (**C**) Number of autophagic vesicles per cell in unstimulated control cells and surviving/dying cells five hours after medium exchange/stimulation with PLY (mean ± SD from n = 3 independent experiments, Welch ANOVA).

4 Discussion

4.1 Summary of the main results

In this present study, the alveolar epithelial cell line A549 and primary alveolar epithelial type II cells were investigated with regards to cell survival after PLY challenge. A machine-learning based method was established to longitudinally track individual cells and relate individual cellular parameters associated with alveolar epithelial cell survival after PLY challenge *in vitro*.

This study showed that alveolar epithelial cells can recover from activation of executioner caspases-3/7 and survive after challenge with 0.1 µg/ml of the pore-forming toxin PLY *in vitro*. The number of surviving cells after stimulation with PLY increased in the presence of a pan-caspase inhibitor. Surviving cells recovered from cell shrinkage, mitochondrial fragmentation and loss of $\Delta\Psi_m$. Some surviving cells also partially regained their pre-PLY-exposure mitochondrial ATP levels. The in-depth analysis of $[Ca^{2+}]_m$ fluxes on a single cell level revealed the $[Ca^{2+}]_m$ influx amplitude and $[Ca^{2+}]_m$ efflux rate as decisive parameters for survival after PLY challenge. Accordingly, inhibition of $[Ca^{2+}]_m$ efflux resulted in a decrease of surviving A549 cells. Further findings indicated that induction of autophagy might be important for survival of alveolar epithelial cells after PLY challenge. Overall, this study indicates that $[Ca^{2+}]_m$ regulation is critical for the survival of alveolar epithelial cells after PLY-related activation of executioner caspases-3/7.

4.2 Alveolar epithelial cells survive caspase-3/7 activation

Pneumonia is still the 4th most common cause of death worldwide [2]. It is associated with significant morbidity and mortality, and poses a major clinical and economic burden to healthcare systems [5]. The leading cause of CAP is *S.pn.,* which produces the pore forming toxin PLY [1]. In spite of great advances in medicine, around 12.2 % of hospital-treated pneumonia patients still die in Germany [15]. It has been assumed that during severe pneumonia increased endothelial and alveolar permeability lead to deleterious complications such as pulmonary edema formation and sepsis [51]. Several studies indicate that PLY disrupts the alveolar-capillary barrier, and thus favours edema formation and the spread of bacteria into the pulmonary tissue and ultimately into the bloodstream [49, 50, 73]. It may damage the alveolar-capillary barrier, among other things, by inducing cell death of alveolar epithelial cells [145]. A study by Nerlich *et al.* showed that alveolar

epithelial A549 cells undergoing PLY-induced cell death displayed strong activation of executioner caspases-3/7 [97]. In this current study it was shown that A549 cells infected with PLY-producing *S.pn.* showed caspase-3/7 activation, while infection of A549 cells with PLY-deficient mutant *S.pn.* did not result in caspase-3/7 activation. This indicates that caspase-3/7 activation during *S.pn.* infection is indeed PLY-dependent. However, further studies need to determine whether this mechanism can also be observed *in vivo* in humans.

Furthermore, it was uncovered in this study that a subpopulation of A549 cells was able to recover from activation of executioner caspases-3/7 and able to survive after stimulation with 0.1 µg/ml of PLY. It is important to note that the recovery process from caspase-3/7 activation was not only detected in A549 cells but also in freshly isolated phAEC II, since A549 cells may have *eo ipso* modified cell death mechanisms. Again, it should be noted that these studies were performed on isolated cells.

Survival of alveolar epithelial cells after PLY challenge during *S.pn.* infection might be beneficial for improved clinical outcomes, since maintaining the alveolar epithelial cell barrier permits the exchange of oxygen and carbon dioxide along the alveolar-capillary barrier. Furthermore, survival of alveolar epithelial cells after PLY challenge might decrease the risk of lung edema formation, as the alveolar-capillary barrier integrity is maintained [10]. Additionally, survival of alveolar epithelial type II cells especially could be of great advantage after lung injury caused by *S.pn.* pneumonia, since reepithelization of epithelial alveolar barriers occurs mainly by proliferation of alveolar epithelial type II cells which can differentiate into type I cells [51, 52]. Survival of alveolar epithelial type II cells might be additionally beneficial, as alveolar epithelial type II cells produce surfactant which lowers the surface tension in alveoli. Lack of surfactant can lead to alveolar collapse and respiratory failure [52]. In summary, surviving alveolar epithelial cells might help to maintain the integrity of epithelial layers after PLY challenge during *S.pn.* infection, thereby preventing development of lung edema. A study by Witzenrath *et al.* also showed that low PLY concentrations lead to a reversible increase of paracellular permeability in A549 cells [73].

Pan-caspase inhibition by ZVAD led to a reduced number of dying cells, which further underlines that caspases are involved in PLY-induced cell death. However, the ZVAD concentration of 10.7 µM did not lead to a total inhibition of cell death. A study conducted by Stringaris *et al.* with SH-SY5Y human neuronal cells treated with 0.5 µg/ml PLY

and 20 µM ZVAD also showed that pan-caspase inhibition did not fully prevent PLY-induced cell death [68]. In future experiments, A549 cells should be treated with increasing ZVAD concentrations to test whether higher concentrations might inhibit all caspase activity after PLY stimulation.

In vivo, alveolar epithelial type II cells are connected to type I cells and in tight proximity to lung capillary endothelial cells [54]. Furthermore, cells are part of a complex three-dimensional architecture, grow in an organotypic matrix and are continuously exposed to physical forces [146]. Since virtually all of these factors, among other things, influence alveolar epithelial type II cell behaviour [52, 146], it is of outmost importance to verify the results presented here in more complex models to better estimate the occurrence and relevance of cell survival despite caspase-3/7 activation for human *S.pn.* pneumonia. Moreover, alveolar epithelial type I cells cover 95 % of the alveolar surface and are thus of high importance for lung barrier function [54], and it is hitherto unclear, if these type I cells might also react in the same way as observed here for type II cells.

4.3 Possible mechanisms of alveolar epithelial cell survival after pneumolysin stimulation

During the experiments, alveolar epithelial cells exposed to 0.1 µg/ml PLY recovered from activation of executioner caspases-3/7 and strong mitochondrial alterations. The core question arises: how can executioner caspases be activated after PLY stimulation without killing the alveolar epithelial cell?

It is widely accepted that MOMP with consequent loss of $\Delta\Psi m$ leads to activation of executioner caspases, which then results in cell death [109]. MOMP was often considered a point of no return concerning cell death [113]. However, recent studies have shown that MOMP can occur to varying degrees within a single cell [121]. This event has been termed minority MOMP. A study by Ichim *et al.* showed that only few mitochondria are permeabilized during minority MOMP, resulting in small amounts of cytochrome c being released, causing only limited caspase activation. Apoptosis here appears to be triggered, but then stopped before the point of no return and the cell stays alive [121, 128].

In a past study, our group showed that MOMP was not detectable when using lytic concentrations of PLY – neither by cytosolic cytochrome c staining via antibodies or by release of a fluorescent protein targeted in the inner mitochondrial space [97]. It is

tempting to speculate that minimal amounts of cytochrome c are released below the detection limit, leading to induction of minority MOMP. Minority MOMP would then lead to a minimal activation of caspases-3/7. In surviving cells, caspase-3/7 activation was measurable, even though it was not as high as in dying cells. One explanation for the measured increase of caspase-3/7 activation in surviving cells might be explained by the high sensitivity of the caspase-3/7 activity sensor. Similar caspase sensor designs have also been shown to be highly sensitive [147].

Taken together, it could be speculated that A549 cells survive sublytic PLY concentrations because they undergo minority MOMP. In line with this, surviving A549 cells showed lower levels of mitochondrial alterations compared with dying cells. Mitochondrial fragmentation and decrease of $\Delta\Psi m$ was not as pronounced in surviving cells compared with dying cells.

Twig *et al.* showed that mitochondria crossing a threshold towards low $\Delta\Psi m$ are segregated from the functional mitochondrial pool and will subsequently be degraded by autophagic removal of mitochondria [148]. Autophagy selective for mitochondrial elimination is called mitophagy and is associated with mitochondrial fragmentation [148, 149]. Mitochondrial fragmentation may serve to produce smaller mitochondria that can be engulfed by autophagosomes. Furthermore, it might also function to isolate damaged mitochondria from the rest of the network, as mitochondria with lower membrane potential are less fusion competent. On the other hand, only moderately affected mitochondria that do not experience such a strong drop down of $\Delta\Psi m$ may be rescued from mitophagy [148]. Mitochondria that are left intact will subsequently proliferate and repopulate the mitochondrial pool enabling cell survival [121].

Recovery of mitochondrial membrane potential, ATP production and reversal of mitochondrial fragmentation in surviving A549 cells demonstrates that cells that survived PLY challenge were able to rescue mitochondrial integrity and functions. The number of autophagic vesicles in A549 cells treated with PLY was increased in surviving cells compared with dying cells. These differences suggest that autophagy might promote survival of A549 cells after PLY stimulation. However, further experiments are needed to discover the underlying molecular mechanisms and to elucidate whether autophagy (and specifically mitophagy) is a driving force for cell recovery after PLY challenge.

Interestingly, several recent studies have shown that cells are able to recover from caspase-3/7 activation and apoptosis initiation, stay alive and presumably repair any damage caused [129, 130]. This process has been termed anastasis meaning “rising to life” in Greek. The underlying molecular mechanisms are still almost unknown, but the researchers argue that it is an active process during which several genes are upregulated [130]. In this current work, we did not test for upregulation of anastasis typical genes. To determine whether a form of anastasis might also occur during apoptosis of alveolar epithelial cells after PLY challenge, further studies would have to be executed. For example, upregulation and silencing of the transcription factor Snail should be tested in PLY-stimulated cells. Sun *et al.* showed that Snail, which is known to downregulate E-cadherin, was upregulated during anastasis and that silencing Snail prevented cell recovery [130].

An important prerequisite for the elimination of executioner caspase activation during anastasis is that the apoptotic stimulus is temporary [129]. In this context, it is noteworthy that Wolfmeier *et al.* reported that human embryonic kidney cells were able to recover from PLY-induced pore formation. As long as a certain threshold of cytosolic Ca^{2+} influx was not surpassed, cells were able to repair damaged membranes by shedding the affected regions via microvesicles into the extracellular milieu [132].

Whether cells can recover from elevated Ca^{2+} influx due to pore formation by PLY probably depends on the activity of intracellular Ca^{2+} sequestrating mechanisms, as will be discussed below.

4.4 Importance of mitochondrial calcium regulation for survival after pneumolysin challenge

Well-controlled intracellular $[Ca^{2+}]_c$ levels are important for balanced cellular signalling [150]. However, pore formation by PLY floods the cell with high $[Ca^{2+}]_c$ concentrations [131, 132]. Several other bacterial pathogens have been reported to cause strong $[Ca^{2+}]_c$ influx to induce mitochondria-dependent apoptosis and facilitate tissue invasion [151, 152].

Increased $[Ca^{2+}]_c$ levels are first buffered by the endoplasmic reticulum and then by mitochondria [99, 100]. Accordingly, the conducted experiments showed an increase of $[Ca^{2+}]_m$ levels in all A549 cells after PLY stimulation. The fast increase of $[Ca^{2+}]_m$ immediately after PLY stimulation suggests that affected A549 cells try to prevent

excessive Ca^{2+} accumulation in the cytosol and endoplasmic reticulum by transferring Ca^{2+} to mitochondria. Similar effects have been observed in HepG2 cells, primary hippocampal neurones and U2OS cells stimulated with the Ca^{2+} ionophore ionomycin [153, 154]. Excessive $[Ca^{2+}]_m$ load can lead to mitochondrial membrane depolarization, mitochondrial ROS production and initiation of cell death [101, 120]. Therefore, $[Ca^{2+}]_m$ uptake in and release from mitochondria have to be carefully controlled to avoid $[Ca^{2+}]_m$ overload and subsequent cell death. The analysis of $[Ca^{2+}]_m$ load at the single cell level demonstrated that surviving A549 cells showed a significantly higher efflux rate.

Ca^{2+} efflux from mitochondria can occur through NCLX, which pumps Ca^{2+} back into the cytosol, and by the opening of the mPTP. The opening of the mPTP can occur in two different modes: a high conductance state and a low conductance state [155]. The high conductance state leads to an irreversible, complete opening and initiation of cell death mechanisms [107]. Interestingly, studies by Stringaris *et al.* and Marriott *et al.* showed that survival after PLY stimulation was improved when the mPTP was blocked [68, 126]. The low conductance mode is characterized by transient opening of the pore and release of Ca^{2+} from mitochondria [156, 157]. The latter mode could be active in surviving A549 cells.

Our group showed in a recent study that high concentrations of PLY induce a rapid opening of the mPTP. Lower concentrations lead to slow decrease of the mitochondrial calcein signal in the cell populations [97]. These findings might indicate a transient opening of the mPTP. To test whether opening of the mPTP is decisive for cell survival of alveolar epithelial cells, mPTP inhibition by molecules such as bongkrekic acid or cyclosporine A should be tested.

Since $[Ca^{2+}]_m$ efflux seemed to play a crucial role for survival, A549 cells were treated with the NCLX inhibitor CGP-37157 for efflux inhibition. Treatment with the NCLX inhibitor CGP-37157 led to a reduced $[Ca^{2+}]_m$ efflux. Furthermore, inhibitor treatment also significantly reduced the number of surviving A549 cells after PLY stimulation. This underlines the importance of $[Ca^{2+}]_m$ efflux for survival of alveolar epithelial cells. A similar function in cell survival has been shown *in vivo* in a NCLX knockout model, as well as *in vitro* in neuronal cells by upregulation of NCLX [158, 159].

Taken together, survival of alveolar epithelial A549 cells after PLY challenge seems dependent on effective $[Ca^{2+}]_m$ efflux that prevents $[Ca^{2+}]_m$ overload and subsequent cell death.

What are the reasons for some cells being able to cope better with the strong $[Ca^{2+}]_m$ influx than others? First, it could be that even before PLY stimulation some cells have better functioning mitochondria with a higher metabolic activity. Since $[Ca^{2+}]_m$ efflux through NCLX is ATP-dependent they might be able to handle $[Ca^{2+}]_m$ overload better. However, the experiments on mitochondrial ATP production in this work did not show that surviving cells had a higher ATP content before stimulation compared with cells that died over the course of the experiment. Another explanation might be that surviving A549 cells are affected by lower amounts of PLY, leading to reduced formation of PLY pores in their cell membranes. Therefore, the cytosolic and subsequent $[Ca^{2+}]_m$ influx are lower and mitochondrial functions can be maintained. Hence, no cell death mechanisms are activated. In contrast, when more PLY pores are formed $[Ca^{2+}]_c$ and $[Ca^{2+}]_m$ reach higher levels, mitochondrial functions are strongly affected, leading to more widespread MOMP and executioner caspase activation. Past studies have shown that even cells that are next to each other can be affected by different loads of PLY [160, 161]. This mirrors the *in vivo* situation in the lung during pneumonia, where cells are confronted with locally variable amounts of bacteria and toxin during infection.

In line with this, surviving cells showed a lower $[Ca^{2+}]_m$ amplitude than surviving cells. Furthermore, surviving cells experienced less actin polymerization. Dying cells, on the other hand, displayed very prominent actin polymerization, which can be interpreted as a strong stress response. Thus, it can be hypothesized that surviving A549 cells were exposed to lower amounts of PLY. Consequently, their recovery was favoured, which was visualized by reversal of actin polymerization to pre-PLY exposure levels.

To verify this hypothesis, in future experiments PLY pores on surviving cells and dying cells could be quantified by using green fluorescent PLY, or by PLY immunostaining and measuring $[Ca^{2+}]_c$ influx. After that, these two parameters should be correlated with survival or death of alveolar epithelial cells after PLY challenge.

Wolfmeier *et al.* reported that human embryonic kidney cells were able to eliminate PLY pores by microvesicle shedding [132]. In future studies, it would be interesting to compare plasma membrane repair in surviving and dying alveolar epithelial cells in order to test whether surviving cells are able to clear PLY pores faster than dying cells.

4.5 Live-cell microscopy and machine learning-based algorithms for single cell analysis

In this work, live-cell microscopy combined with usage of fluorescent dyes was the only method used to assess different cellular parameters such as caspase-3/7 activation or mitochondrial membrane potential. Therefore, parameters like caspase-3/7 activation should be confirmed in future studies by other assays such as western blot. From an experimental and analytical point of view, however, it has to be considered that by using methods where the result is determined by harvesting all cells at a certain point in time, such findings cannot be obtained. Only time-resolved (microscopic) analysis with the examination of individual cell responses makes the collection of such observations possible.

Therefore, live-cell microscopy offers great advantages. Live study of cells and different cellular parameters over long time periods can bring to light otherwise hidden phenomena, such as the survival of a subpopulation of cells. Furthermore, it allows for the study of cellular parameters over time, instead of measuring selected endpoints. This, together with visualization of individual cells, enables the direct measurement of different biological events in individual cells over time, such as changes of mitochondrial membrane potential. Additionally, these different cellular parameters can be measured at the same time if the emission spectra of the fluorogenic probes do not overlap. For example, in this study this enabled the correlation of caspase-3/7 activation with parameters such as $\Delta\Psi_m$ or $[Ca^{2+}]_m$ fluxes.

Even though live-cell light microscopy is a non-invasive method to study cellular processes in living cells, phototoxicity has to be taken into account - especially when high laser intensities are used for long time periods [162]. Phototoxicity can lead to artefacts, abnormal responses and generation of reactive oxygen species [162, 163]. To prevent phototoxicity, high laser intensities were avoided, and light exposure times kept as short as possible during experiments. During experiments, morphologically visible phototoxicity was excluded by control of the DIC channel. Furthermore, control cells did not show increased apoptosis rates or signs of mitochondrial alterations. Therefore, it can be assumed that phototoxicity was very low and probably did not significantly influence the outcome of experiments. Additionally, optimal cell culture conditions were provided by using a microscope equipped with a cell incubator for long-term temperature and CO_2 control.

In order to be able to automatically track cellular parameters in individual cells, a machine learning-based algorithm was applied for the segmentation of nuclei. Subsequently, cells could be tracked, and signal intensities measured in nuclei and cytoplasm. The combination of this cell tracking and machine learning-based image analysis holds the great advantage of being able to measure cellular parameters in individual cells over long time periods. Usually, individual cell analysis with software such as the ZEN 2.0 program requires the drawing of a ROI around each single cell. This time-consuming procedure has to be repeated for each new time frame, since cells tend to move over time. Alternatively, classical computer vision methods can be applied to automatize this process. However, due to strongly increasing SiR-DNA signals in dying cells because of chromatin condensation, and decreasing SiR-DNA signals in surviving cells due to transport of the dye to vesicular structures and cell division, these methods are not reliable in this setup.

Automatic nuclei segmentation and tracking in this study enabled the quantification of parameters such as caspase-3/7 on a large scale, allowing for the analysis and interpretation of more data.

One disadvantage of the machine learning-based algorithm for nuclei recognition and segmentation is that the CNN is only able to detect what it has been trained with. Thus, the training data (in this case images) have to be representative. The more representative the training data on nuclei is, the better the CNN can recognize nuclei and segment the images, and it usually outperforms classic computer vision methods particularly in challenging situations [164].

For future studies, it would be greatly advantageous to develop a convolutional neural network that recognizes nuclei from DIC images without having to label nuclei with a fluorescent marker like SiR-DNA in analogy to the method developed by Ounkomol *et al.* [165]. This would add the option of using another marker in the far red such as SiR-actin and enable correlation of even more cellular read-outs.

4.6 Outlook

This study indicated that $[Ca^{2+}]_m$ fluxes are decisive for survival of A549 cells after PLY challenge *in vitro*. Hereby, a first hint towards why some alveolar epithelial cells might survive PLY challenge has been established. To assess the clinical relevance, and for possible therapeutic consequences of these results, further studies are needed.

Further studies with freshly isolated primary lung epithelial cells, as well as analysis of survival in *ex vivo* infected lung tissue, should be conducted to confirm the obtained results. A pneumococcal infection model in explanted lung tissue has been established in our work group [82, 135, 166-168].

Additionally, further studies with PLY-producing *S.pn.* should be conducted in this setting. PLY concentrations during *S.pn.* infection might differ from the PLY concentrations used in this work. Therefore, it is of utmost importance to investigate whether during infection of human lung tissue with PLY-producing *S.pn.*, alveolar epithelial cells are also able to survive and recover from caspase-3/7 activation, mitochondrial fragmentation and loss of $\Delta\Psi_m$. In this work, only non-encapsulated *S.pn.* strains were used for infection to test specifically for the effects of the *S.pn.* virulence factor PLY without the influence of the effects of the polysaccharide capsule. Since the polysaccharide is an important virulence factor, and nearly all clinically relevant *S.pn.* strains are encapsulated, further studies should disentangle the combinatory effects of encapsulated as well as PLY-producing *S.pn.* [27].

Furthermore, it would be interesting to explore whether cells might recover from stimulation by pore-forming toxins produced by other bacteria such as *Streptococcus pyogenes* or *Clostridium septicum*. Streptolysin O produced by *Streptococcus pyogenes* is known to cause $[Ca^{2+}]_c$ influx, loss of $\Delta\Psi_m$, activation of caspase-3 and cell death of keratinocytes [169]. α-toxin produced by *Clostridium septicum* is known to cause $[Ca^{2+}]_c$ influx, decrease of intracellular ATP and cell death in myoblasts [170]. Since both of these pore-forming toxins also induce $[Ca^{2+}]_c$ influx, lead to mitochondrial dysfunction and cause cell death, it could also be tested whether cells might be able to recover from loss of $\Delta\Psi_m$, decrease of ATP production and caspase-3 activation after exposure to these toxins. Additionally, it should be revealed if pore formation by streptolysin O or α-toxin will likewise induce $[Ca^{2+}]_m$ influx, which might be pharmacologically regulated to foster cell survival rates.

In this current study, PLY challenge led to an increase of $[Ca^{2+}]$ in mitochondria of A549 cells and surviving cells showed a lower $[Ca^{2+}]_m$ influx amplitude as well as a higher $[Ca^{2+}]_m$ efflux rate. MCU knockout mice that were developed by Pan *et al.* revealed that mitochondria lacking MCU showed no $[Ca^{2+}]_m$ increase following the addition of extra-mitochondrial Ca^{2+} [171]. In a future study, it would be of interest to explore how loss of MCU might influence the number of alveolar epithelial cells that survive after PLY

challenge. Additionally, it would also be interesting to investigate whether the increase of $[Ca^{2+}]_m$ efflux might support survival. Currently, a pharmacological intervention which might activate such mechanisms does not exist. However, this could be addressed in future studies.

More survival of alveolar epithelial cells after PLY exposure must be considered as beneficial during pneumococcal pneumonia. Less tissue damage would sustain alveolar-capillary barrier function, and would therefore minimize the accumulation of edema fluid in the lung, thus decreasing the risk of acute respiratory failure by preserving gas exchange and alveolar homeostasis. Additionally, more surviving alveolar epithelial type II cells, which are potentially able to repopulate the epithelial barrier in alveoli, might lead to improved clinical outcomes. To explore whether surviving alveolar cells might be able to restore the epithelial barriers of alveoli after PLY challenge, long-term culture models such as lung organoids are necessary that allow for the monitoring of alveolar epithelial cells over days or even weeks. Organoids are self-organizing three-dimensional cellular structures grown from pluripotent stem cells or adult tissue stem cells partially reflecting the original organ. These *in vitro* models preserve the main aspects of epithelial function, differentiation and polarity, thus providing decisive advantages for studies of potential changes of barrier functions in comparison to 2D cell culture models [172]. The research to establish organoids that reflect key features of alveoli (“alveolospheres”) consisting of alveolar epithelial cells has been advancing significantly in the last years [173-175]. Our group successfully established the first stable long-term cultures (> 6 months) of human lung organoids from adult stem cells that contain differentiated type II cells (personal communication, manuscript in preparation). In such an experimental setting, it would be possible to follow the fate of surviving cells in alveolospheres over longer time periods, and it could be examined whether surviving cells might be able to reconstitute epithelial barriers. Additionally, human lung organoids can serve as useful platforms for pre-clinical drug testing [176]. Even partial pharmacological PLY inhibition could significantly reduce pneumococcal tissue damage and possibly mortality. Therapy with antibodies against PLY led to reduced mortality during pneumococcal pneumonia in a murine model, and β-sitosterol protected human alveolar epithelial cells from injury by PLY and prevented lethal pneumococcal infection [177, 178]. More studies to test the pharmacological inhibition of PLY and its cytotoxic effects, especially in human lung models, are of utmost importance.

Bibliography

1. Musher DM, Thorner AR: **Community-acquired pneumonia**. *The New England journal of medicine* 2014, **371**(17):1619-1628.

2. **The top 10 causes of death** [https://www.who.int/en/news-room/fact-sheets/detail/the-top-10-causes-of-death] (Accessed August 25, 2020)

3. Wardlaw TMJ, Emily White; Hodge, Matthew; World Health Organization; UNICEF: **Pneumonia: the forgotten killer of children.** 2006:4.

4. Kolditz M, Ewig S: **Community-Acquired Pneumonia in Adults**. *Dtsch Arztebl Int* 2017, **114**(49):838-848.

5. Welte T, Torres A, Nathwani D: **Clinical and economic burden of community-acquired pneumonia among adults in Europe**. *Thorax* 2012, **67**(1):71-79.

6. Kolditz M, Tesch F, Mocke L, Hoffken G, Ewig S, Schmitt J: **Burden and risk factors of ambulatory or hospitalized CAP: A population based cohort study**. *Respir Med* 2016, **121**:32-38.

7. Lim WS, van der Eerden MM, Laing R, Boersma WG, Karalus N, Town GI, Lewis SA, Macfarlane JT: **Defining community acquired pneumonia severity on presentation to hospital: an international derivation and validation study**. *Thorax* 2003, **58**(5):377-382.

8. Ewig S, Hoffken G, Kern WV, Rohde G, Flick H, Krause R, Ott S, Bauer T, Dalhoff K, Gatermann S, Kolditz M, Kruger S, Lorenz J, Pletz M, de Roux A, Schaaf B, Schaberg T, Schutte H, Welte T: **[Management of Adult Community-acquired Pneumonia and Prevention - Update 2016]**. *Pneumologie* 2016, **70**(3):151-200.

9. Force ADT, Ranieri VM, Rubenfeld GD, Thompson BT, Ferguson ND, Caldwell E, Fan E, Camporota L, Slutsky AS: **Acute respiratory distress syndrome: the Berlin Definition**. *JAMA* 2012, **307**(23):2526-2533.

10. Matthay MA, Zemans RL: **The acute respiratory distress syndrome: pathogenesis and treatment**. *Annu Rev Pathol* 2011, **6**:147-163.

11. Caya CA, Boikos C, Desai S, Quach C: **Dosing regimen of the 23-valent pneumococcal vaccination: a systematic review**. *Vaccine* 2015, **33**(11):1302-1312.

12. Ewald H, Briel M, Vuichard D, Kreutle V, Zhydkov A, Gloy V: **The Clinical Effectiveness of Pneumococcal Conjugate Vaccines: A Systematic Review and Meta-analysis of Randomized Controlled Trials**. *Dtsch Arztebl Int* 2016, **113**(9):139-146.

13. Impfkommission S: **Empfehlungen der Ständigen Impfkommission beim Robert Koch-Institut – 2019/2020**. *Epidemiologisches Bulletin* 2019(34):313--364.

14. Lynch JP, 3rd, Zhanel GG: **Escalation of antimicrobial resistance among Streptococcus pneumoniae: implications for therapy**. *Semin Respir Crit Care Med* 2005, **26**(6):575-616.

15. Welte T, Kohnlein T: **Global and local epidemiology of community-acquired pneumonia: the experience of the CAPNETZ Network**. *Semin Respir Crit Care Med* 2009, **30**(2):127-135.

16. Garcia-Suarez Mdel M, Florez N, Astudillo A, Vazquez F, Villaverde R, Fabrizio K, Pirofski LA, Mendez FJ: **The role of pneumolysin in mediating lung damage in a lethal pneumococcal pneumonia murine model**. *Respir Res* 2007, **8**:3.

17. Herrero R, Sanchez G, Lorente JA: **New insights into the mechanisms of pulmonary edema in acute lung injury**. *Ann Transl Med* 2018, **6**(2):32.

18. van der Poll T, Opal SM: **Pathogenesis, treatment, and prevention of pneumococcal pneumonia**. *Lancet* 2009, **374**(9700):1543-1556.

19. Kadioglu A, Weiser JN, Paton JC, Andrew PW: **The role of Streptococcus pneumoniae virulence factors in host respiratory colonization and disease**. *Nat Rev Microbiol* 2008, **6**(4):288-301.

20. Bogaert D, De Groot R, Hermans PW: **Streptococcus pneumoniae colonisation: the key to pneumococcal disease**. *Lancet Infect Dis* 2004, **4**(3):144-154.

21. Loughran AJ, Orihuela CJ, Tuomanen EI: **Streptococcus pneumoniae: Invasion and Inflammation**. *Microbiol Spectr* 2019, **7**(2).

22. Ganaie F, Saad JS, McGee L, van Tonder AJ, Bentley SD, Lo SW, Gladstone RA, Turner P, Keenan JD, Breiman RF, Nahm MH: **A New Pneumococcal Capsule Type, 10D, is the 100th Serotype and Has a Large cps Fragment from an Oral Streptococcus**. *mBio* 2020, **11**(3).

23. **Pneumococcal conjugate vaccine for childhood immunization--WHO position paper**. *Wkly Epidemiol Rec* 2007, **82**(12):93-104.

24. AlonsoDeVelasco E, Verheul AF, Verhoef J, Snippe H: **Streptococcus pneumoniae: virulence factors, pathogenesis, and vaccines**. *Microbiol Rev* 1995, **59**(4):591-603.

25. Nelson AL, Roche AM, Gould JM, Chim K, Ratner AJ, Weiser JN: **Capsule enhances pneumococcal colonization by limiting mucus-mediated clearance**. *Infect Immun* 2007, **75**(1):83-90.

26. Abeyta M, Hardy GG, Yother J: **Genetic alteration of capsule type but not PspA type affects accessibility of surface-bound complement and surface antigens of Streptococcus pneumoniae**. *Infect Immun* 2003, **71**(1):218-225.

27. Hyams C, Camberlein E, Cohen JM, Bax K, Brown JS: **The Streptococcus pneumoniae capsule inhibits complement activity and neutrophil phagocytosis by multiple mechanisms**. *Infect Immun* 2010, **78**(2):704-715.

28. Tong HH, Blue LE, James MA, DeMaria TF: **Evaluation of the virulence of a Streptococcus pneumoniae neuraminidase-deficient mutant in nasopharyngeal colonization and development of otitis media in the chinchilla model**. *Infect Immun* 2000, **68**(2):921-924.

29. King SJ, Hippe KR, Weiser JN: **Deglycosylation of human glycoconjugates by the sequential activities of exoglycosidases expressed by Streptococcus pneumoniae**. *Mol Microbiol* 2006, **59**(3):961-974.

30. Burnaugh AM, Frantz LJ, King SJ: **Growth of Streptococcus pneumoniae on human glycoconjugates is dependent upon the sequential activity of bacterial exoglycosidases**. *J Bacteriol* 2008, **190**(1):221-230.

31. Pritchard DG, Lin B, Willingham TR, Baker JR: **Characterization of the group B streptococcal hyaluronate lyase**. *Arch Biochem Biophys* 1994, **315**(2):431-437.

32. Martner A, Dahlgren C, Paton JC, Wold AE: **Pneumolysin released during Streptococcus pneumoniae autolysis is a potent activator of intracellular oxygen radical production in neutrophils**. *Infect Immun* 2008, **76**(9):4079-4087.

33. Tuomanen E, Liu H, Hengstler B, Zak O, Tomasz A: **The induction of meningeal inflammation by components of the pneumococcal cell wall**. *J Infect Dis* 1985, **151**(5):859-868.

34. Seo HS, Michalek SM, Nahm MH: **Lipoteichoic acid is important in innate immune responses to gram-positive bacteria**. *Infect Immun* 2008, **76**(1):206-213.

35. Ren B, McCrory MA, Pass C, Bullard DC, Ballantyne CM, Xu Y, Briles DE, Szalai AJ: **The virulence function of Streptococcus pneumoniae surface protein A involves inhibition of complement activation and impairment of complement receptor-mediated protection**. *J Immunol* 2004, **173**(12):7506-7512.

36. Hammerschmidt S, Bethe G, Remane PH, Chhatwal GS: **Identification of pneumococcal surface protein A as a lactoferrin-binding protein of Streptococcus pneumoniae**. *Infect Immun* 1999, **67**(4):1683-1687.

37. Hammerschmidt S, Talay SR, Brandtzaeg P, Chhatwal GS: **SpsA, a novel pneumococcal surface protein with specific binding to secretory immunoglobulin A and secretory component**. *Mol Microbiol* 1997, **25**(6):1113-1124.

38. Zhang JR, Mostov KE, Lamm ME, Nanno M, Shimida S, Ohwaki M, Tuomanen E: **The polymeric immunoglobulin receptor translocates pneumococci across human nasopharyngeal epithelial cells**. *Cell* 2000, **102**(6):827-837.

39. Boyton RJ, Openshaw PJ: **Pulmonary defences to acute respiratory infection**. *Br Med Bull* 2002, **61**:1-12.

40. Paterson GK, Mitchell TJ: **Innate immunity and the pneumococcus**. *Microbiology* 2006, **152**(Pt 2):285-293.

41. Akira S, Uematsu S, Takeuchi O: **Pathogen recognition and innate immunity**. *Cell* 2006, **124**(4):783-801.

42. Widdicombe J: **Relationships among the composition of mucus, epithelial lining liquid, and adhesion of microorganisms**. *Am J Respir Crit Care Med* 1995, **151**(6):2088-2092; discussion 2092-2083.

43. Nicod LP: **Lung defences: an overview**. *Eur Respir Rev* 2005, **14: 45–50.**

44. Jacquot J, Puchelle E, Zahm JM, Beck G, Plotkowski MC: **Effect of human airway lysozyme on the in vitro growth of type I Streptococcus pneumoniae**. *Eur J Respir Dis* 1987, **71**(4):295-305.

45. Whitsett JA, Alenghat T: **Respiratory epithelial cells orchestrate pulmonary innate immunity**. *Nature immunology* 2015, **16**(1):27-35.

46. Vermaelen KY, Carro-Muino I, Lambrecht BN, Pauwels RA: **Specific migratory dendritic cells rapidly transport antigen from the airways to the thoracic lymph nodes**. *The Journal of experimental medicine* 2001, **193**(1):51-60.

47. West AP, Shadel GS, Ghosh S: **Mitochondria in innate immune responses**. *Nature reviews Immunology* 2011, **11**(6):389-402.

48. Mitchell AM, Mitchell TJ: **Streptococcus pneumoniae: virulence factors and variation**. *Clin Microbiol Infect* 2010, **16**(5):411-418.

49. Goldenberg NM, Steinberg BE, Slutsky AS, Lee WL: **Broken barriers: a new take on sepsis pathogenesis**. *Sci Transl Med* 2011, **3**(88):88ps25.

50. Opal SM, van der Poll T: **Endothelial barrier dysfunction in septic shock**. *J Intern Med* 2015, **277**(3):277-293.

51. Matthay MA, Ware LB, Zimmerman GA: **The acute respiratory distress syndrome**. *J Clin Invest* 2012, **122**(8):2731-2740.

52. Olajuyin AM, Zhang X, Ji HL: **Alveolar type 2 progenitor cells for lung injury repair**. *Cell Death Discov* 2019, **5**:63.

53. Crapo JD, Barry BE, Gehr P, Bachofen M, Weibel ER: **Cell number and cell characteristics of the normal human lung**. *Am Rev Respir Dis* 1982, **125**(6):740-745.

54. Herzog EL, Brody AR, Colby TV, Mason R, Williams MC: **Knowns and unknowns of the alveolus**. *Proceedings of the American Thoracic Society* 2008, **5**(7):778-782.

55. Lucas R, Czikora I, Sridhar S, Zemskov E, Gorshkov B, Siddaramappa U, Oseghale A, Lawson J, Verin A, Rick FG, Block NL, Pillich H, Romero M, Leustik M, Schally AV, Chakraborty T: **Mini-review: novel therapeutic strategies to blunt actions of pneumolysin in the lungs**. *Toxins (Basel)* 2013, **5**(7):1244-1260.

56. Marriott HM, Mitchell TJ, Dockrell DH: **Pneumolysin: a double-edged sword during the host-pathogen interaction**. *Current molecular medicine* 2008, **8**(6):497-509.

57. Price KE, Camilli A: **Pneumolysin localizes to the cell wall of Streptococcus pneumoniae**. *J Bacteriol* 2009, **191**(7):2163-2168.

58. Tilley SJ, Orlova EV, Gilbert RJ, Andrew PW, Saibil HR: **Structural basis of pore formation by the bacterial toxin pneumolysin**. *Cell* 2005, **121**(2):247-256.

59. Vogele M, Bhaskara RM, Mulvihill E, van Pee K, Yildiz O, Kuhlbrandt W, Muller DJ, Hummer G: **Membrane perforation by the pore-forming toxin pneumolysin**. *Proc Natl Acad Sci U S A* 2019, **116**(27):13352-13357.

60. van Pee K, Neuhaus A, D'Imprima E, Mills DJ, Kuhlbrandt W, Yildiz O: **CryoEM structures of membrane pore and prepore complex reveal cytolytic mechanism of Pneumolysin**. *eLife* 2017, **6**.

61. Berry AM, Yother J, Briles DE, Hansman D, Paton JC: **Reduced virulence of a defined pneumolysin-negative mutant of Streptococcus pneumoniae**. *Infect Immun* 1989, **57**(7):2037-2042.

62. Canvin JR, Marvin AP, Sivakumaran M, Paton JC, Boulnois GJ, Andrew PW, Mitchell TJ: **The role of pneumolysin and autolysin in the pathology of pneumonia and septicemia in mice infected with a type 2 pneumococcus**. *J Infect Dis* 1995, **172**(1):119-123.

63. Rubins JB, Charboneau D, Paton JC, Mitchell TJ, Andrew PW, Janoff EN: **Dual function of pneumolysin in the early pathogenesis of murine pneumococcal pneumonia**. *J Clin Invest* 1995, **95**(1):142-150.

64. Berry AM, Alexander JE, Mitchell TJ, Andrew PW, Hansman D, Paton JC: **Effect of defined point mutations in the pneumolysin gene on the virulence of Streptococcus pneumoniae**. *Infect Immun* 1995, **63**(5):1969-1974.

65. Mitchell TJ, Dalziel CE: **The biology of pneumolysin**. *Subcell Biochem* 2014, **80**:145-160.

66. Steinfort C, Wilson R, Mitchell T, Feldman C, Rutman A, Todd H, Sykes D, Walker J, Saunders K, Andrew PW, et al.: **Effect of Streptococcus pneumoniae on human respiratory epithelium in vitro**. *Infect Immun* 1989, **57**(7):2006-2013.

67. Bermpohl D, Halle A, Freyer D, Dagand E, Braun JS, Bechmann I, Schroder NW, Weber JR: **Bacterial programmed cell death of cerebral endothelial cells involves dual death pathways**. *J Clin Invest* 2005, **115**(6):1607-1615.

68. Stringaris AK, Geisenhainer J, Bergmann F, Balshusemann C, Lee U, Zysk G, Mitchell TJ, Keller BU, Kuhnt U, Gerber J, Spreer A, Bahr M, Michel U, Nau R: **Neurotoxicity of pneumolysin, a major pneumococcal virulence factor, involves calcium influx and depends on activation of p38 mitogen-activated protein kinase**. *Neurobiol Dis* 2002, **11**(3):355-368.

69. Braun JS, Hoffmann O, Schickhaus M, Freyer D, Dagand E, Bermpohl D, Mitchell TJ, Bechmann I, Weber JR: **Pneumolysin causes neuronal cell death through mitochondrial damage**. *Infect Immun* 2007, **75**(9):4245-4254.

70. Rayner CF, Jackson AD, Rutman A, Dewar A, Mitchell TJ, Andrew PW, Cole PJ, Wilson R: **Interaction of pneumolysin-sufficient and -deficient isogenic variants of Streptococcus pneumoniae with human respiratory mucosa**. *Infect Immun* 1995, **63**(2):442-447.

71. Feldman C, Mitchell TJ, Andrew PW, Boulnois GJ, Read RC, Todd HC, Cole PJ, Wilson R: **The effect of Streptococcus pneumoniae pneumolysin on human respiratory epithelium in vitro**. *Microb Pathog* 1990, **9**(4):275-284.

72. Rubins JB, Duane PG, Charboneau D, Janoff EN: **Toxicity of pneumolysin to pulmonary endothelial cells in vitro**. *Infect Immun* 1992, **60**(5):1740-1746.

73. Witzenrath M, Gutbier B, Hocke AC, Schmeck B, Hippenstiel S, Berger K, Mitchell TJ, de los Toyos JR, Rosseau S, Suttorp N, Schutte H: **Role of pneumolysin for the development of acute lung injury in pneumococcal pneumonia**. *Crit Care Med* 2006, **34**(7):1947-1954.

74. Lucas R, Yang G, Gorshkov BA, Zemskov EA, Sridhar S, Umapathy NS, Jezierska-Drutel A, Alieva IB, Leustik M, Hossain H, Fischer B, Catravas JD, Verin AD, Pittet JF, Caldwell RB, Mitchell TJ, Cederbaum SD, Fulton DJ, Matthay MA, Caldwell RW, Romero MJ, Chakraborty T: **Protein kinase C-alpha and arginase I mediate pneumolysin-induced pulmonary endothelial hyperpermeability**. *Am J Respir Cell Mol Biol* 2012, **47**(4):445-453.

75. Hippenstiel S, Suttorp N: **Interaction of pathogens with the endothelium**. *Thromb Haemost* 2003, **89**(1):18-24.

76. Ratner AJ, Hippe KR, Aguilar JL, Bender MH, Nelson AL, Weiser JN: **Epithelial cells are sensitive detectors of bacterial pore-forming toxins**. *J Biol Chem* 2006, **281**(18):12994-12998.

77. Ratner AJ, Lysenko ES, Paul MN, Weiser JN: **Synergistic proinflammatory responses induced by polymicrobial colonization of epithelial surfaces**. *Proc Natl Acad Sci U S A* 2005, **102**(9):3429-3434.

78. Rogers PD, Thornton J, Barker KS, McDaniel DO, Sacks GS, Swiatlo E, McDaniel LS: **Pneumolysin-dependent and -independent gene expression identified by cDNA microarray analysis of THP-1 human mononuclear cells stimulated by Streptococcus pneumoniae**. *Infect Immun* 2003, **71**(4):2087-2094.

79. Dessing MC, Hirst RA, de Vos AF, van der Poll T: **Role of Toll-like receptors 2 and 4 in pulmonary inflammation and injury induced by pneumolysin in mice**. *PLoS One* 2009, **4**(11):e7993.

80. Malley R, Henneke P, Morse SC, Cieslewicz MJ, Lipsitch M, Thompson CM, Kurt-Jones E, Paton JC, Wessels MR, Golenbock DT: **Recognition of pneumolysin by Toll-like receptor 4 confers resistance to pneumococcal infection**. *Proc Natl Acad Sci U S A* 2003, **100**(4):1966-1971.

81. McNeela EA, Burke A, Neill DR, Baxter C, Fernandes VE, Ferreira D, Smeaton S, El-Rachkidy R, McLoughlin RM, Mori A, Moran B, Fitzgerald KA, Tschopp J, Petrilli V, Andrew PW, Kadioglu A, Lavelle EC: **Pneumolysin activates the NLRP3 inflammasome and promotes proinflammatory cytokines independently of TLR4**. *PLoS Pathog* 2010, **6**(11):e1001191.

82. Fatykhova D, Rabes A, Machnik C, Guruprasad K, Pache F, Berg J, Toennies M, Bauer TT, Schneider P, Schimek M, Eggeling S, Mitchell TJ, Mitchell AM, Hilker R, Hain T, Suttorp N, Hippenstiel S, Hocke AC, Opitz B: **Serotype 1 and 8 Pneumococci Evade Sensing by Inflammasomes in Human Lung Tissue**. *PLoS One* 2015, **10**(8):e0137108.

83. Alcantara RB, Preheim LC, Gentry-Nielsen MJ: **Pneumolysin-induced complement depletion during experimental pneumococcal bacteremia**. *Infect Immun* 2001, **69**(6):3569-3575.

84. Yuste J, Botto M, Paton JC, Holden DW, Brown JS: **Additive inhibition of complement deposition by pneumolysin and PspA facilitates Streptococcus pneumoniae septicemia**. *J Immunol* 2005, **175**(3):1813-1819.

85. Galluzzi L, Kepp O, Trojel-Hansen C, Kroemer G: **Mitochondrial control of cellular life, stress, and death**. *Circ Res* 2012, **111**(9):1198-1207.

86. Kuhlbrandt W: **Structure and function of mitochondrial membrane protein complexes**. *BMC biology* 2015, **13**:89.

87. Falkenberg M: **Mitochondrial DNA replication in mammalian cells: overview of the pathway**. *Essays Biochem* 2018, **62**(3):287-296.

88. Detmer SA, Chan DC: **Functions and dysfunctions of mitochondrial dynamics**. *Nature reviews Molecular cell biology* 2007, **8**(11):870-879.

89. Friedman JR, Nunnari J: **Mitochondrial form and function**. *Nature* 2014, **505**(7483):335-343.

90. Lackner LL: **Shaping the dynamic mitochondrial network**. *BMC biology* 2014, **12**:35.

91. Chen H, McCaffery JM, Chan DC: **Mitochondrial fusion protects against neurodegeneration in the cerebellum**. *Cell* 2007, **130**(3):548-562.

92. Chang CR, Blackstone C: **Dynamic regulation of mitochondrial fission through modification of the dynamin-related protein Drp1**. *Ann N Y Acad Sci* 2010, **1201**:34-39.

93. Frank S, Gaume B, Bergmann-Leitner ES, Leitner WW, Robert EG, Catez F, Smith CL, Youle RJ: **The role of dynamin-related protein 1, a mediator of mitochondrial fission, in apoptosis**. *Developmental cell* 2001, **1**(4):515-525.

94. Jagasia R, Grote P, Westermann B, Conradt B: **DRP-1-mediated mitochondrial fragmentation during EGL-1-induced cell death in C. elegans**. *Nature* 2005, **433**(7027):754-760.

95. Lee YJ, Jeong SY, Karbowski M, Smith CL, Youle RJ: **Roles of the mammalian mitochondrial fission and fusion mediators Fis1, Drp1, and Opa1 in apoptosis**. *Molecular biology of the cell* 2004, **15**(11):5001-5011.

96. Mills EL, Kelly B, O'Neill LAJ: **Mitochondria are the powerhouses of immunity**. *Nature immunology* 2017, **18**(5):488-498.

97. Nerlich A, Mieth M, Letsiou E, Fatykhova D, Zscheppang K, Imai-Matsushima A, Meyer TF, Paasch L, Mitchell TJ, Tonnies M, Bauer TT, Schneider P, Neudecker J, Ruckert JC, Eggeling S, Schimek M, Witzenrath M, Suttorp N, Hippenstiel S, Hocke AC: **Pneumolysin induced mitochondrial dysfunction leads to release of mitochondrial DNA**. *Sci Rep* 2018, **8**(1):182.

98. Zhang Q, Raoof M, Chen Y, Sumi Y, Sursal T, Junger W, Brohi K, Itagaki K, Hauser CJ: **Circulating mitochondrial DAMPs cause inflammatory responses to injury**. *Nature* 2010, **464**(7285):104-107.

99. Rizzuto R, De Stefani D, Raffaello A, Mammucari C: **Mitochondria as sensors and regulators of calcium signalling**. *Nature reviews Molecular cell biology* 2012, **13**(9):566-578.

100. Raffaello A, Mammucari C, Gherardi G, Rizzuto R: **Calcium at the Center of Cell Signaling: Interplay between Endoplasmic Reticulum, Mitochondria, and Lysosomes**. *Trends Biochem Sci* 2016, **41**(12):1035-1049.

101. Giorgi C, Marchi S, Pinton P: **The machineries, regulation and cellular functions of mitochondrial calcium**. *Nature reviews Molecular cell biology* 2018, **19**(11):713-730.

102. Patron M, Raffaello A, Granatiero V, Tosatto A, Merli G, De Stefani D, Wright L, Pallafacchina G, Terrin A, Mammucari C, Rizzuto R: **The mitochondrial calcium uniporter (MCU): molecular identity and physiological roles**. *J Biol Chem* 2013, **288**(15):10750-10758.

103. De Stefani D, Raffaello A, Teardo E, Szabo I, Rizzuto R: **A forty-kilodalton protein of the inner membrane is the mitochondrial calcium uniporter**. *Nature* 2011, **476**(7360):336-340.

104. Baughman JM, Perocchi F, Girgis HS, Plovanich M, Belcher-Timme CA, Sancak Y, Bao XR, Strittmatter L, Goldberger O, Bogorad RL, Koteliansky V, Mootha VK: **Integrative genomics identifies MCU as an essential component of the mitochondrial calcium uniporter**. *Nature* 2011, **476**(7360):341-345.

105. Palty R, Silverman WF, Hershfinkel M, Caporale T, Sensi SL, Parnis J, Nolte C, Fishman D, Shoshan-Barmatz V, Herrmann S, Khananshvili D, Sekler I: **NCLX is an essential component of mitochondrial Na+/Ca2+ exchange**. *Proc Natl Acad Sci U S A* 2010, **107**(1):436-441.

106. Drago I, De Stefani D, Rizzuto R, Pozzan T: **Mitochondrial Ca2+ uptake contributes to buffering cytoplasmic Ca2+ peaks in cardiomyocytes**. *Proc Natl Acad Sci U S A* 2012, **109**(32):12986-12991.

107. Orrenius S, Gogvadze V, Zhivotovsky B: **Calcium and mitochondria in the regulation of cell death**. *Biochem Biophys Res Commun* 2015, **460**(1):72-81.

108. Ashida H, Mimuro H, Ogawa M, Kobayashi T, Sanada T, Kim M, Sasakawa C: **Cell death and infection: a double-edged sword for host and pathogen survival**. *The Journal of cell biology* 2011, **195**(6):931-942.

109. Galluzzi L, Vitale I, Aaronson SA, Abrams JM, Adam D, Agostinis P, Alnemri ES, Altucci L, Amelio I, Andrews DW, Annicchiarico-Petruzzelli M, Antonov AV, Arama E, Baehrecke EH, Barlev NA, Bazan NG, Bernassola F, Bertrand MJM, Bianchi K, Blagosklonny MV, Blomgren K, Borner C, Boya P, Brenner C, Campanella M, Candi E, Carmona-Gutierrez D, Cecconi F, Chan FK, Chandel NS, Cheng EH, Chipuk JE, Cidlowski JA, Ciechanover A, Cohen GM, Conrad M, Cubillos-Ruiz JR, Czabotar PE, D'Angiolella V, Dawson TM, Dawson VL, De Laurenzi V, De Maria R, Debatin KM, DeBerardinis RJ, Deshmukh M, Di Daniele N, Di Virgilio F, Dixit VM, Dixon SJ, Duckett CS, Dynlacht BD, El-Deiry WS, Elrod JW, Fimia GM, Fulda S, Garcia-Saez AJ, Garg AD, Garrido C, Gavathiotis E, Golstein P, Gottlieb E, Green DR, Greene LA, Gronemeyer H, Gross A, Hajnoczky G, Hardwick JM, Harris IS, Hengartner MO, Hetz C, Ichijo H, Jaattela M, Joseph B, Jost PJ, Juin PP, Kaiser WJ, Karin M, Kaufmann T, Kepp O, Kimchi A, Kitsis RN, Klionsky DJ, Knight RA, Kumar S, Lee SW, Lemasters JJ, Levine B, Linkermann A, Lipton SA,

Lockshin RA, Lopez-Otin C, Lowe SW, Luedde T, Lugli E, MacFarlane M, Madeo F, Malewicz M, Malorni W, Manic G, Marine JC, Martin SJ, Martinou JC, Medema JP, Mehlen P, Meier P, Melino S, Miao EA, Molkentin JD, Moll UM, Munoz-Pinedo C, Nagata S, Nunez G, Oberst A, Oren M, Overholtzer M, Pagano M, Panaretakis T, Pasparakis M, Penninger JM, Pereira DM, Pervaiz S, Peter ME, Piacentini M, Pinton P, Prehn JHM, Puthalakath H, Rabinovich GA, Rehm M, Rizzuto R, Rodrigues CMP, Rubinsztein DC, Rudel T, Ryan KM, Sayan E, Scorrano L, Shao F, Shi Y, Silke J, Simon HU, Sistigu A, Stockwell BR, Strasser A, Szabadkai G, Tait SWG, Tang D, Tavernarakis N, Thorburn A, Tsujimoto Y, Turk B, Vanden Berghe T, Vandenabeele P, Vander Heiden MG, Villunger A, Virgin HW, Vousden KH, Vucic D, Wagner EF, Walczak H, Wallach D, Wang Y, Wells JA, Wood W, Yuan J, Zakeri Z, Zhivotovsky B, Zitvogel L, Melino G, Kroemer G: **Molecular mechanisms of cell death: recommendations of the Nomenclature Committee on Cell Death 2018**. *Cell death and differentiation* 2018, **25**(3):486-541.

110. Haanen C, Vermes I: **Apoptosis and inflammation**. *Mediators Inflamm* 1995, **4**(1):5-15.

111. Silva MT: **Secondary necrosis: the natural outcome of the complete apoptotic program**. *FEBS letters* 2010, **584**(22):4491-4499.

112. Green DR, Kroemer G: **The pathophysiology of mitochondrial cell death**. *Science* 2004, **305**(5684):626-629.

113. Galluzzi L, Kepp O, Kroemer G: **Mitochondrial regulation of cell death: a phylogenetically conserved control**. *Microb Cell* 2016, **3**(3):101-108.

114. Grosse L, Wurm CA, Bruser C, Neumann D, Jans DC, Jakobs S: **Bax assembles into large ring-like structures remodeling the mitochondrial outer membrane in apoptosis**. *The EMBO journal* 2016, **35**(4):402-413.

115. Salvador-Gallego R, Mund M, Cosentino K, Schneider J, Unsay J, Schraermeyer U, Engelhardt J, Ries J, Garcia-Saez AJ: **Bax assembly into rings and arcs in apoptotic mitochondria is linked to membrane pores**. *The EMBO journal* 2016, **35**(4):389-401.

116. Kroemer G, Martin SJ: **Caspase-independent cell death**. *Nat Med* 2005, **11**(7):725-730.

117. Norberg E, Orrenius S, Zhivotovsky B: **Mitochondrial regulation of cell death: processing of apoptosis-inducing factor (AIF)**. *Biochem Biophys Res Commun* 2010, **396**(1):95-100.

118. Joza N, Susin SA, Daugas E, Stanford WL, Cho SK, Li CY, Sasaki T, Elia AJ, Cheng HY, Ravagnan L, Ferri KF, Zamzami N, Wakeham A, Hakem R, Yoshida H, Kong YY, Mak TW, Zuniga-Pflucker JC, Kroemer G, Penninger JM: **Essential role of the mitochondrial apoptosis-inducing factor in programmed cell death**. *Nature* 2001, **410**(6828):549-554.

119. Lemasters JJ, Theruvath TP, Zhong Z, Nieminen AL: **Mitochondrial calcium and the permeability transition in cell death**. *Biochimica et biophysica acta* 2009, **1787**(11):1395-1401.

120. Hurst S, Hoek J, Sheu SS: **Mitochondrial Ca(2+) and regulation of the permeability transition pore**. *J Bioenerg Biomembr* 2017, **49**(1):27-47.

121. Tait SW, Parsons MJ, Llambi F, Bouchier-Hayes L, Connell S, Munoz-Pinedo C, Green DR: **Resistance to caspase-independent cell death requires persistence of intact mitochondria**. *Developmental cell* 2010, **18**(5):802-813.

122. Braun JS, Sublett JE, Freyer D, Mitchell TJ, Cleveland JL, Tuomanen EI, Weber JR: **Pneumococcal pneumolysin and H(2)O(2) mediate brain cell apoptosis during meningitis**. *J Clin Invest* 2002, **109**(1):19-27.

123. Dockrell DH, Lee M, Lynch DH, Read RC: **Immune-mediated phagocytosis and killing of Streptococcus pneumoniae are associated with direct and bystander macrophage apoptosis**. *J Infect Dis* 2001, **184**(6):713-722.

124. Zysk G, Schneider-Wald BK, Hwang JH, Bejo L, Kim KS, Mitchell TJ, Hakenbeck R, Heinz HP: **Pneumolysin is the main inducer of cytotoxicity to brain microvascular endothelial cells caused by Streptococcus pneumoniae**. *Infect Immun* 2001, **69**(2):845-852.

125. Beurg M, Hafidi A, Skinner L, Cowan G, Hondarrague Y, Mitchell TJ, Dulon D: **The mechanism of pneumolysin-induced cochlear hair cell death in the rat**. *J Physiol* 2005, **568**(Pt 1):211-227.

126. Marriott HM, Ali F, Read RC, Mitchell TJ, Whyte MK, Dockrell DH: **Nitric oxide levels regulate macrophage commitment to apoptosis or necrosis during pneumococcal infection**. *FASEB J* 2004, **18**(10):1126-1128.

127. Srivastava A, Henneke P, Visintin A, Morse SC, Martin V, Watkins C, Paton JC, Wessels MR, Golenbock DT, Malley R: **The apoptotic response to pneumolysin is Toll-like receptor 4 dependent and protects against pneumococcal disease**. *Infect Immun* 2005, **73**(10):6479-6487.

128. Ichim G, Lopez J, Ahmed SU, Muthalagu N, Giampazolias E, Delgado ME, Haller M, Riley JS, Mason SM, Athineos D, Parsons MJ, van de Kooij B, Bouchier-Hayes L, Chalmers AJ, Rooswinkel RW, Oberst A, Blyth K, Rehm M, Murphy DJ, Tait SWG: **Limited mitochondrial permeabilization causes DNA damage and genomic instability in the absence of cell death**. *Molecular cell* 2015, **57**(5):860-872.

129. Tang HL, Tang HM, Mak KH, Hu S, Wang SS, Wong KM, Wong CS, Wu HY, Law HT, Liu K, Talbot CC, Jr., Lau WK, Montell DJ, Fung MC: **Cell survival, DNA damage, and oncogenic transformation after a transient and reversible apoptotic response**. *Molecular biology of the cell* 2012, **23**(12):2240-2252.

130. Sun G, Guzman E, Balasanyan V, Conner CM, Wong K, Zhou HR, Kosik KS, Montell DJ: **A molecular signature for anastasis, recovery from the brink of apoptotic cell death**. *The Journal of cell biology* 2017, **216**(10):3355-3368.

131. Wolfmeier H, Schoenauer R, Atanassoff AP, Neill DR, Kadioglu A, Draeger A, Babiychuk EB: **Ca(2)(+)-dependent repair of pneumolysin pores: A new paradigm for host cellular defense against bacterial pore-forming toxins**. *Biochimica et biophysica acta* 2015, **1853**(9):2045-2054.

132. Wolfmeier H, Radecke J, Schoenauer R, Koeffel R, Babiychuk VS, Drucker P, Hathaway LJ, Mitchell TJ, Zuber B, Draeger A, Babiychuk EB: **Active release of**

pneumolysin prepores and pores by mammalian cells undergoing a Streptococcus pneumoniae attack. *Biochimica et biophysica acta* 2016, **1860**(11 Pt A):2498-2509.

133. Giard DJ, Aaronson SA, Todaro GJ, Arnstein P, Kersey JH, Dosik H, Parks WP: **In vitro cultivation of human tumors: establishment of cell lines derived from a series of solid tumors**. *Journal of the National Cancer Institute* 1973, **51**(5):1417-1423.

134. Imamura H, Nhat KP, Togawa H, Saito K, Iino R, Kato-Yamada Y, Nagai T, Noji H: **Visualization of ATP levels inside single living cells with fluorescence resonance energy transfer-based genetically encoded indicators**. *Proc Natl Acad Sci U S A* 2009, **106**(37):15651-15656.

135. Berg J, Zscheppang K, Fatykhova D, Tonnies M, Bauer TT, Schneider P, Neudecker J, Ruckert JC, Eggeling S, Schimek M, Gruber AD, Suttorp N, Hippenstiel S, Hocke AC: **Tyk2 as a target for immune regulation in human viral/bacterial pneumonia**. *Eur Respir J* 2017, **50**(1).

136. Mulisch M, Aescht E, Romeis B: **Romeis - Mikroskopische Technik**. In., 19th edn. Edited by Mulisch M, Welsch U. Berlin: Springer Spektrum; 2015.

137. Schmidt U, Weigert M, Broaddus C, Myers G: **Cell Detection with Star-Convex Polygons**. In*: 2018; Cham*: Springer International Publishing; 2018: 265-273.

138. Schindelin J, Arganda-Carreras I, Frise E, Kaynig V, Longair M, Pietzsch T, Preibisch S, Rueden C, Saalfeld S, Schmid B, Tinevez JY, White DJ, Hartenstein V, Eliceiri K, Tomancak P, Cardona A: **Fiji: an open-source platform for biological-image analysis**. *Nature methods* 2012, **9**(7):676-682.

139. McQuin C, Goodman A, Chernyshev V, Kamentsky L, Cimini BA, Karhohs KW, Doan M, Ding L, Rafelski SM, Thirstrup D, Wiegraebe W, Singh S, Becker T, Caicedo JC, Carpenter AE: **CellProfiler 3.0: Next-generation image processing for biology**. *PLoS biology* 2018, **16**(7):e2005970.

140. Tinevez JY, Perry N, Schindelin J, Hoopes GM, Reynolds GD, Laplantine E, Bednarek SY, Shorte SL, Eliceiri KW: **TrackMate: An open and extensible**

platform for single-particle tracking. *Methods (San Diego, Calif)* 2017, **115**:80-90.

141. Nerlich A, von Wunsch Teruel I, Mieth M, Honzke K, Ruckert JC, Mitchell TJ, Suttorp N, Hippenstiel S, Hocke AC: **Reversion of pneumolysin induced executioner caspase activation redirects cells to survival**. *J Infect Dis* 2020.

142. Scarlett JL, Sheard PW, Hughes G, Ledgerwood EC, Ku HH, Murphy MP: **Changes in mitochondrial membrane potential during staurosporine-induced apoptosis in Jurkat cells**. *FEBS letters* 2000, **475**(3):267-272.

143. Cox DA, Conforti L, Sperelakis N, Matlib MA: **Selectivity of inhibition of Na(+)-Ca2+ exchange of heart mitochondria by benzothiazepine CGP-37157**. *Journal of cardiovascular pharmacology* 1993, **21**(4):595-599.

144. Altman BJ, Rathmell JC: **Metabolic stress in autophagy and cell death pathways**. *Cold Spring Harbor perspectives in biology* 2012, **4**(9):a008763.

145. Schmeck B, Gross R, N'Guessan PD, Hocke AC, Hammerschmidt S, Mitchell TJ, Rosseau S, Suttorp N, Hippenstiel S: **Streptococcus pneumoniae-induced caspase 6-dependent apoptosis in lung epithelium**. *Infect Immun* 2004, **72**(9):4940-4947.

146. Waters CM, Roan E, Navajas D: **Mechanobiology in lung epithelial cells: measurements, perturbations, and responses**. *Compr Physiol* 2012, **2**(1):1-29.

147. Cen H, Mao F, Aronchik I, Fuentes RJ, Firestone GL: **DEVD-NucView488: a novel class of enzyme substrates for real-time detection of caspase-3 activity in live cells**. *Faseb j* 2008, **22**(7):2243-2252.

148. Twig G, Elorza A, Molina AJ, Mohamed H, Wikstrom JD, Walzer G, Stiles L, Haigh SE, Katz S, Las G, Alroy J, Wu M, Py BF, Yuan J, Deeney JT, Corkey BE, Shirihai OS: **Fission and selective fusion govern mitochondrial segregation and elimination by autophagy**. *The EMBO journal* 2008, **27**(2):433-446.

149. Nowikovsky K, Reipert S, Devenish RJ, Schweyen RJ: **Mdm38 protein depletion causes loss of mitochondrial K+/H+ exchange activity, osmotic swelling and mitophagy**. *Cell death and differentiation* 2007, **14**(9):1647-1656.

150. Clapham DE: **Calcium signaling**. *Cell* 2007, **131**(6):1047-1058.

151. Lobet E, Letesson JJ, Arnould T: **Mitochondria: a target for bacteria**. *Biochem Pharmacol* 2015, **94**(3):173-185.

152. TranVan Nhieu G, Clair C, Grompone G, Sansonetti P: **Calcium signalling during cell interactions with bacterial pathogens**. *Biol Cell* 2004, **96**(1):93-101.

153. Abramov AY, Duchen MR: **Actions of ionomycin, 4-BrA23187 and a novel electrogenic Ca2+ ionophore on mitochondria in intact cells**. *Cell calcium* 2003, **33**(2):101-112.

154. Chakrabarti R, Ji WK, Stan RV, de Juan Sanz J, Ryan TA, Higgs HN: **INF2-mediated actin polymerization at the ER stimulates mitochondrial calcium uptake, inner membrane constriction, and division**. *The Journal of cell biology* 2018, **217**(1):251-268.

155. Wacquier B, Combettes L, Dupont G: **Cytoplasmic and Mitochondrial Calcium Signaling: A Two-Way Relationship**. *Cold Spring Harbor perspectives in biology* 2019, **11**(10).

156. Bernardi P, Petronilli V: **The permeability transition pore as a mitochondrial calcium release channel: a critical appraisal**. *J Bioenerg Biomembr* 1996, **28**(2):131-138.

157. Ichas F, Jouaville LS, Mazat JP: **Mitochondria are excitable organelles capable of generating and conveying electrical and calcium signals**. *Cell* 1997, **89**(7):1145-1153.

158. Ludtmann MHR, Kostic M, Horne A, Gandhi S, Sekler I, Abramov AY: **LRRK2 deficiency induced mitochondrial Ca(2+) efflux inhibition can be rescued by Na(+)/Ca(2+)/Li(+) exchanger upregulation**. *Cell Death Dis* 2019, **10**(4):265.

159. Luongo TS, Lambert JP, Gross P, Nwokedi M, Lombardi AA, Shanmughapriya S, Carpenter AC, Kolmetzky D, Gao E, van Berlo JH, Tsai EJ, Molkentin JD, Chen X, Madesh M, Houser SR, Elrod JW: **The mitochondrial Na(+)/Ca(2+) exchanger is essential for Ca(2+) homeostasis and viability**. *Nature* 2017, **545**(7652):93-97.

160. Iliev AI, Djannatian JR, Nau R, Mitchell TJ, Wouters FS: **Cholesterol-dependent actin remodeling via RhoA and Rac1 activation by the Streptococcus pneumoniae toxin pneumolysin**. *Proc Natl Acad Sci U S A* 2007, **104**(8):2897-2902.

161. Drucker P, Bachler S, Wolfmeier H, Schoenauer R, Koffel R, Babiychuk VS, Dittrich PS, Draeger A, Babiychuk EB: **Pneumolysin-damaged cells benefit from non-homogeneous toxin binding to cholesterol-rich membrane domains**. *Biochim Biophys Acta Mol Cell Biol Lipids* 2018, **1863**(8):795-805.

162. Waldchen S, Lehmann J, Klein T, van de Linde S, Sauer M: **Light-induced cell damage in live-cell super-resolution microscopy**. *Sci Rep* 2015, **5**:15348.

163. Magidson V, Khodjakov A: **Circumventing photodamage in live-cell microscopy**. *Methods Cell Biol* 2013, **114**:545-560.

164. Caicedo JC, Goodman A, Karhohs KW, Cimini BA, Ackerman J, Haghighi M, Heng C, Becker T, Doan M, McQuin C, Rohban M, Singh S, Carpenter AE: **Nucleus segmentation across imaging experiments: the 2018 Data Science Bowl**. *Nature methods* 2019, **16**(12):1247-1253.

165. Ounkomol C, Seshamani S, Maleckar MM, Collman F, Johnson GR: **Label-free prediction of three-dimensional fluorescence images from transmitted-light microscopy**. *Nature methods* 2018, **15**(11):917-920.

166. Hocke AC, Suttorp N, Hippenstiel S: **Human lung ex vivo infection models**. *Cell Tissue Res* 2017, **367**(3):511-524.

167. Peter A, Fatykhova D, Kershaw O, Gruber AD, Rueckert J, Neudecker J, Toennies M, Bauer TT, Schneider P, Schimek M, Eggeling S, Suttorp N, Hocke AC, Hippenstiel S: **Localization and pneumococcal alteration of junction proteins**

in the human alveolar-capillary compartment. *Histochem Cell Biol* 2017, **147**(6):707-719.

168. Hocke AC, Becher A, Knepper J, Peter A, Holland G, Tonnies M, Bauer TT, Schneider P, Neudecker J, Muth D, Wendtner CM, Ruckert JC, Drosten C, Gruber AD, Laue M, Suttorp N, Hippenstiel S, Wolff T: **Emerging human middle East respiratory syndrome coronavirus causes widespread infection and alveolar damage in human lungs**. *Am J Respir Crit Care Med* 2013, **188**(7):882-886.

169. Cywes Bentley C, Hakansson A, Christianson J, Wessels MR: **Extracellular group A Streptococcus induces keratinocyte apoptosis by dysregulating calcium signalling**. *Cell Microbiol* 2005, **7**(7):945-955.

170. Kennedy CL, Smith DJ, Lyras D, Chakravorty A, Rood JI: **Programmed cellular necrosis mediated by the pore-forming alpha-toxin from Clostridium septicum**. *PLoS Pathog* 2009, **5**(7):e1000516.

171. Pan X, Liu J, Nguyen T, Liu C, Sun J, Teng Y, Fergusson MM, Rovira, II, Allen M, Springer DA, Aponte AM, Gucek M, Balaban RS, Murphy E, Finkel T: **The physiological role of mitochondrial calcium revealed by mice lacking the mitochondrial calcium uniporter**. *Nat Cell Biol* 2013, **15**(12):1464-1472.

172. Barkauskas CE, Chung MI, Fioret B, Gao X, Katsura H, Hogan BL: **Lung organoids: current uses and future promise**. *Development* 2017, **144**(6):986-997.

173. Barkauskas CE, Cronce MJ, Rackley CR, Bowie EJ, Keene DR, Stripp BR, Randell SH, Noble PW, Hogan BL: **Type 2 alveolar cells are stem cells in adult lung**. *J Clin Invest* 2013, **123**(7):3025-3036.

174. Jacob A, Vedaie M, Roberts DA, Thomas DC, Villacorta-Martin C, Alysandratos KD, Hawkins F, Kotton DN: **Derivation of self-renewing lung alveolar epithelial type II cells from human pluripotent stem cells**. *Nat Protoc* 2019, **14**(12):3303-3332.

175. Jacobson EF, Tzanakakis ES: **Human pluripotent stem cell differentiation to functional pancreatic cells for diabetes therapies: Innovations, challenges and future directions**. *J Biol Eng* 2017, **11**:21.

176. Xu H, Jiao Y, Qin S, Zhao W, Chu Q, Wu K: **Organoid technology in disease modelling, drug development, personalized treatment and regeneration medicine**. *Exp Hematol Oncol* 2018, **7**:30.

177. Musher DM, Phan HM, Baughn RE: **Protection against bacteremic pneumococcal infection by antibody to pneumolysin**. *J Infect Dis* 2001, **183**(5):827-830.

178. Li H, Zhao X, Wang J, Dong Y, Meng S, Li R, Niu X, Deng X: **beta-sitosterol interacts with pneumolysin to prevent Streptococcus pneumoniae infection**. *Sci Rep* 2015, **5**:17668.

Statutory declaration

“I, Iris Vera von Wunsch-Rolshoven Teruel, by personally signing this document in lieu of an oath, hereby affirm that I prepared the submitted dissertation on the topic “Role of mitochondria for the survival of alveolar epithelial cells after pneumolysin challenge”, independently and without the support of third parties, and that I used no other sources and aids than those stated.
All parts which are based on the publications or presentations of other authors, either in letter or in spirit, are specified as such in accordance with the citing guidelines. The sections on methodology (in particular regarding practical work, laboratory regulations, statistical processing) and results (in particular regarding charts, tables and all figures **except figure 10**) are exclusively my responsibility.

My contributions to any publications to this dissertation correspond to those stated in the below joint declaration made together with the supervisor. All publications created within the scope of the dissertation comply with the guidelines of the ICMJE (International Committee of Medical Journal Editors; www.icmje.org) on authorship. In addition, I declare that I shall comply with the regulations of Charité – Universitätsmedizin Berlin on ensuring good scientific practice.

I declare that I have not yet submitted this dissertation in identical or similar form to another Faculty.

The significance of this statutory declaration and the consequences of a false statutory declaration under criminal law (Sections 156, 161 of the German Criminal Code) are known to me.”

Date Signature

Declaration of own contribution to the top-journal publication

Iris Vera von Wunsch-Rolshoven Teruel contributed the following to the below listed publication:

Publication:

Nerlich A, **von Wunsch Teruel I,** Mieth M, Hönzke K, Rückert JC, Mitchell TJ, Suttorp N, Hippenstiel S, Hocke AC: Reversion of pneumolysin induced executioner caspase activation redirects cells to survival. *The Journal of Infectious Diseases*; 12 October 2020; jiaa639, https://doi.org/10.1093/infdis/jiaa639.

Detailed declaration of own contribution:

Iris von Wunsch Teruel started this project in 2017 and, first, contributed elaborately to the development and optimization of the experimental settings. She performed pilot experiments and analyses with different toxin concentrations and varying cell culture conditions and established life-cell microscopy conditions as well as image analysis settings.

After this initial phase almost all experiments were carried out autonomously. Only those with primary human cells isolated from alveolar tissue as well as infection with *Streptococcus pneumoniae* were conducted with help of Drs. Andreas Nerlich, Maren Mieth and Katja Hönzke. Additionally, acquisition of images by structured illumination microscopy was executed with the help of Dr. Andreas Nerlich.

All semi-automatic and machine learning based single cell analysis approaches were set up by Dr. Andreas Nerlich but image and statistical analyses were performed by Iris von Wunsch Teruel after thorough introduction. By supervision of Prof. Dr. Andreas Hocke and Dr. Andreas Nerlich she interpreted the data and prepared the figures.

The first draft of the publication was written by Dr. Andreas Nerlich, which was then revised by all co-authors under leading supervision of Prof. Dr. Andreas Hocke before submission to the journal.

Date Signature

Curriculum vitae

Mein Lebenslauf wird aus datenschutzrechtlichen Gründen in der elektronischen Version meiner Arbeit nicht veröffentlicht.

Publications

Peer-reviewed journals:

Nerlich A, von Wunsch Teruel I, Mieth M, Hönzke K, Rückert JC, Mitchell TJ, Suttorp N, Hippenstiel S, Hocke AC: **Reversion of pneumolysin induced executioner caspase activation redirects cells to survival**. *The Journal of Infectious Diseases*; 12 October 2020; jiaa639, https://doi.org/10.1093/infdis/jiaa639.

Presentations:

Nerlich A, von Wunsch Teruel I, Mieth M, Hönzke K, Rückert JC, Mitchell TJ, Suttorp N, Hippenstiel S, Hocke AC: **Mitochondrial calcium flux is decisive for survival of pneumolysin induced cell death.** Autumn Meeting 2019, German Respiratory Society (DGP), Berlin 29.11.2019-30.11.2019.

Acknowledgements

I would never have been able to finish my dissertation without the guidance of my supervisors, help from my colleagues, and support from my parents and friends.
First of all, I would like to thank Prof. Dr. Suttorp for giving me the opportunity to conduct my research at the Department of Infectious Diseases and Respiratory Medicine at the Charité. I would like to express my profound gratitude to my supervisor Prof. Dr. Andreas Hocke for introducing me to this interesting research field, for his guidance and the caring support. His advice and the numerous conversations we had were very enriching – on a personal and an intellectual level. I am also very thankful to Prof. Dr. Stefan Hippenstiel for proofreading this work and for the excellent scientific advice he provided.
I would like to express my very great appreciation to Dr. Andreas Nerlich for co-supervising my dissertation. He was always there for me whenever I had a question. Working with him was a pleasure and the many fruitful exchanges we had motivated me to continue this work. He was a great teacher and I am thankful for all the scientific skills he taught me. I am well aware of how lucky I was to have him as my co-supervisor.
I also want to thank Dr. Maren Mieth for introducing me to the laboratory work and for her excellent help during experiments in the lab. I especially want to thank Dr. Diana Fatykhova and Katharina Hellwig for their caring presence and support. I was not only able to learn a lot from Diana's scientific experience but also looked forward to seeing her in the office every day. It was a delight to share an office with her. I also enjoyed all the uplifting and interesting conversations and moments I shared with all the other members of our research group. Therefore, I would also like to thank my colleagues Dr. Katja Hönzke, Dr. Mirjana Kessler, Dr. Karen Hoffmann, Dr. Mirja Mittermeier, Dr. Melanie Dohmen and Eva Pappe for the friendly atmosphere in the lab.
Finally, I wish to express my deepest gratitude to my parents and all my friends for their continuous support over the past years. I especially want to thank Dr. Sarah Starossom who taught me a great deal about scientific thinking and writing. I also want to thank my friends Peter Grabitz, Lydia König and Stephan Kolling for proofreading this work and for their very helpful remarks. Without the love and immense support from my parents I would never have been able to start such a project, never mind finishing it. Their love and guidance are with me in whatever I pursue. Finally, I also want to thank Steffi who motivated me lovingly to run the last mile.